

Aus der Abt. Vaskuläre Biologie und Tumorangiogenese  
der Medizinischen Fakultät Mannheim  
European Center for Angioscience  
(Direktor: Prof. Dr. Hellmut Augustin)

The increased concentration of 4-Hydroxynonenal in *aldh3a1* zebrafish mutants disrupts pancreas development, leading to hyperglycaemia and retina hyaloid vasculature alteration

Inauguraldissertation  
zur Erlangung des medizinischen Doktorgrades  
der  
Medizinischen Fakultät Mannheim  
der Ruprecht-Karls-Universität  
zu  
Heidelberg

vorgelegt von  
Bowen Lou

aus  
Shaanxi, China  
2020

Dekan: Prof. Dr. med. Sergij Goerd  
Referent: Prof. Dr. Jens Kroll

太阳只是颗启明星，来日方长。

亨利·戴维·梭罗（瓦尔登湖）

*"There is more day to dawn. The sun is but a morning star."*

*Henry David Thoreau (Walden)*

# CONTENTS

	Page
ABBREVIATIONS.....	1
<b>1 INTRODUCTION.....</b>	<b>5</b>
1.1 Diabetes mellitus (DM).....	5
1.2 Chronic diabetic complications and diabetic retinopathy (DR).....	7
1.3 Mechanisms of pancreas development in diabetes .....	9
1.4 4-Hydroxynonenal (4-HNE) and its function in Diabetes.....	10
1.5 Aldehyde dehydrogenase (ALDH) superfamily and ALDH3A1.....	11
1.6 Aim of the thesis.....	13
<b>2 MATERIALS AND METHODS .....</b>	<b>15</b>
2.1 Material .....	15
2.1.1 Equipment .....	15
2.1.2 Chemicals.....	16
2.1.3 Consumables .....	16
2.1.4 Buffers and Solutions .....	17
2.1.5 Kits and Reagents .....	18
2.1.6 Plasmids.....	19
2.1.7 Enzymes and buffers.....	19
2.1.8 Oligonucleotides.....	19
2.1.9 Morpholinos.....	22
2.1.10 Bacteria strain .....	22
2.1.11 Zebrafish transgenic lines .....	22
2.2 Methods .....	23
2.2.1 Animal studies .....	23
2.2.2 Molecular biology .....	25
2.2.3 Biochemical analysis .....	30
2.2.4 Software .....	31
2.2.5 Statistical analysis .....	31

3 RESULTS.....	33
3.1 Sequence alignment of Aldh3a1 across different species and analysis of the <i>aldh3a1</i> mRNA expression in larvae and adult organs of zebrafish.....	33
3.2 Generation and validation of Aldh3a1 knock out in zebrafish. ....	34
3.3 Vasculature alternations in <i>aldh3a1</i> mutants are enhanced by <i>pxd1</i> morpholino injection. ....	36
3.4 Early pancreas is impaired by <i>aldh3a1</i> morpholino injection. ....	40
3.5 <i>Ins</i> mRNA level is reduced and the whole-body glucose is elevated in both Aldh3a1 transient knockdown and permanent knockout zebrafish larvae. ....	42
3.6 Detoxification of 4-HNE but not MG is impaired and causes hyperglycaemia in Aldh3a1 knock out. ....	47
3.7 Overfeeding leads to obesity and alters retina morphology but does not develop hyperglycaemia in <i>aldh3a1</i> <sup>-/-</sup> adult zebrafish. ....	53
4 DISSCUSSION .....	58
4.1 The Aldh3a1 enzyme system in zebrafish .....	59
4.2 <i>Aldh3a1</i> <sup>-/-</sup> larvae exhibit abnormal angiogenesis in the trunk and retinal hyaloid vasculature, which was accelerated by hyperglycaemia. ....	60
4.3 <i>Aldh3a1</i> <sup>-/-</sup> larvae display imbalance energy metabolism and moderate hyperglycaemia, which is caused by the destruction of pancreas development. ..	62
4.4 Defective 4-HNE detoxification and increased internal 4-HNE concentration regulate metabolic diseases via glucose homeostasis after Aldh3a1 loss.....	64
4.5 Overfeeding induced obesity alters retina morphology in <i>aldh3a1</i> <sup>-/-</sup> adult zebrafish.....	67
SUMMARY.....	69
REFERENCE.....	71
PUBLICATION LIST .....	82
CURRICULUM VITAE .....	83
ACKNOWLEDGEMENT .....	84

## ABBREVIATIONS

°C	Degree Celsius
∞	Forever
μl	Microliter
μm	Micrometre
μM	Micromolar
%	Percent
4-HNE	4-Hydroxynonenal
AD	Alzheimer's disease
ADP	Adenosine diphosphate
AGE	Advanced glycation end product
AKR	Aldo keto reductase
Ala	Alanine
ALDH	Aldehyde dehydrogenase
Aldh3a1	Aldehyde dehydrogenase 3 family, member a1
ALE	Advanced lipoxidation end product
AMP	Adenosine monophosphate
Amp	Ampicillin
approx.	Approximately
Arg	Arginine
Asn	Asparagine
Asp	Aspartate/aspartic acid
ATP	Adenosine triphosphate
bp	Base pairs
BSA	Bovine serum albumin
Cas9	CRISPR associated protein 9
CD36	Cluster of differentiation 36
cDNA	Complementary deoxyribonucleic acid
CL	Cardiolipin
cm	Centimetre
Con	Control
CRISPR	Clustered regularly-interspaced short palindromic repeats
CTGF	Connective tissue growth factor
Cys	Cysteine
DM	Diabetes
DME	Diabetic macular edema
DLAV	Dorsal longitudinal anastomotic vessel
DKFZ	German Cancer Research Center
DNA	Deoxyribonucleic acid
dpf	Days after post fertilization
DPP4	Dipeptidyl peptidase 4
DR	Diabetic retinopathy
E. coli	Escherichia coli
EGFP	Enhanced green fluorescent protein
FFA	fluorescein angiography
fli1	Friend leukemia integration1
Frc-6-P	Fructose-6-phosphate
g	Gram

GABA	Gamma-aminobutyric acid
GC-MS	Gas chromatography-mass spectrometry
GDM	Gestational diabetes
Gln	Glutamine
Glo1	Glyoxalase1
Glp1	Glucagon-like peptide
Glu	Glutamic acid
Gly	Glycine
GPx	Glutathione peroxidase
gRNA	Guide RNA
GSEA	Gene set enrichment analysis
GSH	Glutathione
GSSG	Glutathione disulphide
GST	Glutathione S-transferase
h	Hours
H <sub>2</sub> O	Histidine
HbA1C	Glycated hemoglobin
HCE	human corneal epithelial cell line
HIF1	Hypoxia-inducible transcription factor 1
hpf	Hours after post fertilization
HPLC	High performance liquid chromatography
Hz	Hertz
Ile	Isoleucine
kb	Kilo bases
KCl	Potassium chloride
l	Litre
IDDM	Insulin-dependent diabetes mellitus
IFG	Impaired fasting glycaemia
IGT	Impaired glucose tolerance
Ins	Preproinsulin
Insb	Preproinsulin b
Isl1	ISL LIM homeobox 1
Isl2a	ISL LIM homeobox 2a
Isl2b	ISL LIM homeobox 2b
IOC	Inner optic circle
ISV	Intersegment vessel
LB	Lysogeny broth
LC-MS/MS	Liquid chromatography-tandem mass spectrometry
LD50	Median lethal dose
Leu	Leucine
LRP	LDL receptor-related protein
Lys	Lysine
KATP	ATP-regulated potassium
M	Molar
MARD	mild age-related diabetes
MDA	malondialdehyde
Met	Methionine
MG	Methylglyoxal
mg	Milligram
min	Minutes
ml	Millilitre

mM	Millimolar
Mnx1/Hb9	Motor neuron and pancreas homeobox 1
MO	Morpholino
MOD	mild obesity-related diabetes
MODY	maturity onset diabetes of the young
Mpc1	Mitochondrial pyruvate carrier 1
Mpc2	Mitochondrial pyruvate carrier 2
mRNA	Messenger RNA
MTA	Methylthioadenosine
n	Number of samples
NAC	N-acetyl-cysteine
NaCl	Sodium chloride
NADH	Nicotinamide adenine dinucleotide
NADPH	Nicotinamide adenine dinucleotide phosphate
NCBI	National Center for Biotechnology Information
NDM	Neonatal diabetes mellitus
NECA	5'-N-ethylcarboxamidoadenosine
NF	Normal feeding
NF- $\kappa$ B	Nuclear factor kappa-light-chain-enhancer of activated B cells
nl	Nanolitre
nm	Nanometre
nmol	Nanomole
NO	Nitrate Oxygen
NOX	NADPH oxidase
NSAIDs	Non-steroidal anti-inflammatory drugs
OCT	Optical coherence tomography
OGTT	Oral glucose tolerance test
OF	Overfeeding
Orn	Ornithine
p	p-value
PAM	Protospacer adjacent motif
PAS	Periodic acid Schiff
PBS	Phosphate buffered saline
PCA	Principal component analysis
PCR	Polymerase chain reaction
PD	Parkinson's disease
PDK4	Pyruvate dehydrogenase lipoamide kinase isozyme 4
PDH	pyruvate dehydrogenase
PDR	Proliferative diabetic retinopathy
Pdx1	Pancreatic and duodenal homeobox 1
PFA	Paraformaldehyde
Phe	Phenylalanine
PKC	Protein kinase C
PLC	Phospholipase C
pmol	Picomol
PNDM	permanent neonatal diabetes mellitus
PPAR	Peroxisome proliferator-activated receptor
PP cell	Pancreatic polypeptide cell
Pro	Proline
PTF1A	Pancreas transcription factor 1 subunit alpha
PTU	Phenylthiourea



RAS	Renin angiotensin system
RFX6	Regulatory factor X, 6
ROS	Reactive-oxygen species
RPE	Retinal pigmented epithelium
rpm	Rounds per minute
RT-PCR	Reverse transcription polymerase chain reaction
RT-qPCR	Real time-quantitative polymerase chain reaction
SAM	S-adenosyl methionine
SAID	Severe autoimmune diabetes
SA	segmental artery
SB	Splice blocking
SD	Standard deviation
SDS	Sodium dodecyl sulfate
Ser	Serine
SGLT2	Sodium/glucose cotransporter 2
SHC	S-adenosyl homocysteine
SIDD	Severe insulin-deficient diabetes
SIRD	severe insulin-resistant diabetes
SV	Segmental vein
T1DM	Type 1 diabetes
T2DM	Type 2 diabetes
TCA	Tricarboxylic acid
Tg	Transgenic
Thr	Threonine
Tris	Tris-aminomethan
Tyr	Tyrosine
UCP2	mitochondrial uncoupling protein 2
UPLC-FSR	Ultra-performance liquid chromatography with fluorescence detection
UV	Ultraviolet
Val	Valine
VEGF	Vascular endothelial growth factor

# 1 INTRODUCTION

## 1.1 Diabetes mellitus (DM).

Diabetes mellitus (DM) is a group of metabolic disorders characterized by high blood glucose levels <sup>1</sup>. Over recent years the global prevalence of diabetes was increasing rapidly<sup>2</sup>, according to the IDF DIABETES ATLAS 9<sup>th</sup> edition, by approximately 463 million people in 2019 and was expected to 700 million in 2045<sup>3</sup>. In the meantime, the number of deaths resulting from diabetes and its complications is estimated to be 4.2 million, and annual global health expenditure on diabetes treatment including its complications is estimated to be USD 760 billion in 2019.

Currently, there are three main types of diabetes: Type 1 diabetes(T1DM), type 2 diabetes(T2DM) and gestational diabetes (GDM), which is more like a temporary status in pregnant women that carries long-term risk of T2DM<sup>4</sup>. Results from the failure of pancreas and  $\beta$  cells, T1DM is an autoimmune dysfunction by insufficient/absolute insulin secretion in the body <sup>5</sup>. Referred to as "insulin-dependent diabetes mellitus" (IDDM) or "juvenile diabetes"<sup>6</sup>, patients with T1DM require insulin therapy every day to regulate their blood glucose level. T2DM, making up the majority of diabetic patients worldwide, results from insulin resistance with relative insulin deficiency to an extensive secretory defect<sup>7</sup>. T2DM is often diagnosed after the occurrence of late complications and accompanied with other disorders such as metabolic syndrome<sup>8</sup>. Furthermore, due to the high heterogeneity of T2DM, a refined classification of Diabetes was identified as five subgroups: severe autoimmune diabetes (SAID), severe insulin-deficient diabetes (SIDDD), severe insulin-resistant diabetes (SIRD), mild obesity-related diabetes (MOD), mild age-related diabetes (MARD) <sup>9</sup>. This new sub stratification could help to tailor and target early treatment to patients and may represent a primary step towards precision medicine in diabetes.

Besides, one of several single-gene mutations can also cause destruction of  $\beta$  cell and lead to Diabetes, including neonatal diabetes mellitus (NDM) and maturity onset diabetes of the young(MODY). Apart from diabetes, impaired glucose tolerance (IGT) and impaired fasting glycaemia (IFG) are pre-diabetic states and intermediate conditions between normal blood glucose and hyperglycaemia. As IGT and IFG are

curable disease states and often considered the precursors for T2DM, appropriate diagnose and lifestyle management are essential to enhance diabetes prevention<sup>10</sup>.

Insulin is the hormone to regulate glucose uptake from the blood into most cells of the body<sup>11</sup>. Hence, insulin secretion deficiency or insulin resistance plays a central role in all types of DM. Insulin is released into the blood by beta cells ( $\beta$  cells) from pancreas islet in the response of glucose alternation in the body<sup>12</sup>. In the normal physiological condition, elevated internal glucose level, especially after eating, will promote the secretion of insulin. Then two-third of the cells will absorb the glucose as energy substrate via insulin usage. To the contrary, lower glucose levels will reduce the secretion and elevate the glucagon amount, which is produced by alpha cells of the pancreas and convert the stored glycogen into glucose<sup>13</sup>. When the secretion of insulin is insufficient, or cells respond poorly because of insulin resistance, the glucose cannot enter into cells properly, and the blood sugar level remains high<sup>14</sup>.

As diabetes is characterized by recurrent or persistent hyperglycaemia, the diagnose criteria is based on the blood sugar level by any one of the following: Fasting plasma glucose level  $\geq 7.0$  mmol/L (126 mg/dL), plasma glucose  $\geq 11.1$  mmol/L (200 mg/dL) two hours after a 75 gram oral glucose load as in an oral glucose tolerance test (OGTT) and glycated haemoglobin (HbA1C)  $\geq 48$  mmol/L ( $\geq 6.5\%$ )<sup>15</sup>. The basic idea of diabetes management is to keep a healthy blood sugar level and avoid causing hypoglycaemia. Avoid the high-risk factors, including smoking, hypertension, lack of exercise and keep a healthy lifestyle are the preliminary rules for curing diabetes. Further, proper medication is necessary for diabetes treatment. In T1DM, exogenous insulin administration is necessary, and immunotherapies which will prevent  $\beta$  cell destruction are developing rapidly according to the development of medical technology<sup>16</sup>. While in T2DM, metformin remains the primary option and treatment has been widely expanded<sup>17</sup>, including sulfonylureas, sodium/glucose cotransporter 2 (SGLT2) inhibitors, glucagon-like peptide 1 (GLP1) receptor agonists, and dipeptidyl peptidase 4 (DPP4) inhibitors. Moreover, a medication that has cardiovascular or renal benefits should be prescribed, but depends well on the accompanying complications<sup>18</sup>.

## 1.2 Chronic diabetic complications and diabetic retinopathy (DR)

The complications of DM include the problems that they develop rapidly (acute) and over time (chronic) and may affect several organ systems. Most acute complications occur due to the glucose disorders, such as hypoglycaemia, diabetic ketoacidosis and hyperosmolar hyperglycaemic non-ketotic coma<sup>19</sup>. While chronic complications are caused by a mixture of microvascular, macrovascular disorders and immune dysfunction. Microvascular disorders lead to microangiopathy in several vital organs, including brain, heart, kidneys, eyes and nerves, and finally results in diabetic nephropathy, neuropathy, retinopathy, cardiomyopathy etc.

Since 2001, Brownlee proposed a unifying hypothesis which was identified to be responsible for the development of complications. The whole hypothesis includes four pathways: the polyol pathway, hexosamine pathway, protein kinase C (PKC) pathway and the advanced glycation end product (AGE) pathway<sup>20</sup>. All the above pathways lead to the elevation of stress and metabolic imbalances. Several increased reactive metabolites during the imbalances, such as  $O_2^-$  and  $H_2O_2$ , accelerate the formation of AGE, activate the polyol pathway and phospholipase C(PLC)<sup>21</sup>. Consequently, the increased accumulation of AGEs sorbitol, oxidative stress and inflammation, while also the dysregulation of epigenetic genes, resulting in the formation of diabetic tissue and microvascular damage<sup>22</sup>.

Diabetic retinopathy(DR) is a common microvascular complication of diabetics and the leading cause of vision loss in working-age people in the world<sup>23</sup>. Although just one-third of diabetic patients have the signs of DR and only one-third of DR patients may suffer from vision-threatening retinopathy including proliferative DR and diabetic macular edema (DME)<sup>24, 25</sup>. The individual lifetime risk of DR is 50–60% in a person with T2DM and up to even 90% in T1DM patients<sup>26, 27</sup>. Moreover, DR gets fifth place among the common causes of blindness or severe vision impairment<sup>28</sup>. The quality of life may be impaired in patients with severe degrees of DR by reduced physical, emotional and social well-being and increased health-care resources<sup>29</sup>.

The understanding of the pathophysiological mechanisms of DR is constantly updated<sup>30, 31</sup>. Before the overt microvascular complications, retinal neurodegeneration can take place and causing neuronal dysfunction right up to neural apoptosis<sup>32</sup> or altered neurovascular coupling<sup>33</sup>. Besides, chronic exposure to hyperglycaemia and other

high-risk factors such as hypertension can initiate a cascade of biochemical and physiological alternations and finally lead to microvascular damage and retinal dysfunction<sup>34</sup>.

Several biochemical mechanisms have evolved in the modulation of DR pathophysiology. Vascular endothelial growth factor (VEGF) expressed by retinal endothelial cells and pericytes can stimulate angiogenesis and increase capillary permeability in response to hypoxia. At the meantime, angiotensin II, up regulated in diabetes, might also increase VEGF expression in retinal endothelial cells [32]. In response to retinal ischaemia, erythropoietin may have neuroprotective effects and act independently of VEGF during retinal angiogenesis in proliferative retinopathy<sup>35</sup>. Besides, hyperglycaemia induces oxidative stress via increased reactive-oxygen species (ROS) production, leading to PKC as well as polyol pathway activation and AGE formation. They together regulate cell signalling, cell metabolism and angiogenic factor expression and result in retinal neurodegeneration and angiogenesis at end<sup>36</sup>.

The progression of DR pathology can be slow and divide into four overlapping clinical stages<sup>25</sup>: 1. Retinal damage by microaneurysms formation via a fundoscopic examination but without any visible microvascular abnormalities; 2. Mild or moderate non-proliferative retinal microvascular; 3. Severe non-proliferative DR; 4. Proliferative and advanced stages of DR. The diagnosis of DR is usually performed by an eye examination: visual acuity test, ophthalmoscopy, pupil dilation and some advanced tests such as fundus fluorescein angiography (FFA) and optical coherence tomography (OCT). With the restriction to patients with Diabetes, a spectrum of retinal microvascular lesions is a typical sign for diagnosing<sup>25</sup>.

Within five years of diagnosing, approximately half of the high-risk proliferative diabetic retinopathy (PDR) patients will suffer from visual impairments without effective treatments<sup>37</sup>. Optimal control of blood glucose and blood pressure is the foundation stone for preventing the progression of DR<sup>25</sup>. Current main medications include corticosteroids, non-steroidal anti-inflammatory drugs (NSAIDs), renin angiotensin system (RAS) blockers and surgery. Laser and vitrectomy surgery is sufficient to avoid vision loss before retina is severely damaged<sup>38</sup>. Moreover, intravitreal anti-VEGF agents have heralded a new treatment paradigm for DME, with the potential to improve vision and quality of life<sup>39</sup>.

### 1.3 Mechanisms of pancreas development in diabetes

The pancreas is composed of two morphologically and functionally distinct compartments<sup>40</sup>: the exocrine compartment, as a part of the digestive system, comprises acinar cells and secretes pancreatic juice and digestive enzymes into the duodenum through the pancreatic duct; the endocrine compartment, throughout the pancreatic parenchyma in functional units known as “islets of Langerhans”<sup>41</sup>. Pancreatic islets include five major types of cells and each cell synthesizes and secretes a principle hormone: insulin from  $\beta$  cells, glucagon from  $\alpha$ -cells, somatostatin from  $\delta$ -cells, and pancreatic polypeptide from pancreatic polypeptide (PP) cells and ghrelin from  $\epsilon$ -cells. Insulin and glucagon are released directly into the circulation to regulate blood sugar levels.

$\beta$  cells, the primary type of cells in endocrine lineage, makeup 50–70% of the cells in human islets, synthesize and secrete insulin and amylin and play a central role in glucose homeostasis<sup>42</sup>. Hence, the reduction of  $\beta$  cell mass or loss of function can lead to insufficient insulin secretion and cause diabetes:  $\beta$  cells are lost due to autoimmune destruction in T1DM while in T2DM, a developing failure of  $\beta$  cells cannot satisfy body's insulin demand<sup>43</sup>. Besides, the disruption of a range of pancreas development relevant transcription factors by mutation, such as pancreatic and duodenal homeobox 1 (PDX1), pancreas transcription factor 1 subunit alpha (PTF1A), motor neuron and pancreas homeobox 1 (MNX1) and regulatory factor X, 6 (RFX6), can lead to  $\beta$  cell failure and permanent neonatal diabetes mellitus (PNDM)<sup>44-49</sup>. PNDM tends to show low birth weight, permanent inadequate secretion of insulin because of the insufficient function of  $\beta$  cells, and the corresponding mutation is supposed as the leading cause of monogenic DM.

Unlike mammals, zebrafish can regenerate  $\beta$  cells throughout their entire life<sup>50</sup>. After around seven thousand small molecules screen, Anderson *et al.* found adenosine agonist 5'-N-ethylcarboxamidoadenosine (NECA) can increase  $\beta$  cell proliferation and promote the restoration of normal glucose level in zebrafish larvae<sup>51</sup>. Delaspre *et al.* illuminated centroacinar cells (Notch-On) contribute to  $\beta$  cell regeneration and neogenesis<sup>52</sup>. Besides,  $\alpha$  cell is also an essential source of  $\beta$  cell regeneration<sup>53</sup>. Taken together, these studies suggest that appropriate signalling pathway and backup

cell systems are essential for  $\beta$  cell regeneration. However, mechanisms for mammalian  $\beta$  cell regeneration is still under investigation. As a unique model, understanding the specific cues that allow for proper pancreatic and  $\beta$  cell regenerative development in zebrafish, can help to accelerate the research progress of diabetes diagnoses and therapies.

#### 1.4 4-Hydroxynonenal (4-HNE) and its function in Diabetes.

4-Hydroxynonenal (4-HNE) is an  $\alpha$ ,  $\beta$ -unsaturated hydroxyalkenal that is produced by lipid peroxidation in cells. Three functional groups, an aldehyde, a double-bond at carbon 2, and a hydroxyl group at carbon 4<sup>54</sup>, makes it a very reactive and dangerous compound.

As the most prominent lipid peroxidation specific aldehydes, 4-HNE has drawn significant attention during the last 40 years and is known to be a significant aldehyde product after the peroxidation of  $\omega$ 6 polyunsaturated fatty acids, including linoleic acid and arachidonic acid<sup>55</sup>. If not detoxified by its corresponding enzymes properly, such as aldehyde dehydrogenase (ALDH), aldo keto reductase (AKR) and glutathione S-transferase (GST), 4-HNE can join in several different chemical reactions with multiple targets<sup>56</sup>. Mostly, 4-HNE can form 1,4-Michael addition adducts with cysteine, while also other two amino acids, histidine and lysine in a lower frequency<sup>57</sup>.

It is widely known that oxidative stress is a precursor to the elevation of ROS<sup>58</sup>. Low levels of ROS play a fundamental role in redox signalling; on the contrary, elevated ROS level, as an oxidative stress marker, reflects the imbalance of the redox system and relates to lipid peroxidation<sup>59</sup>. As the most cytotoxic product generated by lipid peroxidation<sup>60</sup>, 4-HNE is also considered a biomarker of oxidative stress<sup>57</sup>.

In normal physiological conditions, the half-life of 4-HNE is just two minutes because of the metabolism<sup>61</sup>. For example, ALDH isoforms, especially ALDH2 and ALDH3 with the highest efficiency of 4-HNE detoxification, can oxidize the carbonyl group of 4-HNE to become the production of 4-hydroxynonenic acid<sup>61</sup>. The concentration of 4-HNE in the cell membranes can be 10  $\mu$ M to 5 mM in responding to oxidative stress. In physiological concentration, it can evoke proliferation, differentiation, compensatory mechanisms and unfolded protein response in cells; while in pathological

concentration, it can cause damaging effects such as apoptosis, mitochondrial dysfunction, inflammation and proteasome dysfunction<sup>62</sup>.

Due to the high reactive property, 4-HNE has been associated with several different diseases, including but not limited to, Alzheimer's disease (AD), Parkinson's disease (PD), heart disease, atherosclerosis, cancers and diabetes<sup>61, 63-66</sup>. Generally, 4-HNE plays a very complicated role in diabetes depending on its concentration: in physiological concentration, 4-HNE is below the cytotoxic amount and can react to high glucose by active peroxisome proliferator-activated receptor  $\delta$  (PPAR $\delta$ ) complexes, which then induce the transcription and expression of pyruvate dehydrogenase lipoamide kinase isozyme 4 (PDK4) and cluster of differentiation 36 (CD36), finally increasing the secretion of insulin in INS-1E beta cells<sup>67</sup>. When the neutralization capacity of 4-HNE is exceeded, it modifies macromolecules structure, conformation and function, accompanied with AGEs and advanced lipoxidation end products (ALEs)' elevation, leading to  $\beta$  cell dysfunction at the end<sup>68</sup>.

Additionally, several different studies reported the strong correlation between 4-HNE and diabetes complications: G. Liu *et al.* found 4-HNE was highly present in diabetic rat kidneys and led to lipid peroxidative injury<sup>69</sup>. The distal axonopathy generated by 4-HNE treatment mimicked axon pathology observed in neurons isolated from diabetic rats<sup>70</sup>. Asami Mori *et al.* showed an intravitreal injection of 4-HNE significantly prevented the vasodilation of retinal arterioles and may contribute to the retinal vascular dysfunction in DR patients<sup>71</sup>. However, studies regarding the "role" of 4-HNE in diabetes and if it is related to oxidative stress are still restricted. An appropriate model is necessary for next *in vivo* exploration.

### 1.5 Aldehyde dehydrogenase (ALDH) superfamily and ALDH3A1.

The aldehyde dehydrogenase (ALDH) superfamily is composed of nicotinamide adenine dinucleotide (phosphate) (NAD(P)<sup>+</sup>)-dependent enzymes which play an essential role in detoxifying endogenous and exogenous aldehydes<sup>72</sup>. These large superfamily enzyme systems exist in almost all kind of life forms from bacteria, archaea to eukaryotes<sup>73</sup>, which suggest a vital role goes through evolutionary history. Besides, ALDHs have a broad tissue distribution and can be found in all subcellular locations<sup>74</sup>.



Based on the 2002 *ALDH* superfamily update<sup>75</sup>, 555 *ALDH* genes were listed. To date, there are 20 functional *ALDH* genes in the human genome<sup>73</sup> and 21 in zebrafish.

*ALDH* enzymes belong to oxidoreductases family as responsible for aldehydes detoxification. In addition to the capacity of metabolizing aldehydes, *ALDH* exhibit additional enzymatic and non-enzymatic functions, such as they bind several endobiotic and xenobiotic molecules including drugs, hormones etc, as shown for *ALDH1A1*, *ALDH3A1* and *ALDH16A1*<sup>74</sup>; and as structural elements in the eye crystalline, for example *ALDH1A1* and *ALDH3A1*<sup>72</sup>. *ALDH*s are also involved in other physiological processes such as regulation of oxidative stress, neurotransmission, cell proliferation, differentiation and survival, especially in the biosynthesis of retinoic acids<sup>76</sup>.

Mutations in *ALDH* genes can lead to altered *ALDH* activities and defective aldehyde metabolism, which makes individuals vulnerable to aldehyde-related pathogenesis and relates to several diseases<sup>73</sup>, such as cataracts (*ALDH1A1*, *ALDH3A1*, *ALDH18A1*), epileptic seizures (*ALDH7A1*), hyperprolinaemia (*ALDH4A1*), heart disease (*ALDH2*), alcohol sensitivity (*ALDH1A1*, *ALDH1B1*, *ALDH2*), cancers (*ALDH2*) and a wide range of other metabolic and developmental abnormalities<sup>76</sup>.

Aldehyde dehydrogenase 3 families, member A1 (*ALDH3A1*) is a metabolic enzyme that oxidizes mainly toxic lipid peroxidation aldehydes to their corresponding carboxylic acids<sup>77</sup>. It is constitutive in the epithelial layers of lung, stomach, urinary bladder, skin and especially in the cornea<sup>78</sup>. *ALDH3A1* is one of the most abundantly expressed proteins in the corneal epithelium, accounting for 5 to 50% of the total water-soluble protein fraction in mammalian species<sup>79</sup>. Thus it exerts a variety of antioxidant and cytoprotective properties in protecting the cornea during the oxidative stress induced by ultraviolet(UV) light, including such five pathways: a. detoxify several toxic aldehydes during lipid peroxidation<sup>80</sup>; b. absorb the UV light directly<sup>81</sup>; c. antioxidant function by scavenging free radicals<sup>82</sup>; d. regulate the refractive and transparent properties of cornea<sup>83</sup> and e. chaperone-like activity<sup>84</sup>.

Several studies have shown a high *ALDH3A1* affinity for 4-HNE but low ability to detoxify malondialdehyde (MDA), which also supported its multifaceted function<sup>76, 85, 86</sup>. In rabbit corneal stromal fibroblastic cell line (TRK43), human *ALDH3A1* induction reduced the toxic potency of 4-HNE (LD50 increased from 25 to 75  $\mu$ M), decreased 4-

HNE-protein adduct formation and resulted in less DNA fragmentation occurring at higher 4-HNE exposure concentrations<sup>87</sup>. Besides, ectopic expression of ALDH3A1 was associated with cell cycle elongation, reduced DNA synthesis and significant alteration of major cell cycle regulators<sup>77, 88</sup>.

At present few studies have illuminated the role of ALDHs and ALDH3A1 in the disease model: a study in mice showed that ALDH3A1-deficient mice developed cataracts because of the proteasome inhibition by lipid peroxidation [86]. However, further investigations regarding their regulation function especially in diabetes and cancers remain to be essential for disease manifestation, diagnosis and therapy.

## 1.6 Aim of the thesis.

The increased formation of methylglyoxal (MG) under hyperglycaemia is associated with the development of microvascular complications in patients with diabetes mellitus<sup>89</sup>. However, in zebrafish, a permanent knock out of glyoxalase 1(Glo1), the main MG detoxifying system, only led to a two-fold elevation of endogenous MG levels. Importantly, a two-fold increase in ALDH activity, a group of enzymes which catalyse the oxidation of aldehydes and may compensate for the loss of Glo1, was observed. Furthermore, qPCR-based expression data identified increased mRNA levels of *aldh3a1* in the *glo1* mutants suggesting Aldh3a1 as an alternative protein for the detoxification of reactive metabolites<sup>90</sup>.

Besides, in the previous period, few studies focused on the antioxidant function of ALDH3A1 in the corneal epithelium<sup>79, 85, 88</sup>. The function of ALDH3A1 in metabolomics, pancreas development, vascular angiogenesis and diabetes with its complications and if it is related to the 4-HNE detoxifying ability is still unclear. Moreover, in zebrafish, the available data have only reported the existence of the Aldh3a1 enzyme system, but its basic function and properties in organ development and disease processes remain unknown.

Therefore, the thesis aimed to evaluate the short- and long-term effects of Aldh3a1 enzyme system on diabetes and its complications via knockdown and knockout strategies in vivo by using zebrafish as a model organism. The objective was to

generate an Aldh3a1 zebrafish knockout line, to investigate the characteristic of metabolic state and morphology alternation of pancreas and vasculature system under normal, hyperglycaemia and high nutrition intake conditions. The working hypothesis was: 1. Loss of Aldh3a1 enzyme system leads to the dysfunction of 4-HNE detoxification in zebrafish. 2. The accumulation of 4-HNE in vivo results in organ damage, hyperglycaemia, vascular alterations and metabolomics changes subsequently.

## 2 MATERIALS AND METHODS

If not mentioned otherwise, all materials and methods used during the experiments are according to the standard protocols of AG Kroll's Lab, which may be modified from the methods section of the enclosed papers<sup>90-92</sup>.

### 2.1 Material

#### 2.1.1 Equipment

Agarose gel chamber	Peqlab Biotechnologie GmbH
Bench top centrifuge (Rotina 420R)	Hettich
BioPhotometer D30	Eppendorf
Dry bath incubator	Major Science
Electronic balance	Kern & Sohn GmbH
Electrophoresis power supply	Consort
Glucometer Freedom Lite	Abbott(FreeStyle)
Hamilton syringe (Glastight® #1705)	Hamilton
Jun-Air 3-4 Quiet Running Compressor (11 l / min at 8 bar)	Jun-Air
Leica HI1210 water bath	Leica
Leica RM2235 microtome	Leica
QuantStudio 3 Real-Time-PCR-System	Applied Biosystems
Microcentrifuge Mikro 200R	Hettich
PCR cycler	BioRad
pH-meter ProfiLine 197i	WTW ProfiLine
See-saw rocker	Stuart
Table centrifuge	Carl Roth GmbH
UV transilluminator	INTAS
Vertical Micropipette Puller P30	Sutter instruments Co.
Water Bath	Seelbach

### 2.1.2 Chemicals

If not indicated otherwise, all chemicals used during the experiments, were purchased from the following companies:

Carl Roth GmbH & Co. KG  
Merck AG  
Roche Diagnostics GmbH  
Sigma-Aldrich Chemie GmbH  
Thermo Fisher Scientific Inc.

### 2.1.3 Consumables

0.22 µm syringe filter	Millex
Blood glucose test stripes	Abbott (FreeStyle Lite)
Conical tubes (15 ml, 50 ml)	Falcon
Dumont Tweezers No. 5	NeoLabs
Feather disposable scalpel No.10	Feather
Glass culture cyl. (14 mm I.D. x 5 mm)	Biotechs
Microscope slides (76x26 mm)	IDL
Needle 20G x1 ½" nr.1	BD Microlance
Nitrile Gloves	Semperguard
Pasteur Pipettes	Hirschmann
PCR tubes (0.2 ml)	Star Labs
Petri dishes (10cm and quadratic)	Greiner
Pipette filter tips (1000, 100, 20 and 10 µl)	Nerbe plus GmbH
Pipette tip refills (1000, 200, 10 µl)	TipOne Star Labs
Pipettes (P1000, P200, P20 and P2)	Gilson/Eppendorf
Quantitative PCR 96-well reaction plate	Axon
Safe-Lock tubes (0.5, 1.5 and 2.0 ml)	Eppendorf
Stainless steel beads (5 mm)	Qiagen
Syringes (1 ml, 30 ml)	BD Plastipak
Tissue culture plate (6 and 96 well)	Falcon

## 2.1.4 Buffers and Solutions

### 2.1.4.1 Gel electrophoresis

50x TAE buffer	232 g Tris 57.1 ml conc. acetic acid 100 ml 0.5 M EDTA, pH 8.6 ad 1 l deionized water
1x TAE buffer	100 ml 50x TAE buffer ad 5 l deionized water
Denaturing agarose gel sample loading buffer	75 µl deionized formamide 75 µl 10x MOPS buffer 120 µl 37% formaldehyde 90 µl sterile deionized water 50 µl glycerin a spatula's tip bromophenolblue

### 2.1.4.2 Bacteria media

LB agar	35 g LB-Agar (Sigma) ad 1 l MilliQ water
LB medium	20 g LB-Broth (Sigma) ad 1l MilliQ water

### 2.1.4.3 Zebrafish maintenance and work

E3 („eggwater“)	3 g Red Sea Salt ad 10 l MilliQ water
0.1 M KCl	0.745 g KCl ad 100 ml MilliQ water

1-phenyl-2-thiourea (PTU, 10x stock)	304 mg PTU ad 1 l MilliQ water
Lysis buffer	133 µl of 1.5 M Tris/HCl, pH8 40 µl 0.5 M EDTA 60 µl Tween 60 µl Glycerol ad 20 ml MilliQ water
Tricaine (3-amino benzoic acidethylester)	400 mg Tricaine powder 97.9 ml MilliQ water ~2.1 ml 1 M Tris (pH 9) adjust to pH ~7 100 ml total volume
Tris/HCl, pH 7.8	181.17 g Tris Adjust pH to 7.8 with HCl Ad 1 l MilliQ water
4% PFA	4 g PFA dissolved in 100 ml 1xPBS

### 2.1.5 Kits and Reagents

Product	Company
4-Hydroxynonenal (4-HNE) ELISA Kit	Biovision
4-Hydroxynonenal - CAS 75899-68-2	Sigma-Aldrich
Gene Ruler DNA ladder mix (0.5 µg/µl)	Thermo Fisher Scientific
Glucose Assay Kit CBA086	Merck
GoTaq® Green Master Mix	Promega
Illustra PlasmidPrep Mini Spin Kit	GE Healthcare Life Science
Maxima First Strand cDNA Synthesis Kit with dsDNase	molecular biology by thermo scientific
MEGAscript™ T7	invitrogen by Thermo Fisher Scientific
miRNeasy Mini Kit	QIAGEN
mMESSAGE mMach™ T7	invitrogen by Thermo Fisher Scientific

Power SYBR™ Green PCR Master Mix Kit	Applied Biosystems
Qiagen Plasmid Midi Kit	QIAGEN
QIAquick PCR Purification Kit	QIAGEN
RNeasy Mini Kit	QIAGEN
Tricaine (3-amino benzoic acidethylester)	Sigma-Aldrich
Trypsin/EDTA solution (25200-056)	Gibco

### 2.1.6 Plasmids

pT7-gRNA	Addgene
pT3TS-nCas9n	Addgene

### 2.1.7 Enzymes and buffers

All restriction enzymes and buffers, including *Bam*HI-HF, *Bgl*II, NEB Buffer 3, NEB CutSmart Buffer, *Sall*, *Sma*I, T4 DNA Ligase Buffer, T4 Ligase, T7 endonuclease, *Xba*I were purchased from New England Biolabs GmbH.

Proteinase K was purchased from Roche

### 2.1.8 Oligonucleotides

#### **CRISPR-construct name**

#### **Oligonucleotide sequence (5' to 3')**

Aldh3a1-CRISPR#1-for  
Aldh3a1-CRISPR#1-rev

TAGGGGTCTGGATCTGCCTGAC  
AAACGTCAGGCAGATCCAGACC

#### **Genotyping primer name**

#### **Primer sequence (5' to 3')**

Aldh3a1-CRISPR#1.7adjusted-for:  
Aldh3a1-CRISPR#1.10-rev:  
Aldh3a1-rg-1.3adjusted-for:  
Aldh3a1-rg-1.6-rev

ACATGGACTGAACAGTGACCTTGG  
CTCACGCTCTGCCACCTTGAT  
CTCTTTGTGAAATCCTAAACCCT  
TGTCTGCATGGCGTTCAGTGA

<b><u>qPCR primer name</u></b>	<b><u>Primer sequence</u></b>
β-actin-qPCR-for	ACGGTCAGGTCATCACCATC
β-actin-qPCR-rev	TGGATACCGCAAGATTCCAT
b2m-qPCR-for	ACTGCTGAAGAACGGACAGG



b2m-qPCR-rev	GCAACGCTCTTTGTGAGGTG
aldh1a2-qPCR-for	AACCACTGAACACGGACCTC
aldh1a2-qPCR-rev	ATGAGCTCCAGCACACGTC
aldh1a3-qPCR-for	CGTGTTTGCAGACTCAGACC
aldh1a3-qPCR-rev	TGAAGAAAGCCCCCTTCTG
aldh1l1-qPCR-for	GCTGCCCAGACACAGAGG
aldh1l1-qPCR-rev	AACCCTCCCTTCTTATCACCA
aldh1l2-qPCR-for	AGCCGCTTCAATGGATGTAG
aldh1l2-qPCR-rev	GAACACCAGCGCATTCTG
aldh2.1-qPCR-for	CGCACTGTATATCGCCAGTTTA
aldh2.1-qPCR-rev	GGACCAAACCCTGGGATAAT
aldh2.2-qPCR-for	TGCAGTCTCCTTCAGTGTGG
aldh2.2-qPCR-rev	TGCCCAGCCAGCATAATAC
aldh3a1-qPCR-for	CACTGTTGATACTTTACCTTTTGGAG
aldh3a1-qPCR-rev	CAAACGTGTGTTTCCCATGA
aldh3a2a-qPCR-for	TGATGAATCTGAGTGTTACATTGC
aldh3a2a-qPCR-rev	TGGCCCAAAGATCTCTTCC
aldh3a2b-qPCR-for	CACTTCTCTGTCAGCTCTCTGC
aldh3a2b-qPCR-rev	GATAGCGGCCCATACCACT
aldh3b1-qPCR-for	CATGACTCTTCCTGGTTTACCC
aldh3b1-qPCR-rev	TGATAGTTGCCCATCCCACT
aldh4a1-qPCR-for	TGGACCAAAGACATCCGATT
aldh4a1-qPCR-rev	AGCAGAACTTTGCAACTTGGT
aldh5a1-qPCR-for	GGGCCTCTTATCAACTCACG
aldh5a1-qPCR-rev	TCCATGATCCACAGCGTCT

aldh6a1-qPCR-for	GTCTACGTGTCAATGCAGGTG
aldh6a1-qPCR-rev	TCTTTGGCCTGAGGTGAGAT
aldh7a1-qPCR-for	AACCGCAGCACCGAATATGT
aldh7a1-qPCR-rev	TCTGCTATGGTTGCCTGACG
aldh8a1-qPCR-for	CTCCAGCTTCTCCAATCAGG
aldh8a1-qPCR-rev	GTAAACGCTCCGCTCCAC
aldh9a1a.1-qPCR-for	GCTCTGTTTCGAAATCTGTGTTCC
aldh9a1a.1-qPCR-rev	CGACCAGTTGCTGGCTCGTA
aldh9a1a.2-qPCR-for	TCCCATGGTGGCTAAAGTGT
aldh9a1a.2-qPCR-rev	TAGCTGCCATTTCCAAAACC
aldh9a1b-qPCR-for	GGAGCAAGCCAAGAACGA
aldh9a1b-qPCR-rev	GGATCTGCAGGGCTGAAA
aldh16a1-qPCR-for	CCACAGGGTGTTGTGACGGT
aldh16a1-qPCR-rev	AGGAGGCCAGGAAGAGCAGT
aldh18a1-qPCR-for	GCACAGGAAGCCCTGTCTAT
aldh18a1-qPCR-rev	CTCTTCACGAGTGCTCACCA
glo1-qPCR-for	AGCAGACAATGCTGCGGGTG
glo1-qPCR-rev	CTACGGGAGAACGTCCAGGC
ins-qPCR-for	GGTCGTGTCCAGTGTAAGCA
ins-qPCR-rev	GGAAGGAAACCCAGAAGGGG
insb-qPCR-for	CCTGGAGACCTTGCTGGCTTTG
insb-qPCR-rev	CCAGGTGGTAGATGGTGCAGG
isl1-qPCR-for	AGGGTATGGCAGCCGAGGTC
isl1-qPCR-rev	GCTTGCATGCTTAGTACTTGGGC
isl2a-qPCR-for	CATCCCAGAACCTGTGCCAGT

isl2a-qPCR-rev	ACTCGTATGACCCGTGGGCT
isl2b-qPCR-for	GCTGGGAGCGGGATAACAAGG
isl2b-qPCR-rev	TCCGGACTTCTTTTTGGAATGATCC
pdx1-qPCR-for	ACACGCACGCATGGAAAGGACA
pdx1-qPCR-rev	GCGGGCGCGAGATGTATTTGTT

### 2.1.9 Morpholinos

All morpholinos were purchased from GENE TOOLS, LLC.

SB- <i>aldh3a1</i> -MO#1 (targets intron3 – exon4 junction)	5'-GCCGCATTTCTAATCAACAAGAGG-3'
SB- <i>aldh3a1</i> -MO#2 (targets exon4 – intron4 junction)	5'-AACAAATCTATGCACCTTATCCAGA-3'
SB- <i>pdx1</i> -Mo (targets translation start site)	5'-GATAGTAATGCTCTTCCCGATTCAT-3'
Control-MO	5'-CCTCTTACCTCAGTTACAATTTATA-3'

#### **Genotyping primer name**

#### **Primer sequence (5' to 3')**

Aldh3a1-mo-1.5-for  
Aldh3a1-mo-1.4-rev

AGGTGGCAGAGCGTGAGATG  
GAACCCCTCCTGTCACCACC

### 2.1.10 Bacteria strain

*E. coli* stbl3 competent cells

invitrogen by Thermo Fisher Scientific

### 2.1.11 Zebrafish transgenic lines

Three transgenic zebrafish lines were used: *Tg(fli1:EGFP)*<sup>93</sup>, *Tg(hb9:GFP)* (also called as *Tg(mnx1:GFP)*)<sup>94</sup> and *Tg(ins:nfsB-mCherry)*<sup>50</sup> for all the study of zebrafish (*Danio rerio*) experiments.

## 2.2 Methods

### 2.2.1 Animal studies

#### 2.2.1.1 Ethics

All experimental procedures on animals were approved by the local government authority, Regierungspräsidium Karlsruhe and by Medical Faculty Mannheim (license no: G-98/15, G-160/14 and I-19/02) and carried out in accordance with the approved guidelines.

#### 2.2.1.2 Zebrafish maintenance

Zebrafish lines were raised and staged as described<sup>95</sup> under standard husbandry environment. Embryos/larvae were kept in E3 media at 28.5 °C with/without PTU (2.5 ml in 25 ml) to suppress pigmentation. Adult zebrafish were kept under 13 h light/11 h dark cycle and fed with living shrimps in the morning and fish flake food in the afternoon.

#### 2.2.1.3 Morpholino and CRISPR/Cas9-mRNA injection

Morpholino stock (8 or 16 µg/µl) were incubated at 65 °C for 5 minutes and diluted to 4 or 6 µg/µl with 0.1 M KCl for using. CRISPRguide-RNA and Cas9 mRNA were each diluted to 200 ng/µl in 0.1 M KCl and mixed. Freshly laid zebrafish eggs were collected and arranged in a 1% agarose ramp with E3 media. One nanoliter of morpholino or CRISPRguideRNA-Cas9mRNA-mix was injected into the yolk sack or the cell of one-cell staged embryos, respectively. 3-4 h later, the eggs were sorted and undamaged fertilized eggs were kept in the Petri dish.

#### 2.2.1.4 Incubation of zebrafish embryos/larvae

Fertilized zebrafish embryos were transferred into 6-well plate, around 30 embryos per well with 5 ml eggwater containing 0,003% PTU and 5 µM or 10 µM 4-HNE starting at 3-4 hours post fertilization(hpf). Media were changed daily. At 24 hpf the chorion of zebrafish embryos was removed using sharp forceps.

#### 2.2.1.5 Microscopy and analysis of pancreatic and vascular alternations in larvae.

*Tg(hb9:GFP)* embryos and *Tg(fli1:EGFP)* larvae were anesthetized with 0.003% tricaine in egg water and *Tg(hb9:GFP)* were embedded in 1% low-melting-point agarose dissolved in egg water for visualisation on an inverted microscope (Leica DMI

6000 B) with a camera (Leica DFC420 C) and the Leica LAS application suite 3.8 software. The endocrine islet was imaged at 10x and quantified using ImageJ.

For in vivo analysis of pancreatic structure, *Tg(hb9:GFP)* and *Tg(ins:nfsB-mCherry)* larvae were anesthetized in 0.0003% tricaine at 72 hpf. Images were taken with an inverted microscope (Leica DMI 6000 B) with a camera (Leica DFC420 C) and the Leica LAS application suite 3.8 and 4.13. The endocrine pancreatic area and  $\beta$  cell mass were imaged at 20x and 8x, respectively. Quantification were done by using ImageJ.

For in vivo imaging of the zebrafish trunk vasculature, *Tg(fli1:EGFP)* larvae were anesthetized in 0.0003% tricaine at 96 hpf, lying on the side. Images were taken via a DM6000 B microscope with Leica TCS SP5 DS scanner with 600 Hz, 1024x512 pixels and 1  $\mu$ m thick z-stacks. For quantification of altered trunk vessels, the first 5 intersegment vessel (ISV) and dorsal longitudinal anastomotic vessel (DLAV) pairs of each zebrafish larvae were skipped and in the following 17 pairs alterations were counted. The development of new blood vessels referred to 'hyper branches', and altered intersegment vessels that either miss connections to others or show slight malformations(thin, thick or wrong direction) were grouped as 'abnormal ISVs' and counted.

For in vivo imaging of the zebrafish retinal hyaloid vasculature, *Tg(fli1:EGFP)* larvae were anesthetized in 0.0003% tricaine at 120 hpf, and fixed in 4% PFA/PBS overnight at 4°C afterwards. Fixed larvae were washed three times for 20 minutes in double distilled water (ddH<sub>2</sub>O) and incubated for 90 min at 37°C in 0.5% Trypsin/EDTA solution (25200-056, Gibco) buffered with 0.1 M TRIS (Nr. 4855.3, Roth) dilution and adjusted to pH 7.8 with 1 M HCl solution. Larval hyaloid vasculature was dissected under a stereoscope and displayed in PBS for visualisation according to Jung's protocol<sup>96</sup>. Confocal images for phenotype evaluation were acquired using a confocal microscope (DM6000 B) with a scanner (Leica TCS SP5 DS) utilising a 20x0.7 objective, 1024 × 256 pixels, 0.5  $\mu$ m Z-steps. Vascular diameters were measured at two different positions by ImageJ and new blood vessels by neoangiogenesis were counted and addressed as "sprouts" within the circumference of the hyaloid per sample.

#### 2.2.1.6 Overfeeding of adult zebrafish

Adult zebrafish were set in groups based on genotype and feeding method. And the feeding protocol was adapted from Oka<sup>97</sup>. For normal feeding: each fish received a

normal amount of artemia (twice per day and 5 mg dry weight artemia in total). For overfeeding: each fish was overfed by receiving a exceed amount of artemia (three times per day and 60 mg dry weight artemia in total). Animals were sacrificed for experiments after eight weeks feeding.

#### 2.2.1.7 Dissection of adult zebrafish

Adult zebrafish were transferred into single boxes and fasted overnight. 16 hours later, fish were with 0.5 g flake food for 1 hours followed by 1 hours postprandial experiments. Afterwards, fish were euthanized with 0.025% tricaine until the operculum movement stopped entirely. Then blood was collected from the caudal vein and blood glucose was measured by a glucometer. Next, fish were sacrificed by beheaded treatment and transferred into operation stage covered with ice-cold PBS. Livers were isolated, weighed, snap frozen in liquid nitrogen and stored at -80 °C for metabolomics analysis. The whole fish head was transferred into 4% PFA/PBS for 24 h at 4 °C for further retinal analysis.

#### 2.2.1.8 Microdissection and visualisation of retinal vasculature

Retina dissection was prepared according to Wigganhauser's protocol<sup>98</sup>. In brief, PFA-fixed heads from adult zebrafish were transferred into PBS and eyes were removed from the head. Retina was isolated from eye and washed twice with 1xPBS for 5 min. Washed retina was mounted in mounting media and covered with a cover slide. Images were made by using DM6000 B confocal microscope with Leica TCS SP5 DS scanner. Parameter: 600 Hz, 1024x1024 pixels and 1.5 µm thick of z-stacks were. Quantification of branch points and sprouts was performed by using GIMP and ImageJ in squares of 350\*350 µm<sup>2</sup>.

### 2.2.2 Molecular biology

#### 2.2.2.1 Design of CRISPR-oligonucleotides

*Aldh3a1* CRISPR target site was identified and selected using the ZiFiT Targeter 4.1 (<http://zifit.partners.org/ZiFiT/ChoiceMenu.aspx>). Oligonucleotides were synthesized by Sigma-Aldrich.

### 2.2.2.2 Annealing of CRISPR oligonucleotides

Oligonucleotides were dissolved in autoclaved MilliQ water and adjust the concentration to 100  $\mu$ M.

*1x Mix for annealing:*

2  $\mu$ l forward oligonucleotide (*Aldh3a1*-CRISP#1-for)  
2  $\mu$ l reverse oligonucleotide (*Aldh3a1*-CRISP#1-rev)  
2  $\mu$ l NEB Buffer 3  
14  $\mu$ l autoclaved MilliQ water

*Annealing:*

95 °C 5 min  
0.1 °C/sec cooling down  
50 °C 10 min  
1 °C/sec cooling down  
4 °C ( $\infty$ )

### 2.2.2.3 Restriction and ligation of gRNA-plasmids

*1x Mix for annealing:*

1  $\mu$ l annealed oligonucleotide solution (from last section)  
400 ng pT7-gRNA (adjust concentration)  
1  $\mu$ l NEB Buffer 3  
1  $\mu$ l T4 DNA Ligase Buffer  
0.5  $\mu$ l *BsmBI*  
0.3  $\mu$ l *BglII*  
0.3  $\mu$ l *SaII*  
0.5  $\mu$ l T4 Ligase  
ad 10  $\mu$ l sterile MilliQ water

*Restriction:*

37 °C for 60 min and 16 °C for 45 min, three cycles  
37 °C for 30 min  
55 °C for 30 min  
80 °C for 15 min  
4 °C, ( $\infty$ )

Complete ligation mix can be used for the following transformation.

### 2.2.2.4 Transformation of *E. coli*

Competent *E. coli* Stbl3 stock was thawed on ice. 50  $\mu$ l of *E. coli* were added to the ligation mixture (see in last section) and slightly stirred. The mixture was then chilled on ice for 20 min. Afterwards the tube was put in a water bath at 42 °C for exactly 90

sec. Then immediately put it back on ice for at least 90 sec. One ml LB medium was added and the tube was incubated in a bacterial shaker for 45 min (37 °C and 220 rpm). Subsequently, the tube was centrifuged for 5 min (4 °C and 6000 rpm). Discarded 900 µl supernatant and kept the rest to resolve the pellet carefully by avoiding air bubbles. Under hygienic conditions (the flame of a gas burner) the remaining mixture was pipetted on a LB-Amp plate and plated uniformly with a freshly flamed glass pipette. The plate was put overnight in an incubator at 37 °C.

#### 2.2.2.5 Plasmid isolation and sequencing

Single colony was picked from cultured LB-agar plates and inoculated in a 3 ml culture of LB medium with ampicillin. Incubated the whole culture overnight at 37 °C and 220 rpm. Then the Illustra Plasmid Prep Mini Spin Kit was used for plasmids isolation according to the manufacturer's protocol.

For plasmid midi preparations, single colony was picked and inoculated in a 3 ml culture of LB medium with ampicillin. Incubated the whole culture at 37 °C and 220 rpm for 7 h. Plasmid Midi Kit (Qiagen) was used for plasmids isolation according to the manufacturer's protocol.

Purified plasmid was diluted to the following concentration: 75 ng in a volume of 15 µl. Sanger sequencing was performed by Eurofins Genomics.

#### 2.2.2.6 CRISPR-guideRNA and Cas9-mRNA in vitro transcription

SmaI and XbaI cutting enzymes were used for linearization of pT7-gRNA and pT3Ts-nCas9mRNA, respectively. Then linearized plasmids were purified with the PCR purification kit (Qiagen). In vitro RNA transcription was performed using T7 MEGAshortscript kit (Invitrogen) for guideRNAs and mMESSAGING MACHINE Kit (Invitrogen) for Cas9-mRNA. Purification of RNA was done via the miRNeasy Mini (Qiagen) or RNeasy Mini (Qiagen) kit. RNA concentration was determined and RNA samples were made for aliquots and stored at -80 °C, until used for injection.

#### 2.2.2.7 Isolation of genomic DNA

Whole zebrafish larvae or cut fins of adult zebrafish were transferred into 0.2 ml PCR tubes and 20 µl lysis buffer was added. After incubation at 98 °C for 10 min, 10 µl proteinase K was added following incubation at 55 °C for at least 4h. Then flicked the tubes and incubated at 55 °C for another hour. Heated up to 98 °C for 10 min and genomic DNA was stored at -20 °C.



#### 2.2.2.8 Polymerase chain reaction (PCR) and PCR purification

Polymerase chain reaction (PCR) was performed by using 12.5 µl GreenTaq-mix, 2 µl forward primer, 2 µl reverse primer, 6.5 µl sterile MilliQ water and 2 µl DNA template.

The following program was used:

Beginning denaturation 95 °C, 3 min

Denaturation 95 °C, 30 s

Annealing Specific temperature according to the primer, 30 s

Elongation 72 °C, specific elongation time according to the PCR product size

From denaturation to elongation, 34-cycle repetition were performed.

Final elongation 72 °C, 10 min

For genotyping, the QIAquick PCR Purification Kit was used and genotyping PCRs were purified according to the manufacturer's protocol.

#### 2.2.2.9 DNA gel electrophoresis

An agarose gel (1-3% agarose in TAE buffer) was performed for the DNA fragments separation. Using peqlab electrophoresis chambers, the gel was run at 120 V (100 ml gel) in TAE up to 2h.

#### 2.2.2.10 RNA isolation from larvae and adult zebrafish organs.

Larvae from different developmental time point were anesthetized with 0.003% tricaine and the yolk sac was removed by pipetting embryos up and down and centrifuging for 5 min at 14000 rpm. The supernatant was discarded and the sediment was used for the following experiment. Adult zebrafish organs were collected during fish dissection and homogenised samples by tissuelyser were used for the following experiment.

Lysis and purification of the larvae/adult zebrafish organs were performed with the RNeasy Mini Kit (Qiagen) according to the manufacturer's protocol chapter "Purification of Total RNA from Animal Tissue". RNA concentration was measured with a photometer and checked on an 1% agarose gel for integrity. Then samples were made for aliquots and stored at -80 °C until use.

#### 2.2.2.11 cDNA synthesis from RNA (RT-PCR)

The Maxima First Strand cDNA Synthesis Kit was used for reverse transcription PCR (RT-PCR) for generation of cDNA according to the manufacturer's protocol. One  $\mu\text{g}$  RNA were utilised for template. The cDNA was made for aliquots and stored at  $-20\text{ }^{\circ}\text{C}$  until use.

#### 2.2.2.12 Real time quantitative PCR (RT-qPCR)

Primer (see in 2.1.8) were designed with the Primer-BLAST tool from NCBI using the transcript. All samples were used with Power SYBR<sup>™</sup> Green PCR Master Mix Kit in 96-well reaction plates. The qPCR reaction was performed with QuantStudio 3 Real-Time-PCR-System.

A Primer-Mix was prepared for each gene: 2  $\mu\text{l}$  of both forward and reverse primers Stock (100  $\mu\text{M}$ ) were mixed with 96  $\mu\text{l}$  autoclaved MilliQ water.

<i>Each well:</i>	1 $\mu\text{l}$	Primer Mix
	5 $\mu\text{l}$	Power SYBR <sup>™</sup> Green PCR Master Mix
	4 $\mu\text{l}$	cDNA-autoclaved MilliQ water-Mix (containing 20 ng cDNA)
	Total	10 $\mu\text{l}$

#### 2.2.2.13 RNA-Seq Analysis.

RNA were isolated from *aldh3a1*<sup>+/+</sup> and *aldh3a1*<sup>-/-</sup> larvae at 48hpf. Library construction, and sequencing were performed with BGISEQ-500 (Beijing Genomic Institution, www.bgi.com, BGI). Gene expression analysis were conducted by the Core-Lab for microarray analysis, Centre for medical research (ZMF). In brief, main procedure was done with R and bioconductor using the NGS analysis plackage systempipeR<sup>99</sup>. Quality control of raw sequencing reads was performed using FastQC (Babraham Bioinformatics). Low-quality reads were removed using trim\_galore (version 0.6.4). The resulting reads were aligned to zebrafish genome version danRer11 from UCSC and counted using kallisto version 0.46.1<sup>100</sup>. The count data was transformed to log2-counts per million (logCPM) using the voom-function from the limma package<sup>101</sup>. Differential expression analysis was performed using the limma package in R. A false positive rate of  $\alpha = 0.05$  with FDR correction was taken as the level of significance. Volcano plots and heatmaps were created using ggplot2 package (version 2.2.1) and the complexHeatmap (version 2.0.0)<sup>102</sup>.

### 2.2.3 Biochemical analysis

#### 2.2.3.1 Protein sequence alignment

The amino acid sequences of the *aldh3a1* proteins from zebrafish (X1WBM4\_DANRE), human (AL3A1\_HUMAN) and mouse (AL3A1\_MOUSE) were accessed from the UniProt Database (<http://www.uniprot.org/>). For the comparison, the genes were selected and aligned with the UniProt-own alignment tool (<http://www.uniprot.org/align/>).

#### 2.2.3.2 Enzyme activity assay

Enzyme activity assay was performed by the laboratory of Prof. Dr. P. Nawroth (Department of Medicine I and Clinical Chemistry, Heidelberg University, Germany) 96 hpf old larvae were collected for the measurement. ALDH activity was assayed at 25 °C in 75 mM Tris-HCl (pH 9.5) containing 10 mM DL-2-amino-1propanol, 0.5 mM NADP and 2 mM MG/4 mM 4-HNE/ 5Mm Acetaldehyde by measuring the rate of NADP formation at 340 nm<sup>103</sup>. Glo1-activity was determined spectrophotometrically monitoring the change in absorbance at 235 nm caused by the formation of S-D-lactoylglutathione<sup>104</sup>.

#### 2.2.3.3 Determination of methylglyoxal

The determination of MG was performed by stable isotopic dilution analysis via LC-MS/MS<sup>105</sup> by the laboratory of Prof. Dr. P. Nawroth (Department of Medicine I and Clinical Chemistry, Heidelberg University, Germany)

In brief, frozen Zebrafish larvae were treated with precipitation solution (Trichloroacetic acid 20% w/v in 0.9% NaCl), incubated with an internal standard and derivatized with 1,2-Diaminobenzene. Quantification was carried out using a XEVO TQ-S tandem quadrupole mass spectrometer.

#### 2.2.3.4 Metabolomic analysis

Detection was done in cooperation with the Metabolomics Core Technology Platform from the Centre of Organismal Studies Heidelberg by Gernot Poschet and Elena Heidenreich.

Zebrafish larvae at 96 hpf age were anesthetized with 0.003% tricaine. Adult zebrafish organs were collected during fish dissection. The detection was performed either by ultra-performance liquid chromatography with fluorescence detection (UPLC-FLR)<sup>106</sup> or semi-targeted gas chromatography-mass spectrometry (GC/MS)<sup>107</sup> analysis.

#### 2.2.3.5 Whole-body glucose determination in zebrafish larvae.

Zebrafish larvae from different developmental time point were collected and snap frozen. Approximately 20-25 larvae per clutch were homogenized in glucose assay buffer with by the ultrasonic homogenizer sonicator, 90% intensity, and 15seconds for 2 times. Glucose content was determined according to manufacturer's instruction (Glucose Assay Kit, CBA086, Sigma-Aldrich).

#### 2.2.3.6 4-HNE determination in zebrafish larvae

Zebrafish larvae from 96hpf were collected and snap frozen. Approximately 40-50 larvae per clutch were homogenized in PBS with by the ultrasonic homogenizer sonicator, 90% intensity, 15 seconds for 2 times. 4-HNE amount was determined according to manufacturer's instruction (4-Hydroxynonenal ELISA Kit, E4645, Biovision).

#### 2.2.4 Software

Agarose gel images was carried out with IntasGelCaptureEntry (INTAS). For the quantification of trunk vasculature, endocrine pancreatic area and  $\beta$  cell mass, the Leica LAS V3.8 and V4.13 software was used. Analysis of retinal vasculature was carried out by using LAS AF Lite Software from Leica for taking screen shots, Gimp for image cutting and ImageJ for quantification. The "GCMS solution" software (Shimadzu®) was used for data processing of the GC/MS analysis. Statistics were calculated with GraphPad Prism 6.01 and 8.3.0.

#### 2.2.5 Statistical analysis

Results are expressed as mean with standard deviation (mean  $\pm$  SD). Statistical significance between different groups was analysed using Student's *t*-test, Mann-Whitney-U-test, one-way ANOVA (followed either by post hoc Bonferroni's, Sidak's

multiple comparison) in GraphPad Prism 6.01 or 8.3.0. p-values of 0.05 were considered as significant: \* $p < 0.05$ , \*\* $p < 0.01$ , \*\*\* $p < 0.001$ , \*\*\*\* $p < 0.0001$ .

### 3 RESULTS

#### 3.1 Sequence alignment of Aldh3a1 across different species and analysis of the *aldh3a1* mRNA expression in larvae and adult organs of zebrafish.

ALDH3A1 (Aldh3a1) enzyme system exists in human, mouse and zebrafish<sup>108, 109</sup>. At first, the amino acid sequence alignment was blasted among these three species to compare ALDH3A1 (Aldh3a1) proteins among these three species. The alignment showed zebrafish Aldh3a1 shares 61.6% similarity of protein with human ALDH3A1 and 57.6% with mouse; as an enzyme encoding gene, the active site is the same in these three species (Fig.1A).

Then RT-qPCR was performed to investigate the potential expression differences of *aldh3a1* mRNA level in different time points of larvae and adult organs of zebrafish. Results showed an increased trend of *aldh3a1* mRNA as the larva develops by around 3-fold elevation at 96 hpf than 24 hpf. While brain and eye are the most expressed adult organs, which were 11- and 7-fold significant increase compared to heart (reference organ) (Fig.1B).

Altogether, this part identifies *aldh3a1* mRNA exists in zebrafish larvae and different adult organs and the possibility for studying ALDH3A1 (Aldh3a1) enzyme system by using zebrafish model.



**Fig.1** Sequence alignment of Aldh3a1 across different species and the expression of *aldh3a1* mRNA in larvae and adult organs of zebrafish.

(A). Amino acid alignment showed a high similarity between the different species of the active site (red frame) and peptidase dimerization domain (yellow); first line: zebrafish Aldh3a1 dipeptides; second line: human ALDH3A1; third line: mouse Aldh3a1. (B). Heatmap of *aldh3a1* mRNA expression in wildtype zebrafish showed an increased trend from 24hpf to 96hpf in larvae and expressed mostly in brain and eye in adult organs, which is significantly incremental than heart (reference organ). Higher and lower expression is displayed in pink and blue, respectively. Expression of genes was determined by RT-qPCR and normalized to *b2m*. Larvae stage:  $n = 3$  clutches with 30 larvae, adult organs:  $n = 4$  with one organ per sample. For statistical analysis one-way ANOVA followed by Sidak's multiple comparison test was applied,  $*p < 0.05$ ,  $**p < 0.01$ . RT-qPCR, real-time quantitative polymerase chain reaction; hpf, hours post fertilization; *b2m*,  $\beta 2$  microglobulin.

### 3.2 Generation and validation of Aldh3a1 knock out in zebrafish.

Since *aldh3a1* knockout zebrafish model do not exist thus far and in order to explore the function of Aldh3a1 in zebrafish, *aldh3a1*<sup>-/-</sup> zebrafish were generated by CRISPR/CAS9 technology<sup>110</sup>. I designed a CRISPR-guideRNA (gRNA) targeting exon

2 of *aldh3a1* and then identified 11 bases insertion in knockout animal models (Fig.2A), which leads to the formation of a Stop-codon afterwards (Fig.2B).

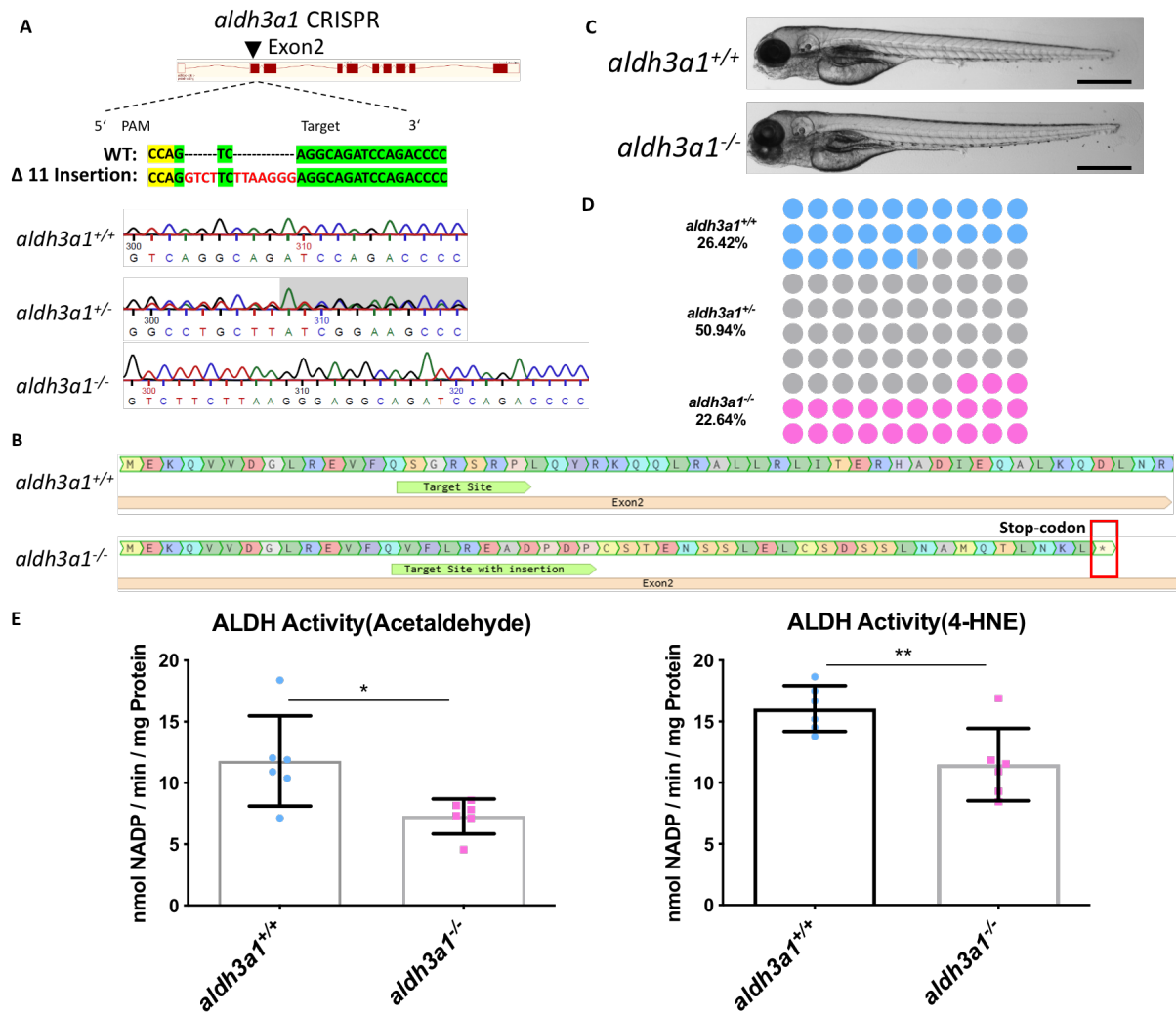


**Fig.2 Generation of Aldh3a1 knockout zebrafish by using CRISPR-Cas9 technology.**

(A). Aldh3a1-CRISPR-target site was designed in exon 2 of *aldh3a1* and CRISPR/Cas9-induced insertions of 11 nucleotides was selected for further *aldh3a1* mutant line generation and maintenance. Genotype was analyzed using sequencing chromatograms of PCR-amplified *aldh3a1* region, containing the *aldh3a1* target site. Chromatogram shows *aldh3a1* wild type, heterozygous, and homozygous sequencing results. (B). Amino acid sequence shows a stop-codon in exon2 of *aldh3a1*<sup>-/-</sup>. (C). Microscopic images showed normal gross morphology of *aldh3a1*<sup>-/-</sup> larvae in comparison with *aldh3a1*<sup>+/+</sup> larvae at 96 hpf. Black scale bar: 500  $\mu$ m. (D). Adult fish number among different genotypes was in line with the Mendelian Inheritance in the first generation of F2: *aldh3a1*<sup>+/+</sup> =14, *aldh3a1*<sup>+/-</sup> =27, *aldh3a1*<sup>-/-</sup> =12. (E). *Aldh3a1*<sup>-/-</sup> zebrafish showed decreased enzyme activity (acetaldehyde and 4-HNE as substrate) measured by spectrophotometric analysis in zebrafish lysates at 96 hpf; n = 6 clutches with 46 to 50 larvae. Mean  $\pm$  SD, for statistical analysis Student's t-test was applied, \*p < 0.05, \*\*p < 0.01. PAM, protospacer-adjacent motif; WT, wild type. Enzyme-activity assays were performed by Jakob Morgenstern/Tomas Fleming.

The gross morphology showed no difference between homozygous and wild type zebrafish larvae at 96hpf (Fig.2C). Meanwhile the fish number was counted by genotype during the first generation of F2, the number of wild type, heterogynous and homogenous adult fish at four months old were 14, 27 and 12 respectively, which was



in line with *the Mendelian Inheritance*<sup>111</sup>(Fig.2D) indicating no survival adversity in *aldh3a1*<sup>-/-</sup> mutants. To evaluate whether the 11 bases insertion in *aldh3a1* mutants causes the non-functional Aldh3a1 protein after translation, ALDH activity was measured by using its different substrates. *Aldh3a1* mutants showed around 30% significant decrease of ALDH activity by both acetaldehyde and 4-HNE substrates (Fig.2E). All the above have proved the successful generation of *aldh3a1* knockout mutants.

### 3.3 Vasculature alternations in *aldh3a1* mutants are enhanced by *pdx1* morpholino injection.

To study vascular developmental effects potentially caused by Aldh3a1 knock out, I investigated the trunk vasculature development in *aldh3a1* mutants at first. *Tg(fli1:EGFP)* zebrafish reporter line, in which endothelial cells express enhanced green fluorescence protein(EGFP) and enables to analyse the vasculature under microscope<sup>93</sup>, was used to perform this experiment. Results showed no difference in hyper branches but a slightly increase in ISVs (including missing, wrong direction, thin, thick intersegment vessels) between *aldh3a1*<sup>+/+</sup> and *aldh3a1*<sup>-/-</sup> zebrafish larvae at 96hpf (Fig.3). As Pdx1 is a transcription factor and necessary for pancreatic development including  $\beta$  cell maturation and duodenal differentiation<sup>112</sup>, transient knock down can cause hyperglycaemia and mimic diabetic condition. According to this strategy, *pdx1* morpholino was used to inject the embryos at one-cell stage to see if it could enhance the phenotype. *Aldh3a1*<sup>-/-</sup> larvae showed enhanced vasculature alternations in both increased hyper branches and abnormal ISV numbers compared to *aldh3a1*<sup>+/+</sup> larvae at 96hpf after *pdx1* morpholino injection (Fig.4).

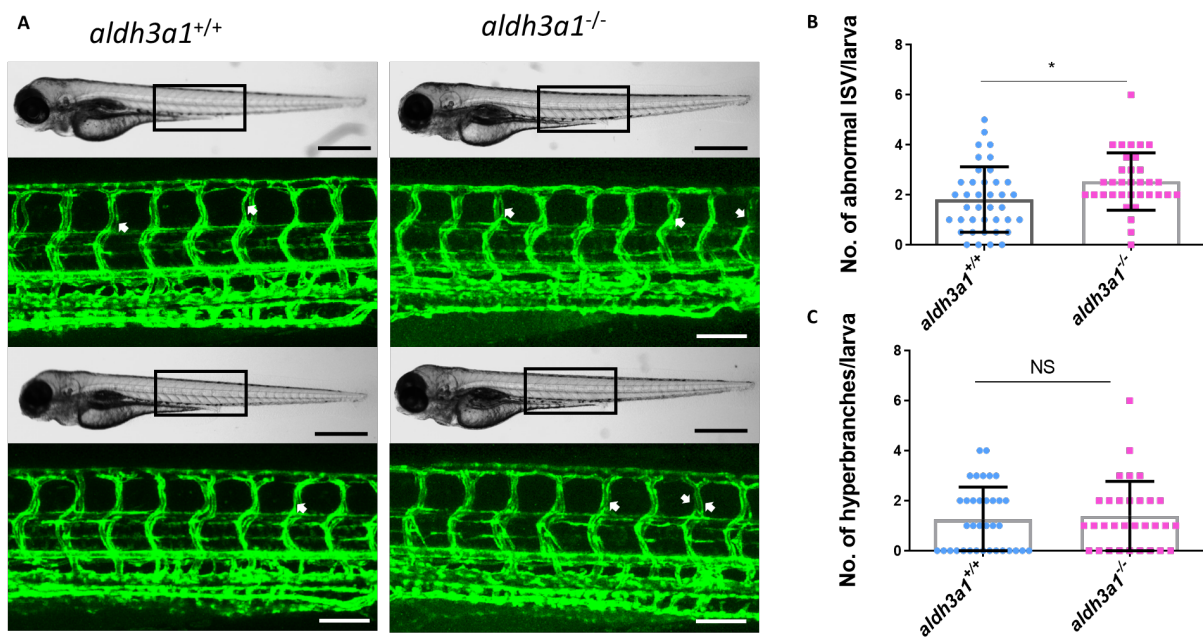


**Fig.3 Trunk vasculature alterations between *aldh3a1*<sup>-/-</sup> and *aldh3a1*<sup>+/+</sup> *Tg(fli1:EGFP)* zebrafish larvae.**

Loss of Aldh3a1 enzyme activity partially altered vasculature morphology, leads to increased formation of abnormal ISV in trunk vasculature of *Tg(fli1:EGFP)* zebrafish larvae at 96hpf. (A). Light microscopic images showed the gross morphology of zebrafish larvae and black boxes indicate region seen in the confocal images. White arrows indicate the abnormal ISV, including missing, wrong direction, thin, thick intersegment vessels. White scale bar = 100  $\mu$ m, black scale bar = 500  $\mu$ m. (B-C). Quantification of abnormal ISV and hyperbranches formation; n = 39 larvae (*aldh3a1*<sup>+/+</sup>) and n = 34 larvae (*aldh3a1*<sup>-/-</sup>). Mean  $\pm$  SD, for statistical analysis Student's t-test was applied \*p<0.05. ISV, intersegmental vessels. NS, not significant.

Since retina conducts one of the most metabolically active tissues in the body<sup>113</sup>, zebrafish retinal hyaloid vasculature is considered as an appropriate model to analyse genetics and disease<sup>114</sup>. To study the short-term influence of *aldh3a1* knock out and hyperglycaemia on the retinal microvasculature, I analysed the retinal hyaloid network in *Tg(fli1:EGFP)* zebrafish larvae at 120 hpf regarding the genotype and diabetic condition. *Aldh3a1*<sup>-/-</sup> larvae showed widen inner optic circle (IOC) branch diameters but no change in sprouts. After the *pdx1* morpholino injection, IOC branch diameters and the number of sprouts increased aggregately in *aldh3a1*<sup>-/-</sup> compared to *aldh3a1*<sup>+/+</sup> larvae (Fig.5).

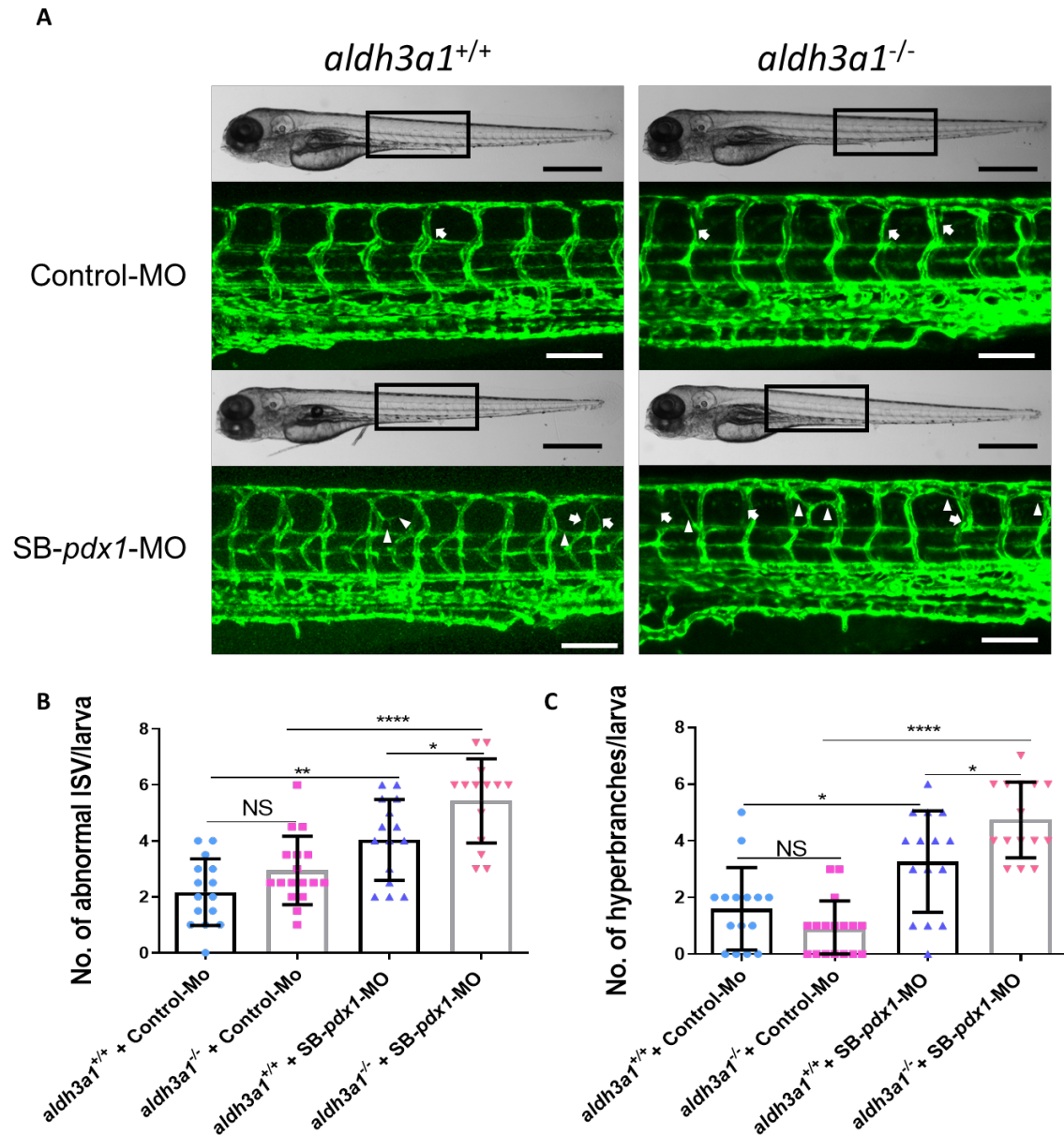
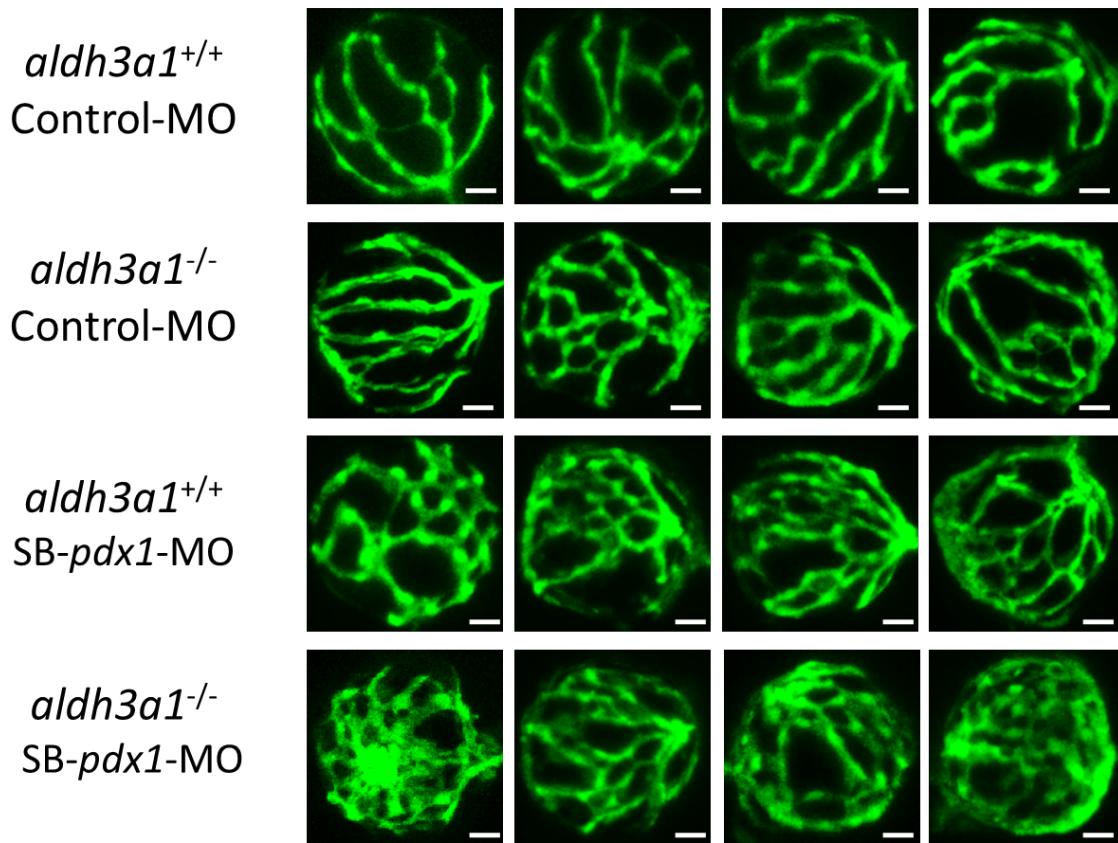


**Fig.4 Trunk vasculature alterations are enhanced by endogenous *pdx1* expression silencing in *aldh3a1*<sup>-/-</sup> *Tg(fli1:EGFP)* zebrafish larvae.**

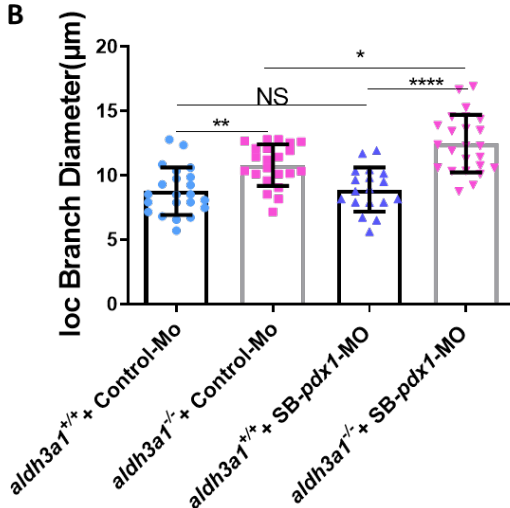
Endogenous *pdx1* expression silencing by *pdx1* morpholino injection leads to enhanced formation of abnormal ISV and hyperbranches in trunk vasculature of *aldh3a1*<sup>-/-</sup> *Tg(fli1:EGFP)* zebrafish larvae at 96hpf. (A). Light microscopic images showed the gross morphology of zebrafish larvae and black boxes indicate region seen in the confocal images. White arrows indicate the abnormal ISV and white deltas indicate the hyperbranches. White scale bar = 100  $\mu$ m, black scale bar = 500  $\mu$ m. (B-C). Quantification of abnormal ISV and hyper branches formation; n = 15-17 per group. 6 ng of morpholinos: Control-MO and SB-*pdx1*-MO were injected into the one-cell stage of zebrafish embryos respectively. Mean  $\pm$  SD, for statistical analysis one-way ANOVA followed by Sidak's multiple comparison test was applied, \* $p$ <0.05, \*\* $p$ <0.01, \*\*\* $p$ <0.001, \*\*\*\* $p$ <0.0001. ISV, intersegmental vessel; MO, morpholino; NS, not significant.

To sum, these data indicate knock out of *aldh3a1* can lead to trunk and hyaloid vasculature alternations and be enhanced under diabetic condition in zebrafish larvae.

A



B



C

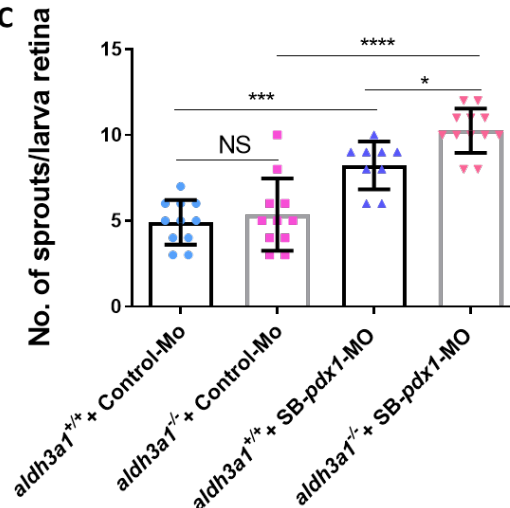


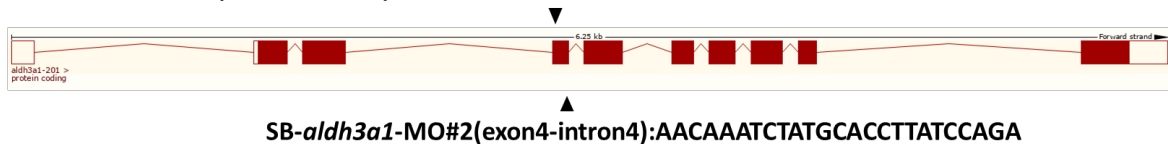
**Fig.5 Retina hyaloid vasculature alterations are enhanced by endogenous *pdx1* expression silencing in *aldh3a1*<sup>-/-</sup> *Tg(fli1:EGFP)* zebrafish larvae.**

Endogenous *pdx1* expression silencing by *pdx1* morpholino injection leads to widen IOC branch diameters and increased sprouts formation in hyaloid vasculature of *aldh3a1*<sup>-/-</sup> *Tg(fli1:EGFP)* zebrafish larvae at 120 hpf. (A). Representative confocal images of hyaloid vasculature after Control-MO or SB-*pdx1*-MO injection. White scale bar = 20 μm. (B-C). Quantification of the IOC branch diameter and sprouts formation, n=8-12 per group. 6 ng of morpholinos: Control-MO and SB-*pdx1*-MO were injected into the one-cell stage of zebrafish embryos respectively. Mean± SD, for statistical analysis one-way ANOVA followed by Sidak's multiple comparison test was applied, \*p<0.05, \*\*p<0.01, \*\*\*p<0.001, \*\*\*\*p<0.0001. MO, morpholino; IOC, inner optic circle. NS, not significant.

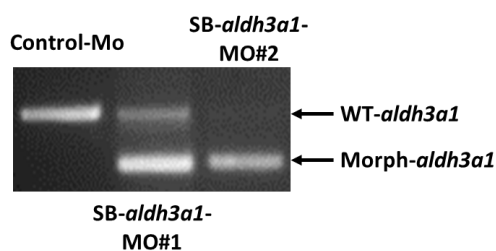
### 3.4 Early pancreas is impaired by *aldh3a1* morpholino injection.

As *aldh3a1* mutants in zebrafish pancreas transgenic reporter line haven't be generated yet, for *Aldh3a1* functional investigation during pancreas development and its interaction with *Pdx1*, an *Aldh3a1* knockdown strategy is essential. Two morpholinos, SB-*aldh3a1*-MO#1 and SB-*aldh3a1*-MO#2, were designed to reduce *aldh3a1* expression in zebrafish transiently by the antisense approach. Two morpholinos target intron3-exon4 and exon4-intron4 junction of *aldh3a1-201* respectively (Fig.6A). Six nanograms of morpholinos were injected into the one-cell stage of zebrafish embryos. The efficiency of morpholino was validated by RT-PCR gel, which showed decreased wild type *aldh3a1* but expression of morphant *aldh3a1* in the gel upon SB-*aldh3a1*-MO#1 and SB-*aldh3a1*-MO#2 injection (Fig.6B). On the other side, microscopic images showed normal gross morphology of SB-*aldh3a1*-MO#1 and SB-*aldh3a1*-MO#2 injected larvae at 48 hpf in comparison with Control-MO injected larvae indicating that the *aldh3a1* morpholinos don't cause other off-target or toxic effects in extra (Fig.6C).

#### A SB-*aldh3a1*-MO#1(intron3-exon4):GCCGCATTCCTAATCAACAAGAGG



#### B



#### C

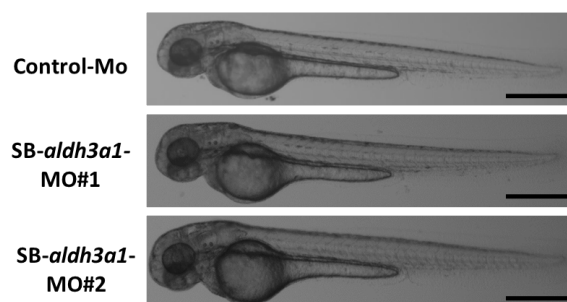


**Fig.6 *Aldh3a1* morpholino design and validation.**

(A). SB-*aldh3a1*-MO#1 and SB-*aldh3a1*-MO#2 target intron3-exon4 and exon4-intron4 junctions of *aldh3a1-201* respectively. (B). Validation of splice-blocking morpholinos: SB-*aldh3a1*-MO#1 and SB-*aldh3a1*-MO#2. RT-PCR of ControlMO, SB-*aldh3a1*-MO#1 and SB-*aldh3a1*-MO#2 injected larvae showed wild type and generation of morphant *aldh3a1* signals at 48 hpf. 6 ng of morpholinos: Control-MO, SB-*aldh3a1*-MO#1 and SB-*aldh3a1*-MO#2 were injected into the one-cell stage of zebrafish embryos respectively. (C) Microscopic images showed normal gross morphology of zebrafish larvae at 48 hpf after morpholino injection. Black scale bar =500  $\mu$ m. WT, wild type; MO, morpholino; Morph: morphant.

Subsequently I wanted to investigate if *Aldh3a1* plays an important role in the development of pancreas. First, the primary pancreas islet size was analysed by using *Tg(hb9:GFP)* transgenic reporter line(also known as *Tg[mnx1:GFP]*), as *hb9* is involved in spinal cord motor neuron cell fate specification and type B pancreatic cell differentiation<sup>115</sup>. The area size of primary endocrine islet showed decreased dimensions with *aldh3a1* morpholino injection in zebrafish larvae at 72hpf (Fig.7). Then  $\beta$  cell mass analyses was carried out by using *Tg(ins:nfsB-mCherry)* transgenic reporter line, which provides not only a suitable model for  $\beta$  cell regeneration, but also an alternative strategy to manipulate cell interactions during early pancreas upgrowth<sup>50</sup>. After the quantification, the early  $\beta$  cell mass size showed significantly decrease with SB-*aldh3a1*-MO#2 injection and a descendant trend with SB-*aldh3a1*-MO#1 injection (Fig.8).

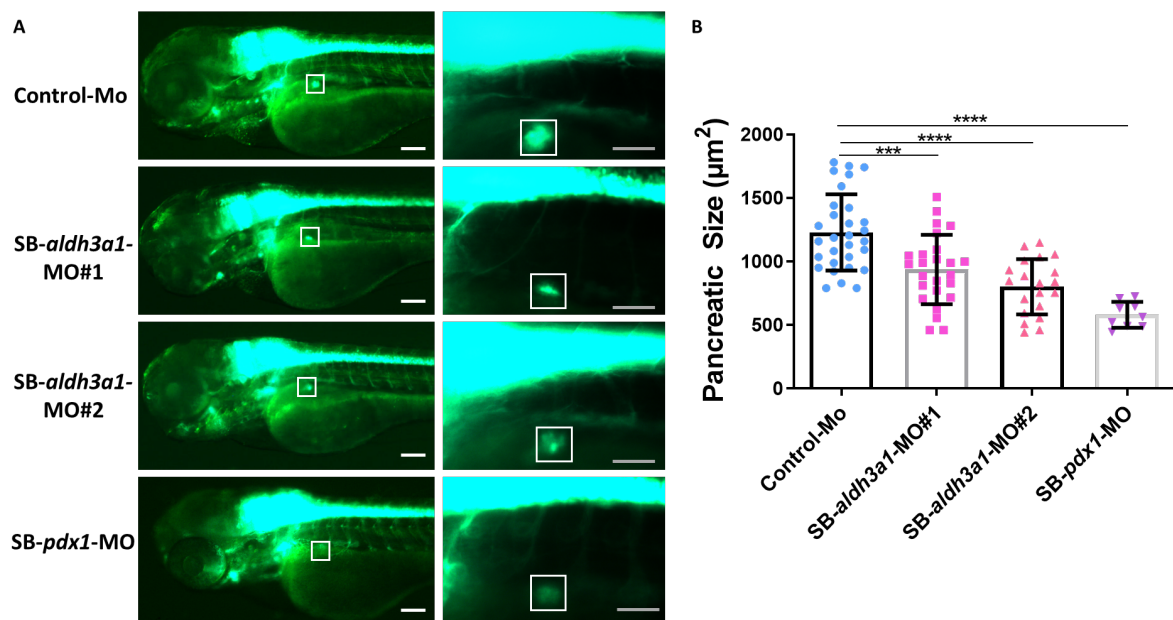


**Fig.7 Area size of the early primary endocrine islet in *Tg(hb9:GFP)* zebrafish larvae shows reduced dimensions by *aldh3a1* morpholino injection.**

*Aldh3a1* morpholino injection induces reduced dimensions of early primary endocrine islet in *Tg(hb9:GFP)* zebrafish larvae at 72hpf. (A). Representative fluorescence microscope pictures of the early developing endocrine pancreas in zebrafish larvae with morpholino injection. White box indicates the developing pancreas. White scale bar = 100  $\mu\text{m}$ , grey scale bar = 50  $\mu\text{m}$ . (B). Quantification of area size of the early primary endocrine islet, n=20-30 per group (SB-*pdx1*-MO injection as positive control, n=9). 6 ng of morpholinos: Control-MO, SB-*aldh3a1*-MO#1, SB-*aldh3a1*-MO#2 and SB-*pdx1*-MO were injected into the one-cell stage of zebrafish embryos respectively. Mean  $\pm$  SD, for statistical analysis one-way ANOVA followed by Sidak's multiple comparison test was applied, \*\*\*p < 0.001, \*\*\*\*p < 0.0001.

Taken together, these results suggest knock down of *Aldh3a1* can impair the primary pancreas development in zebrafish larvae.

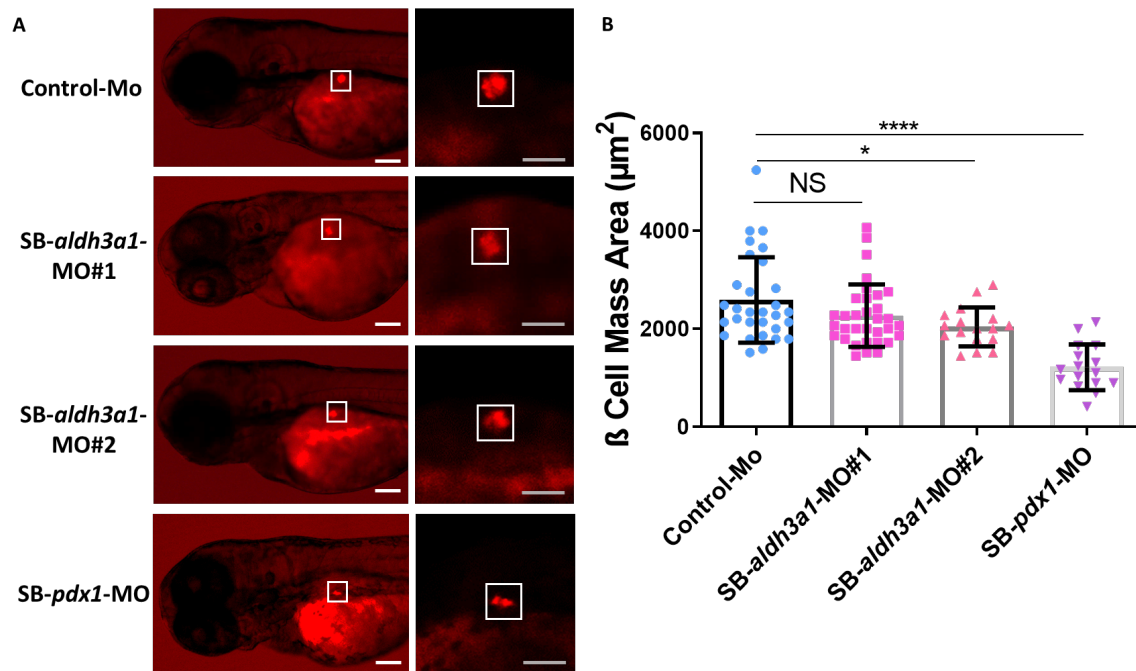


**Fig.8 Early  $\beta$  cell mass in *Tg(ins:nfsB-mCherry)* zebrafish larvae shows reduced trends by *aldh3a1* morpholino injection.**

*Aldh3a1* morpholino injection induces reduced trend of  $\beta$  cell mass in *Tg(ins:nfsB-mCherry)* zebrafish larvae at 72 hpf. (A). Representative fluorescence microscope pictures of the early  $\beta$  cell mass in zebrafish larvae with morpholino injection. White box indicates the  $\beta$  cell mass area. White scale bar = 100  $\mu\text{m}$ , grey scale bar = 50  $\mu\text{m}$ . (B). Quantification of area sizes of the  $\beta$  cell mass area,  $n=16-33$  per group. 6 ng of morpholinos: Control-MO, SB-*aldh3a1*-MO#1, SB-*aldh3a1*-MO#2 and SB-*pdx1*-MO were injected into the one-cell stage of zebrafish embryos respectively. Mean  $\pm$  SD, for statistical analysis one-way ANOVA followed by Sidak's multiple comparison test was applied, \* $p < 0.05$ , \*\*\*\* $p < 0.0001$ .

### 3.5 *Ins* mRNA level is reduced and the whole-body glucose is elevated in both *Aldh3a1* transient knockdown and permanent knockout zebrafish larvae.

Pancreas plays a key role in insulin secretion and glucose homeostasis regulation<sup>116</sup>. In order to clarify the consequence of pancreatic dysplasia caused by *Aldh3a1* knock down while also validate the function role of *Aldh3a1* in diabetes, insulin related gene mRNA expression and the whole-body glucose were determined. I found, *preproinsulin (ins)* and *pdx1* gene mRNA significantly reduced in both *Aldh3a1* knockdown and knockout larvae at 48hpf, while *preproinsulin b (insb)*, another insulin-encoding gene involved in glucose homeostasis regulation and also acting as a pro-growth, survival, and neurotrophic factor during development<sup>117</sup>, is unaltered in *aldh3a1*<sup>-/-</sup> larvae and wild type zebrafish larvae with *aldh3a1* morpholino injection (Fig.9 A-B). Besides, in *aldh3a1*<sup>-/-</sup> larvae, pancreas development related genes, *ISL LIM homeobox 1 (isl1)* and *ISL LIM homeobox 2a (isl2a)* mRNA showed decreased trends while *ISL LIM homeobox 2b (isl2b)* mRNA reduced enormously and

significantly compared to *aldh3a1*<sup>+/+</sup> larvae, which exhibited similar expression level with *aldh3a1*<sup>+/+</sup> larvae after *pdx1* morpholino injection (Fig.9B).

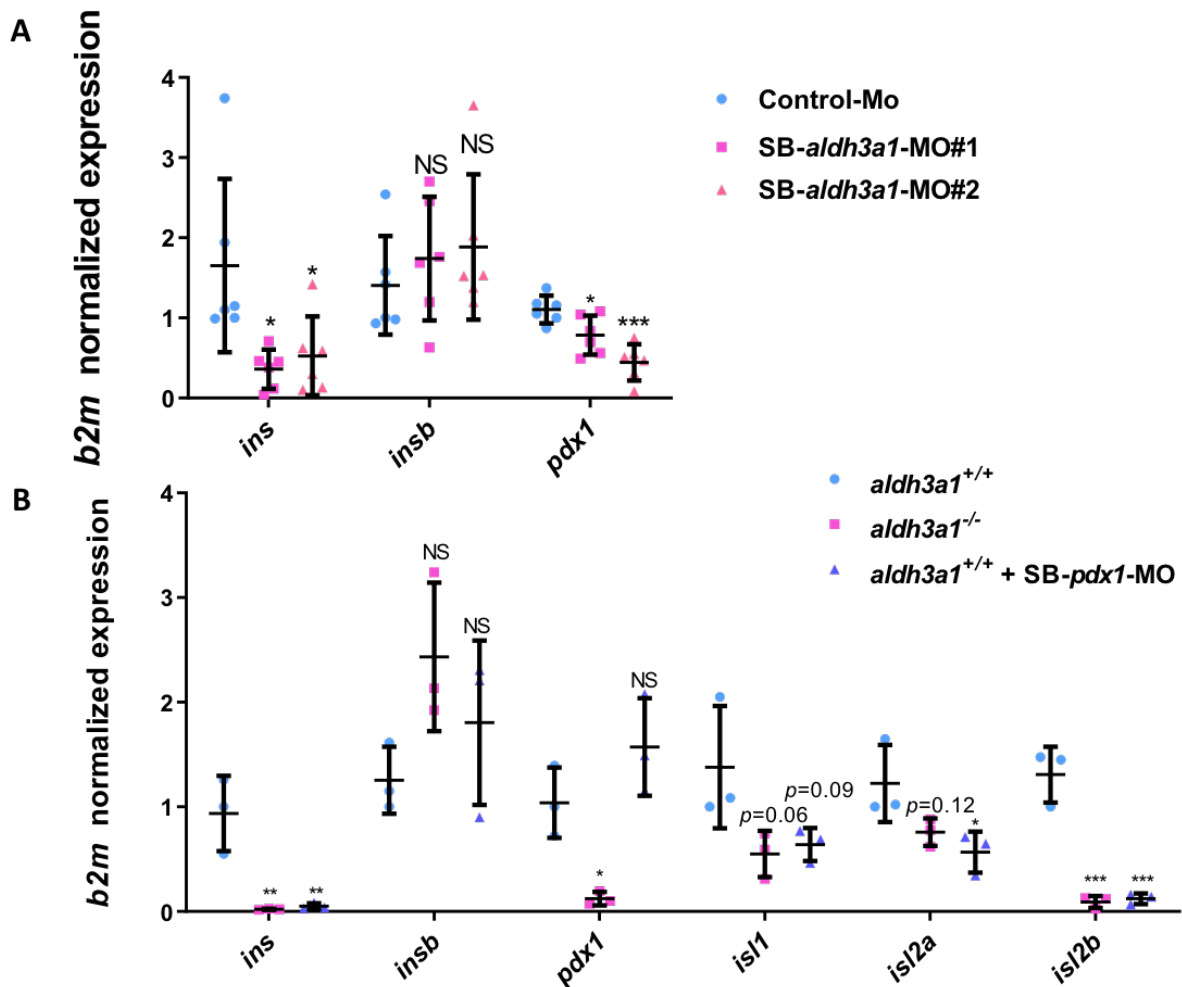


**Fig.9 Both transient knock down and permanent knock out of Aldh3a1 leads to the reduced *pdx1* and *insulin* mRNA level.**

(A). *ins*, *insb* and *pdx1* mRNA expression level in wild type larvae at 48hpf after Control-MO, SB-*aldh3a1*-MO#1 and SB-*aldh3a1*-MO#2 injection. (B). *ins*, *insb*, *pdx1* and pancreas related gene, *isl1*, *isl2a* and *isl2b* mRNA expression level among *aldh3a1*<sup>+/+</sup>, *aldh3a1*<sup>-/-</sup> larvae and SB-*pdx1*-MO injected *aldh3a1*<sup>+/+</sup> larvae at 48hpf. 6 ng of morpholinos: ControlMO, SB-*aldh3a1*-MO#1, SB-*aldh3a1*-MO#2 and SB-*pdx1*-MO were injected into the one-cell stage of zebrafish embryos respectively. Expression of mRNA was analysed by RT-qPCR and expression was normalized to *b2m*. Values for Control-MO injected wild type larvae (A) and *aldh3a1*<sup>+/+</sup> zebrafish larvae (B) were standardized to 1, n = 3-4 clutches with 30 larvae per group. Mean ± SD, for statistical analysis one-way ANOVA followed by Sidak's multiple comparison test was applied, \**p*<0.05, \*\**p*<0.01, \*\*\**p*<0.001. *b2m*, β2 microglobulin; *ins*, preproinsulin; *insb*, preproinsulin b; *isl1*, ISL LIM homeobox 1; *isl2a*, ISL LIM homeobox 2a; *isl2b*, ISL LIM homeobox 2b; NS, not significant.

To further study how gene transcription alters and functions due to Aldh3a1 knock out, all expression patterns were analysed with full genome RNA-Seq between *aldh3a1*<sup>+/+</sup> and *aldh3a1*<sup>-/-</sup> larvae at 48hpf. Principal component analysis (PCA) showed the components of each individual samples<sup>118</sup> and *aldh3a1*<sup>+/+</sup> and *aldh3a1*<sup>-/-</sup> plots are totally separate in PC1 axis (Fig.10A). Volcano plot of statistically significant



differentially expressed genes at P 0.05 identified from the RNA-Seq libraries showed there were around 8 thousand gene down-regulated and 6.5 thousand gene up-regulated in *aldh3a1*<sup>-/-</sup> zebrafish larvae (Fig.10 B). Then, for better understanding how the impaired pancreas reflects in the transcriptome level, gene set enrichment analysis (GSEA), a powerful analytical method for interpreting gene expression data by focusing on gene sets and shared common biological function<sup>119</sup>, was performed. GSEA reveals several biological pathways in common and notably, endocrine pancreas but not exocrine pancreas development pathway was significantly down-regulated in *aldh3a1* mutants (Fig.11).

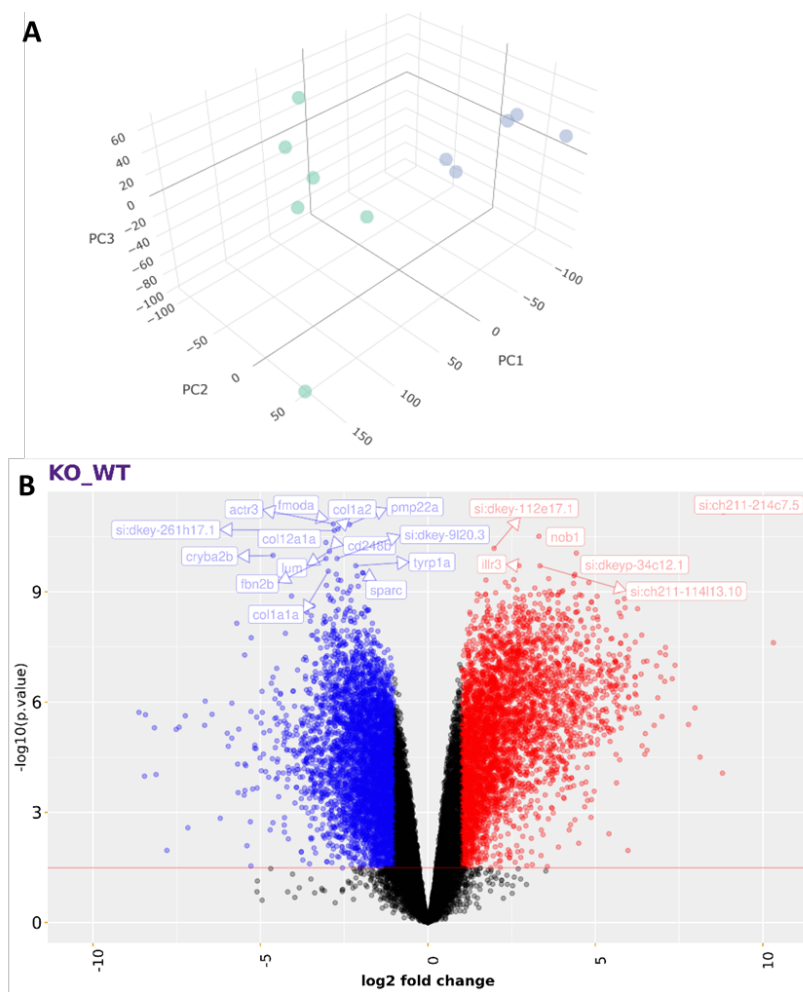
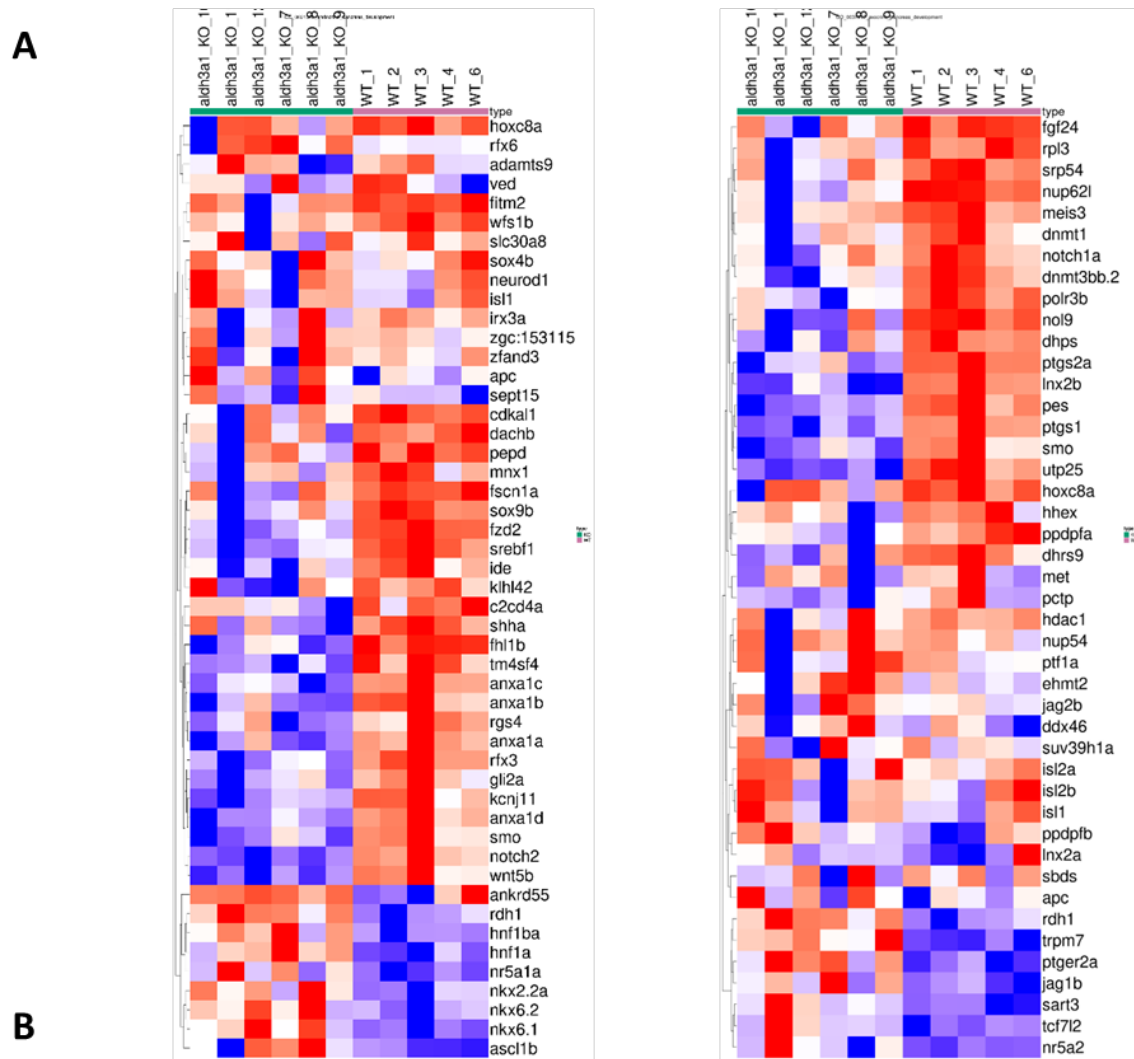


**Fig.10 An overview of RNA Sequence Results.**

(A). Results of the quality control in gene expression analysis between *aldh3a1*<sup>-/-</sup> and *aldh3a1*<sup>+/+</sup> zebrafish larvae at 48hpf. Principal component 1,2 and 3 are on the axis. The plots showed the wild type(n=5) in blue and *aldh3a1* mutants(n=6) in green. (B). Volcano plot showed the down-regulated/up-regulated between *aldh3a1*<sup>-/-</sup> and *aldh3a1*<sup>+/+</sup> zebrafish larvae at 48hpf.

RNA Sequence was analysed by Carsten Sticht.



Pathway	Enrichment Score	NES	p.adjust	Q values
Pancreas development	-0,325	-1,641	0,020	0,011
Endocrine pancreas development	-0,360	-1,576	0,040	0,021
Exocrine pancreas development	-0,326	-1,308	0,189	0,102

**Fig.11 Endocrine pancreas development pathway but not exocrine pancreas development pathway decreased significantly by GSEA analysis.**

(A). Heatmap showed relative mRNA expression in pancreas development between *aldh3a1*<sup>+/+</sup> (n=5) and *aldh3a1*<sup>-/-</sup> (n=6). Higher and lower expression is displayed in red and blue, respectively. (B). Analysis result by GSEA. GSEA, gene set enrichment analysis.

RNA Sequence was analysed by Carsten Sticht.

To evaluate whether the change of *ins* and pancreas dysfunction result in hyperglycaemia, whole-body glucose were measured and *aldh3a1* mutant larvae showed around 40% incremental glucose level at 48hpf (Fig.12A). After *pdx1* morpholino injection, glucose levels were increased in both genotypes and *aldh3a1*<sup>-/-</sup> gained around 30% more glucose than *aldh3a1*<sup>+/+</sup> larvae (Fig.12B). Additionally, *aldh3a1*<sup>-/-</sup> larvae with control morpholino injection showed the same levels of ATP and ADP compared to *aldh3a1*<sup>+/+</sup> larvae with *pdx1* morpholino injection at 96hpf, while achieved significantly lowest ATP and ADP level among all groups with *pdx1* morpholino injection indicating the impaired energy metabolism in *aldh3a1* mutants and may lead to hyperglycaemia directly(Fig.12 C-D).

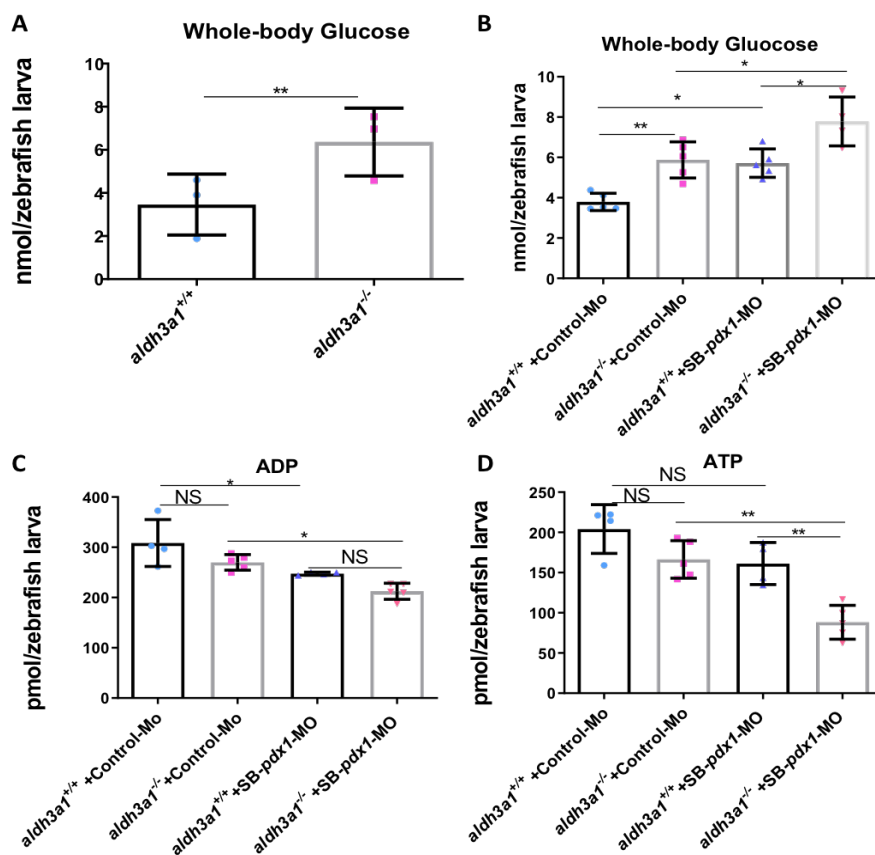


**Fig.12 Whole body glucose is elevated in *aldh3a1*<sup>-/-</sup> zebrafish larvae and enhanced by *pdx1* morpholino injection. *Aldh3a1*<sup>-/-</sup> larvae achieved significantly lowest ATP and ADP level among all groups with *pdx1* morpholino injection.**

(A). Whole body glucose in lysed larvae clutches at 48hpf showed increased glucose levels as an indicator of impaired glucose homeostasis in *aldh3a1*<sup>-/-</sup> larvae. While (B) *Pdx1* morpholino injection enhanced the impaired glucose homeostasis in *aldh3a1*<sup>-/-</sup> larvae at 48 hpf. n = 4-5 clutches with 20-25 larvae per group. (C-D). ADP and ATP showed similar amount levels in Control-MO injected *aldh3a1*<sup>-/-</sup> larvae and SB-*pdx1*-MO injected *aldh3a1*<sup>+/+</sup> larvae, while *aldh3a1*<sup>-/-</sup> larvae achieved significantly lowest ATP and ADP level among all groups with *pdx1* morpholino injection. Derivatives were determined using UPLC-FSR in zebrafish lysates at 96 hpf; n = 4-5 clutches with 50 larvae. 6 ng of morpholinos: Control-MO and SB-*pdx1*-MO were injected into the one-cell stage of zebrafish embryos respectively. Mean  $\pm$  SD, for statistical analysis one-way ANOVA followed by Sidak's multiple comparison test was applied, \*p<0.05, \*\*p<0.01, \*\*\*p<0.001. ADP, adenosine diphosphate; ATP; adenosine triphosphate; Mo, morpholino.

UPLC-FSR analysis was performed by Gernot Poschet/Elena Heidenreich.

Lastly, I also analysed *aldh3a1* expression under diabetic condition. By *pdx1* morpholino injection in wild type zebrafish embryos, I found increased mRNA levels for *aldh3a1* among ALDH genes (Fig.13). This result further suggests Aldh3a1 as an important regulator of glucose homeostasis in diabetes.

In conclusion, all the above results indicate the imbalance of glucose homeostasis in *aldh3a1*<sup>-/-</sup> larvae, which is caused by pancreas dysfunction (see in results 3.4) and leads to vasculature alternations afterwards (see in results 3.3). However, why knock out of Aldh3a1 in zebrafish can result in pancreas dysfunction remained unknown and is therefore further investigated.

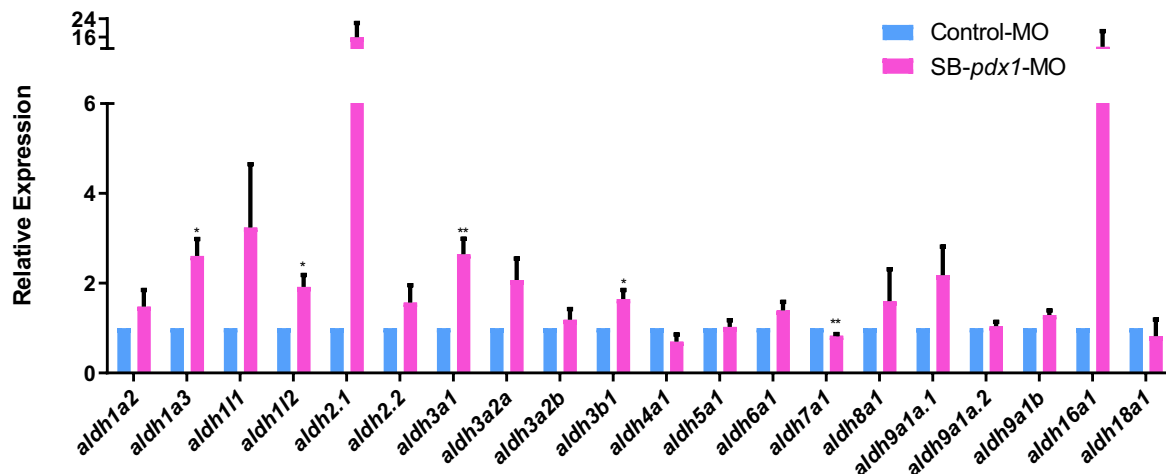


**Fig.13 Aldh mRNA levels in wild type zebrafish larvae.**

*Aldh1a3*, *aldh112*, *aldh3a1* *aldh3b1* mRNA levels were raised and *aldh7a1* was decreased significantly in zebrafish larvae at 48 hpf after *pdx1* morpholino injection. 6 ng of morpholinos: Control-MO and SB-*pdx1*-MO were injected into the one-cell stage of zebrafish embryos respectively. Expression of mRNA was analyzed by RT-qPCR at 48 hpf and expression was normalized to beta-actin. Values for Control-MO injected zebrafish larvae were standardized to 1; n = 3 clutches with 30 larvae per group; Mean $\pm$ SD, for statistical analysis Student's t-test was applied, \*p<0.05, \*\*p<0.01. Mo, morpholino.

### 3.6 Detoxification of 4-HNE but not MG is impaired and causes hyperglycaemia in Aldh3a1 knock out.

Aldehyde dehydrogenase has a board spectrum of substrates such as acetaldehyde, 4-HNE and MG<sup>72</sup>. In addition, our previous study also showed compensatory function of ALDH superfamily in *glo1* mutants<sup>90</sup>, which is the main detoxifying enzyme system for MG and strongly associated with diabetes and its complications<sup>89</sup>. Therefore, I aimed to explore whether MG is increased after loss of Aldh3a1 and criminal for the vascular alternation. The enzyme activity to detoxify MG and the internal

concentrations of MG in zebrafish larvae at 96hpf were determined. Results showed the ability to detoxified MG was not changed neither by ALDH nor by Glo1 in *aldh3a1* mutants (Fig.14 A-B). Moreover, the MG level was unaltered between wild type and *aldh3a1* mutants, which suggest MG is not essential for the observed phenotype after Aldh3a1 knock out (Fig.14C).

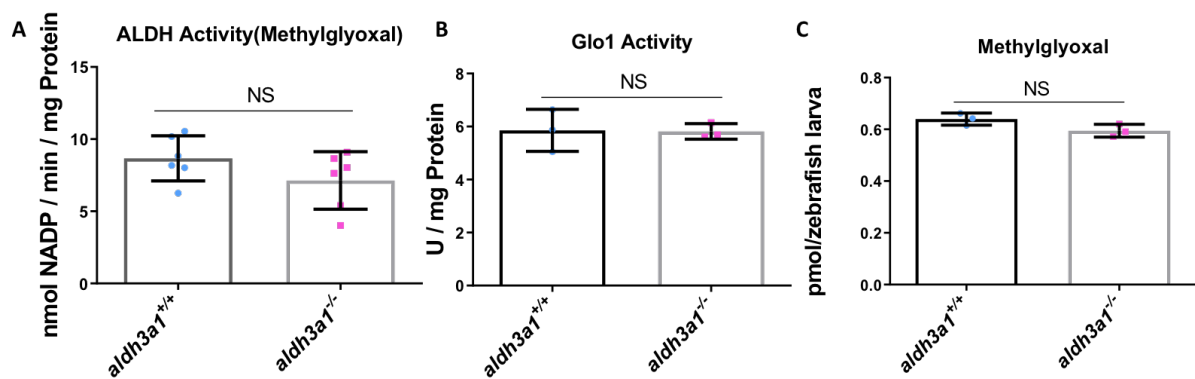


**Fig.14 Detoxification of methylglyoxal (MG) is not impaired by Aldh3a1 knock out.**

*Aldh3a1*<sup>-/-</sup> zebrafish larvae showed unaltered ALDH enzyme activity (A), GLO1 enzyme activity(B) when MG as substrate measured by spectrophotometric analysis and MG amount(C) determined by LC-MS/MS at 96 hpf; n = 3 to 6 clutches with 46 to 50 larvae. Mean ± SD, for statistical analysis Student's t-test was applied. NS: not significant. MG, methylglyoxal.

Enzyme-activity assays and MG measurements were performed by Jakob Morgenstern/Tomas Fleming.

Recent data have shown human ALDH3A1 has high affinity for 4-HNE<sup>76</sup> and *aldh3a1*<sup>-/-</sup> zebrafish caused around 30% reduction of ALDH activity when using 4-HNE as substrate(see in result 3.1). Thus, internal 4-HNE concentration was measured in zebrafish larvae at 96hpf by ELISA and a 60% significant increase in *aldh3a1* mutants was observed (Fig.15A). Besides, 4-HNE facilitates the formation of 1,4-Michael addition adducts primarily with cysteine<sup>120</sup> and around 20% reduction of free cysteine was observed in *aldh3a1*<sup>-/-</sup> larvae at 96hpf (Fig.15B). This suggests more than normal amount of cysteine is united with exceeding 4-HNE and cause the reduced free cysteine level in *aldh3a1* mutants.

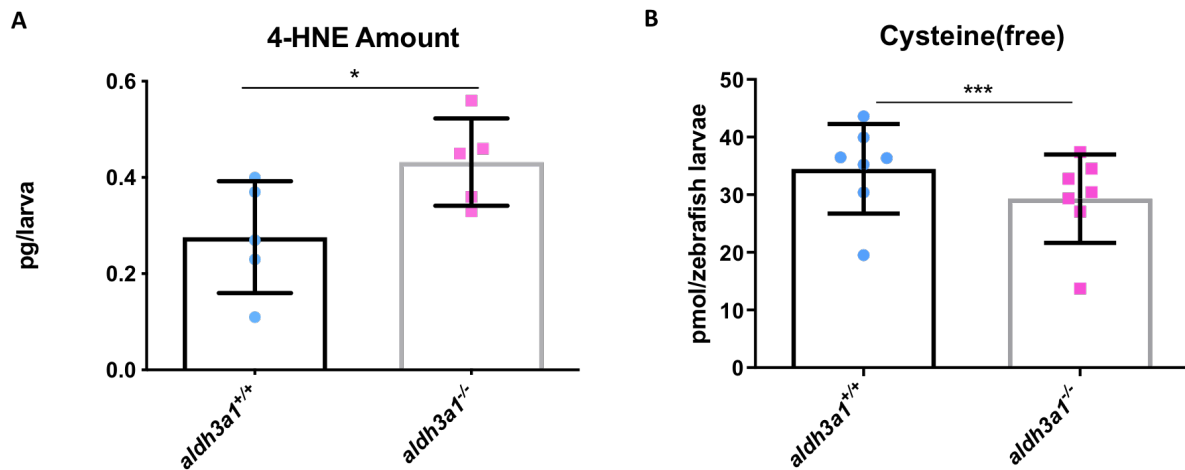


**Fig.15 The amount of 4-HNE increased while cysteine decreased in *aldh3a1*<sup>-/-</sup> zebrafish larvae at 96 hpf.**

*Aldh3a1*<sup>-/-</sup> zebrafish larvae showed increased 4-HNE amount measured by ELISA(A) and decreased free cysteine(B) determined using UPLC-FSR at 96 hpf; n = 5-7 clutches with 45 to 50 larvae. Mean±SD, for statistical analysis Paired samples t-tests was applied. \*p<0.05, \*\*\*p<0.001. 4-HNE, 4-Hydroxynonenal.

UPLC-FSR analysis was performed by Gernot Poschet/Elena Heidenreich.

To evaluate if the increased 4-HNE level causes the phenotype in *aldh3a1*<sup>-/-</sup> larvae, a series of 4-HNE incubation assays were performed. 5 μM and 10 μM were selected to perform the experiments, as they are effective and zebrafish larvae show normal gross morphology after incubation. First of all, both 5 μM and 10 μM incubation partially altered trunk vasculature morphology, led to increased formation of abnormal ISV but not hyper branches in *Tg(fli1:EGFP)* zebrafish larvae at 96hpf (Fig.16). While in hyaloid vasculature of zebrafish larvae at 120 hpf, 5 μM incubation induced more sprouts and 10 μM induced both increased IOC diameter and sprouts formation (Fig.17).

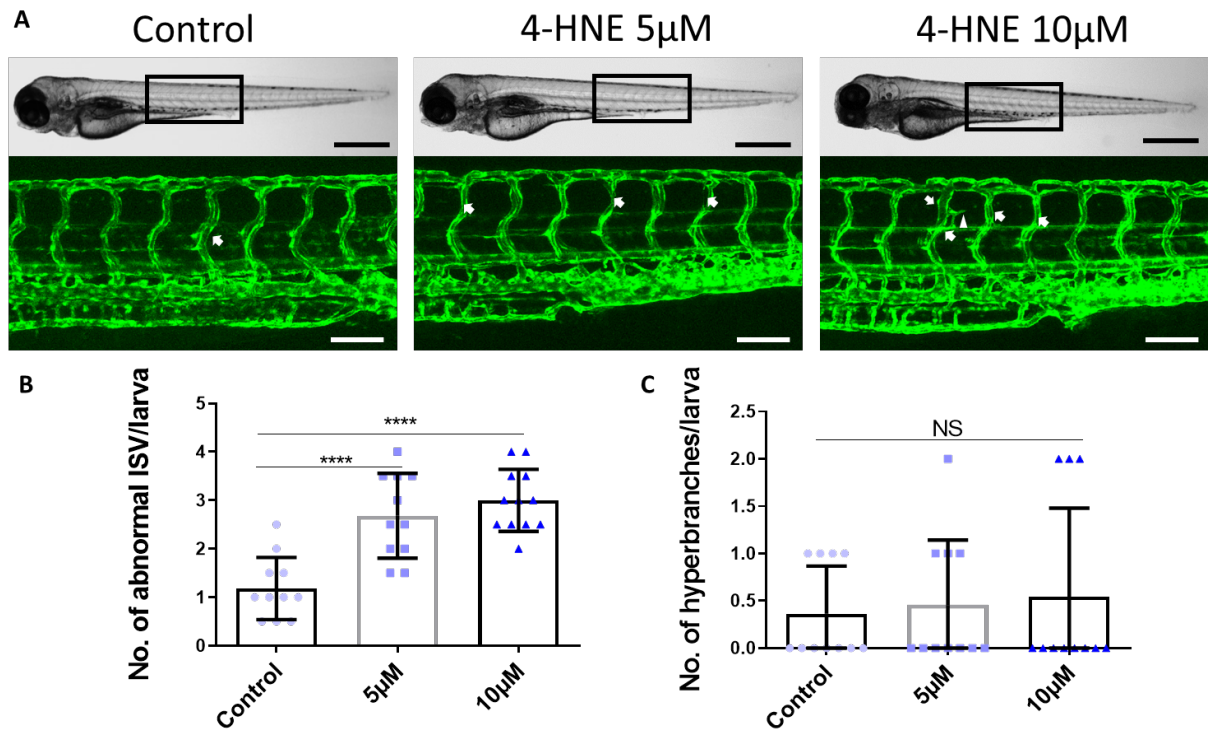


**Fig.16 4-HNE incubation partially alters trunk vasculature morphology, leads to increased formation of abnormal ISV in *Tg(fli1:EGFP)* zebrafish larvae.**

4-HNE incubation partially alters trunk vasculature morphology, leads to increased formation of abnormal ISV (white arrows) in *Tg(fli1:EGFP)* zebrafish larvae at 96hpf. Blank, 5 $\mu$ M and 10 $\mu$ M 4-HNE were added to each group respectively and medium was changed every day. (A). Light microscopic images showed the gross morphology of zebrafish larvae and black boxes indicate region seen in the confocal images. White scale bar = 100  $\mu$ m, black scale bar = 500  $\mu$ m. (B-C). Quantification of abnormal ISV and hyper branches formation; n = 10-12 per group. Mean  $\pm$  SD, for statistical analysis one-way ANOVA followed by Sidak's multiple comparison test was applied, \*\*\*\*p < 0.0001.

All the above results indicate the vasculature alternations after 4-HNE incubation are similar to *Aldh3a1* knock out. Then, for better understanding if 4-HNE causes vasculature alternations via inhibiting the development of pancreas directly, 5  $\mu$ M and 10  $\mu$ M 4-HNE incubation was used in zebrafish pancreas transgenic reporter line. Both concentrations caused reduced dimension of the early primary endocrine islet in *Tg(hb9:GFP)* zebrafish larvae (Fig.18) and reduced size of early  $\beta$  cell mass in *Tg(ins:nfsB-mCherry)* zebrafish larvae at 72hpf (Fig.19), in accordance with the change after *Aldh3a1* knock down. In the end, *ins* and *pdx1* gene mRNA significantly reduced after incubation of both concentrations (Fig.20), which is also in line with both *Aldh3a1* transient knock down and permanent knock out.

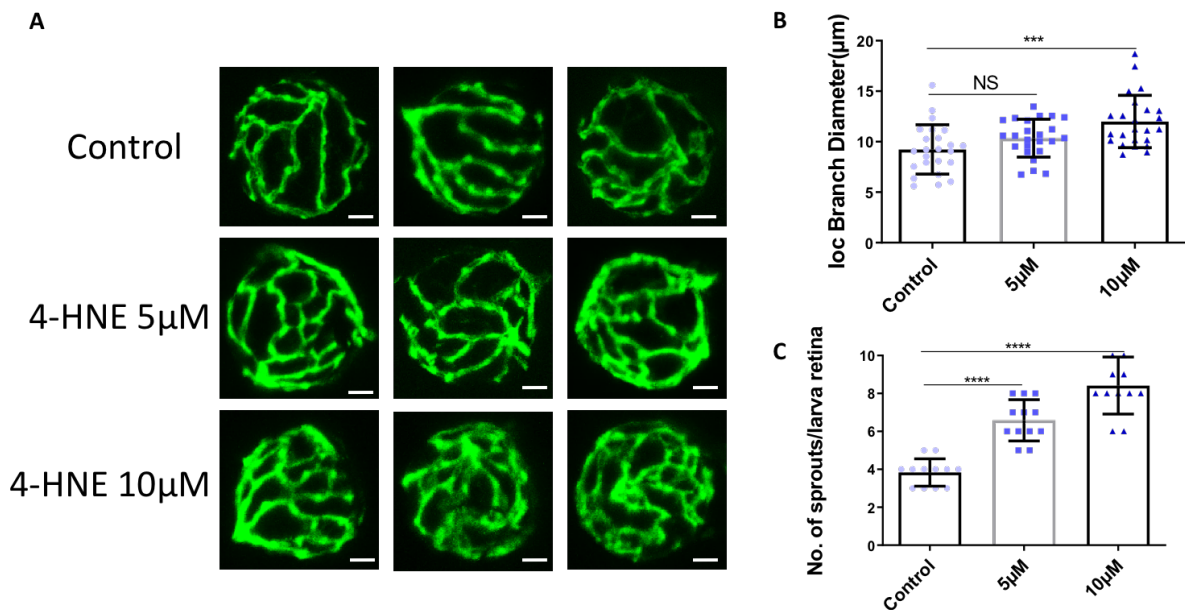


**Fig.17 4-HNE incubation alters hyaloid vasculature morphology, induces increased formation of IOC branch diameters and sprouts in *Tg(fli1:EGFP)* zebrafish larvae.**

4-HNE incubation leads to increased IOC branch diameters (10  $\mu$ M) and sprouts (5 $\mu$ M and 10  $\mu$ M) in hyaloid vasculature of *Tg(fli1:EGFP)* zebrafish larvae at 120hpf. Blank, 5 $\mu$ M and 10  $\mu$ M 4-HNE were added to each group respectively and medium was changed every day. (A). Representative hyaloid vasculature confocal picture after 4-HNE incubation. White scale bar = 20  $\mu$ m. (B-C). Quantification of the IOC branch diameters and sprouts, n=10-12 per group. Mean $\pm$  SD, for statistical analysis one-way ANOVA followed by Sidak's multiple comparison test was applied, \*\*\*p<0.001, \*\*\*\*p<0.0001.

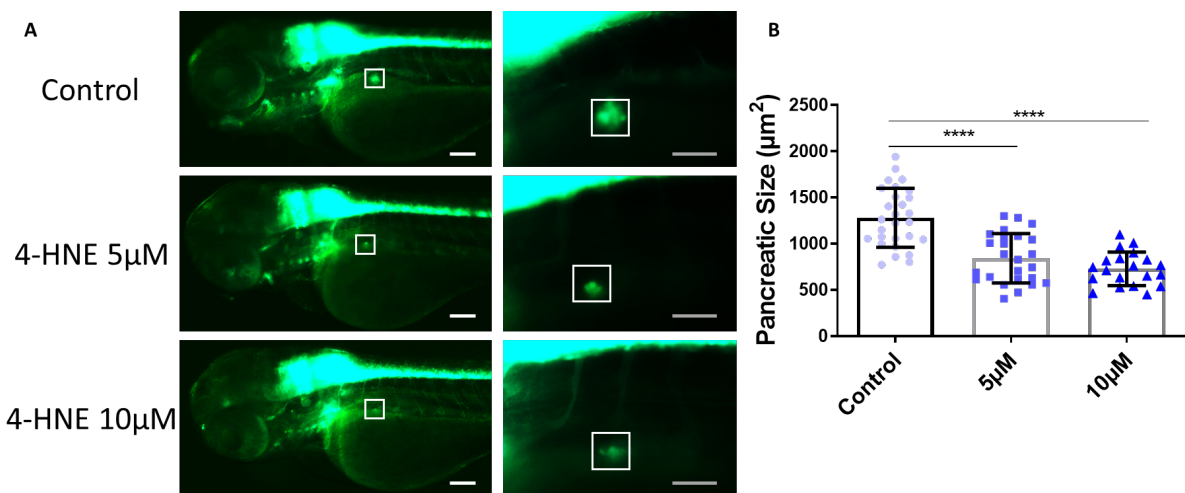


**Fig.18 Area size of the early primary endocrine islet in *Tg(hb9:GFP)* zebrafish larvae shows reduced dimensions with 4-HNE incubation.**

4-HNE incubation induces reduced dimensions of early primary endocrine islet (5 $\mu$ M and 10  $\mu$ M) in *Tg(hb9:GFP)* zebrafish larvae at 72hpf. (A). Representative fluorescence microscope pictures of the early developing endocrine with 4-HNE incubation. White box indicates the developing pancreas. White scale bar = 100  $\mu$ m, grey scale bar = 50  $\mu$ m. (B). Quantification of area sizes of the early primary endocrine islet. Mean $\pm$  SD, for statistical analysis one-way ANOVA followed by Sidak's multiple comparison test was applied, \*\*\*\*p<0.0001.

Overall, this part illuminates the 4-HNE detoxification is impaired after *Aldh3a1* knock out, and hints increased internal 4-HNE concentration can be a dominated factor for



causing pancreas dysfunction, hyperglycaemia and vasculature alternations afterwards.

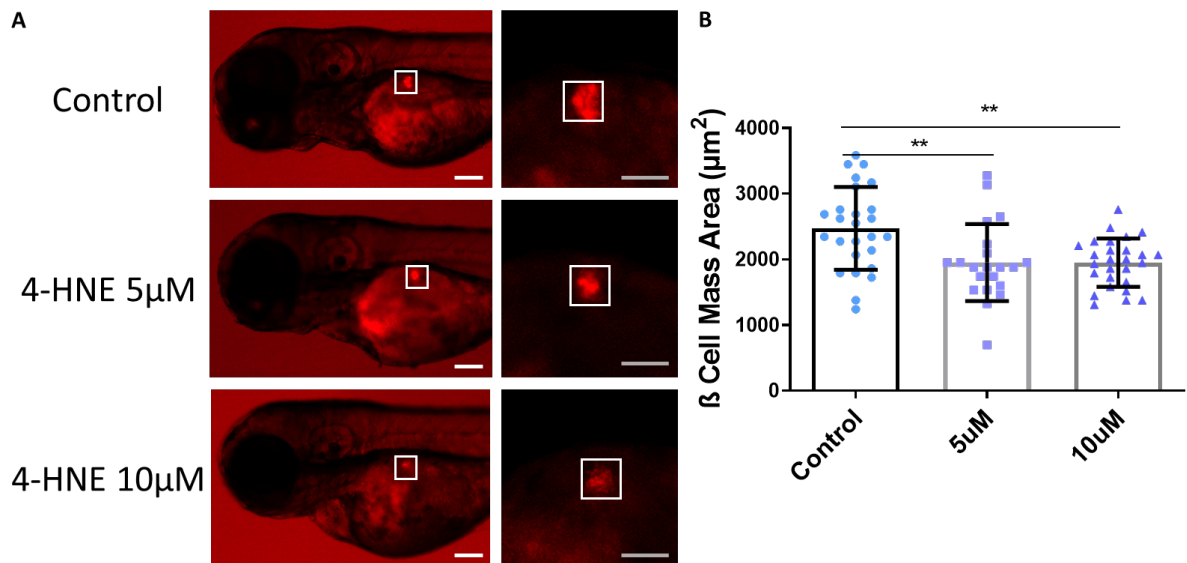


**Fig.19 Early  $\beta$  cell mass in *Tg(ins:nfsB-mCherry)* zebrafish larvae shows reduced size with 4-HNE incubation.**

4-HNE incubation induces reduced trend of  $\beta$ -Cell mass (5  $\mu$ M and 10  $\mu$ M) in *Tg(ins:nfsB-mCherry)* zebrafish larvae at 72 hpf. (A). Representative fluorescence microscope pictures of the early  $\beta$ -Cell mass in with 4-HNE incubation. White box indicates the  $\beta$ -Cell mass area. White scale bar = 100  $\mu$ m, grey scale bar = 50  $\mu$ m. (B). Quantification of area sizes of the  $\beta$ -Cell mass area size. Mean  $\pm$  SD, for statistical analysis one-way ANOVA followed by Sidak's multiple comparison test was applied, \*\* $p < 0.01$ .

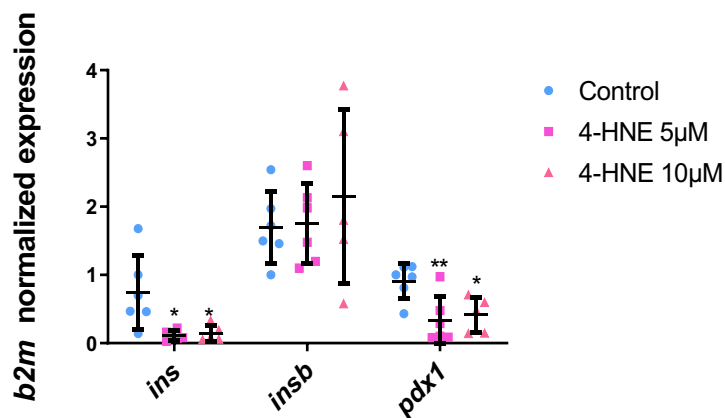


**Fig.20 4-HNE incubation leads to the decreased *pdx1* and *insulin* mRNA level.**

*Ins*, *insb* and *pdx1* mRNA expression level between wild type zebrafish larvae and with 4-HNE incubation at 48hpf. Expression of mRNA was analysed by RT-qPCR normalized to b2m. Values for wild type control zebrafish larvae were standardized to 1, n = 3-4 clutches with 30 larvae per group. Mean + SD, for statistical analysis one-way ANOVA followed by Sidak's multiple comparison test was applied, \* $p < 0.05$ , \*\* $p < 0.01$ .

### 3.7 Overfeeding leads to obesity and alters retina morphology but does not develop hyperglycaemia in *aldh3a1*<sup>-/-</sup> adult zebrafish.

Over nutrition is a main reason for developing diabetes and accelerating the progression of diabetes complications including diabetic retinopathy<sup>121</sup>. As zebrafish is already an appropriate tool for obesity modelling and diabetes research<sup>122</sup>, overfeeding experiments were performed according to the established protocol<sup>97</sup> and sacrificed after 8-week feeding period. Body and liver weight, postprandial glucose, retinal morphology as well as metabolites were examined during the assay.

After 8-week period feeding, all adult zebrafish gained increased weight. Animals from overfeeding group displayed a significantly heavy body weight than normal feeding ones, regardless of genotype (Fig.21A). However, the liver weight, liver/body weight ratio and 1h postprandial blood glucose did not show difference among each group (Fig.21 B-D).

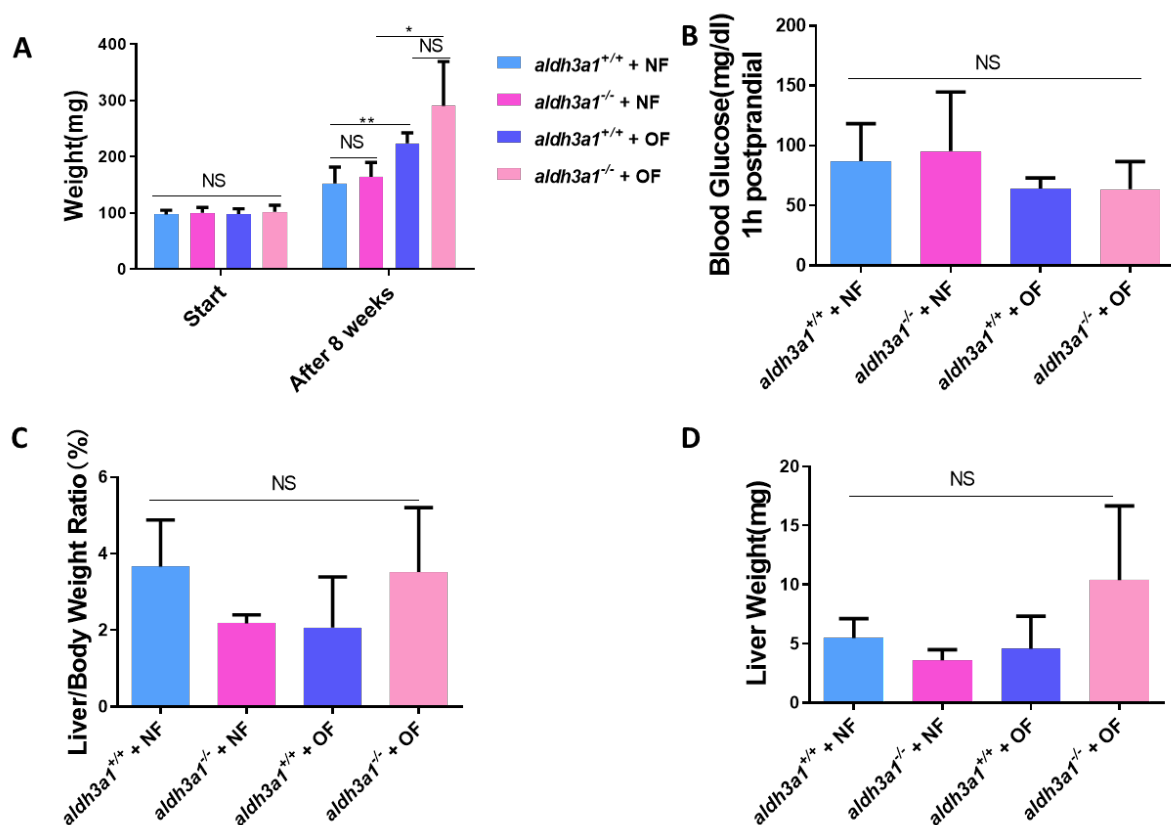


**Fig.21 Overfeeding leads to obesity in both *aldh3a1*<sup>+/+</sup> and *aldh3a1*<sup>-/-</sup> zebrafish but not developed hyperglycaemia.**

(A). After 8-week period feeding, zebrafish in the overfeeding group have gained significantly more weight than zebrafish in the normalfeeding group. Weight was measured at the start and at the end of the feeding period. (B-C). The weight of liver and the liver/body weight ratio showed no difference among each group. (D). 1h postprandial blood glucose levels showed no significant difference between each group. n = 3-4 fish per group. Mean  $\pm$  SD, for statistical analysis one-way ANOVA followed by Sidak's multiple comparison test was applied, \* $p < 0.05$ , \*\* $p < 0.01$ . NS, not significant; NF, normal feeding; OF, overfeeding.

Blood glucose levels were determined jointly with Haozhe Qi (Ryan).

As retina is susceptible to hyperglycaemia and overdoes nutrition, different forms of pathologies including neurodegeneration and angiogenesis may happen after the damage of small vessels and neurons during diabetes and obesity<sup>123</sup>. The retinæ were dissected from overfeeding/normalfeeding group and the architecture was analysed under confocal microscope by following a published protocol<sup>98</sup>. In general, one retina displays three different vascular parts, including low, middle and high density area. Normalfeeding did not affect the structure of retina in each group. However, the *aldh3a1*<sup>-/-</sup> retinal vasculature showed more interconnections between the vascular arcades with significantly increased sprouts and an increased trend of branch points after overfeeding (Fig.22).

To assess the metabolic changes after high nutrition intake and whether it is influenced by the loss of Aldh3a1, metabolites analyse were performed in adult zebrafish liver including amino acids, thiols and adenosines. There is no significant difference of amino acids in adult animal livers among each group even after overfeeding (Fig.23). In adenosine, nicotinamide adenine dinucleotide phosphate (NADPH) showed increased trend in *aldh3a1*<sup>-/-</sup> animal with normalfeeding condition. Nevertheless, this phenomenon disappeared after overfeeding by the elevation in both groups. Moreover, nicotinamide adenine dinucleotide (NADH), total and reduced glutathione (GSH) were incremental significantly in wild type and showed increased trend in knockout animal liver with overfeeding (Fig.24). Which suggests the increased ROS in animal after overload nutrition.

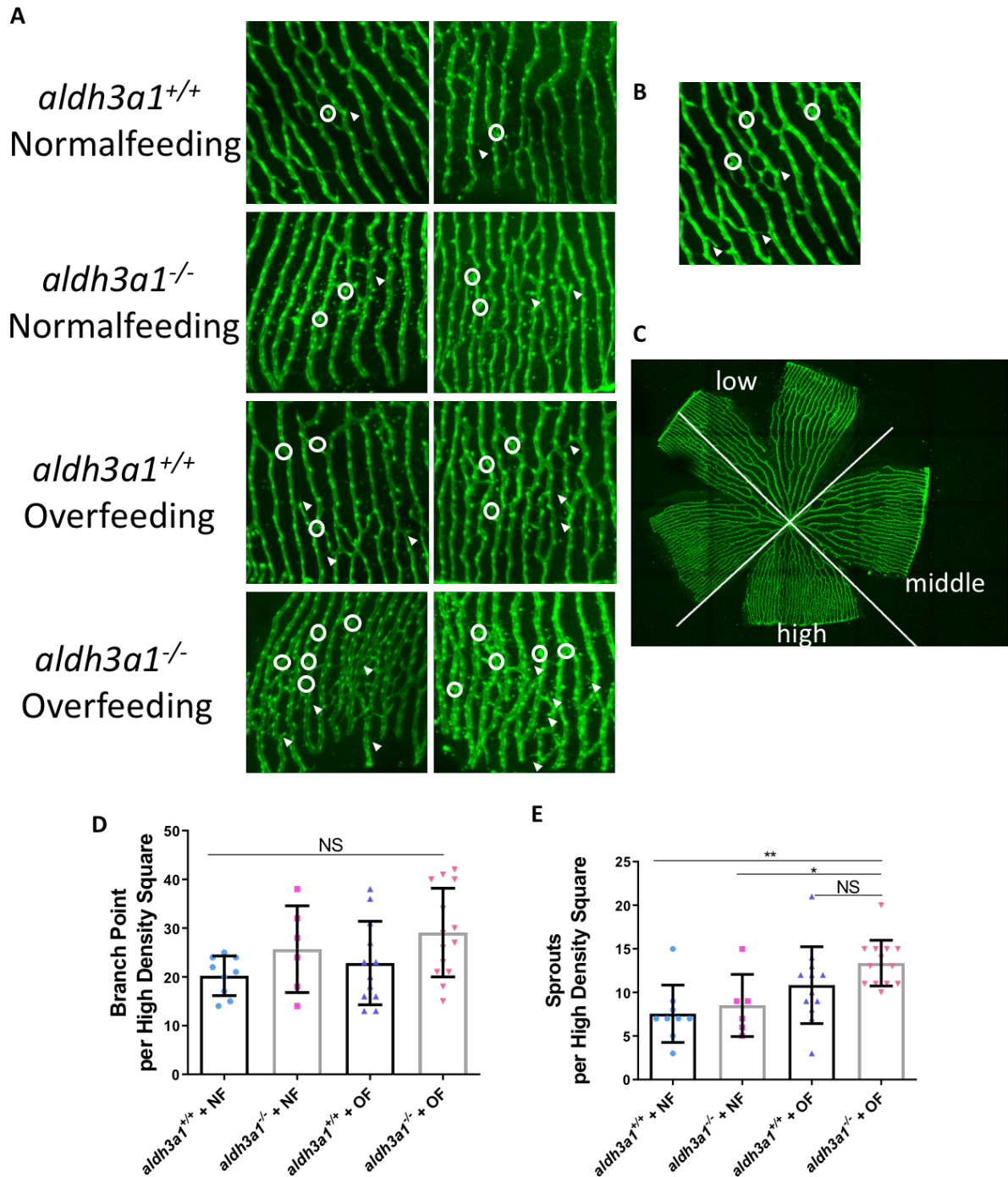


**Fig.22 *Aldh3a1*<sup>-/-</sup> *Tg(fli1:EGFP)* adult zebrafish exhibit altered morphology of the retinal vasculature after overfeeding.**

(A). Representative confocal scans of high density areas of retinal vasculature (350x350  $\mu\text{m}^2$  square with contact to the IOC) in *aldh3a1*<sup>+/+</sup> and *aldh3a1*<sup>-/-</sup> adult zebrafish with normalfed and overfeeding at 8 mpf. B. Quantified sample for branch points (white circle) and sprouts (white arrowhead). C. Representative picture of adult *Tg(fli1:EGFP)* zebrafish retinal vasculature showed different areas of vessel density (including low, middle, high vessel density areas). (D-E). Quantification of vascular parameters in the outer retinal periphery (n = 4 retinae from 3-4 animals per group). Mean  $\pm$  SD, for statistical analysis one-way ANOVA followed by Sidak's multiple comparison test was applied, \* $p < 0.05$ , \*\* $p < 0.01$ . Mpf, month post fertilization. NF, normal feeding; OF, overfeeding.

Adult zebrafish retinae were prepared jointly with Xiaogang Li.

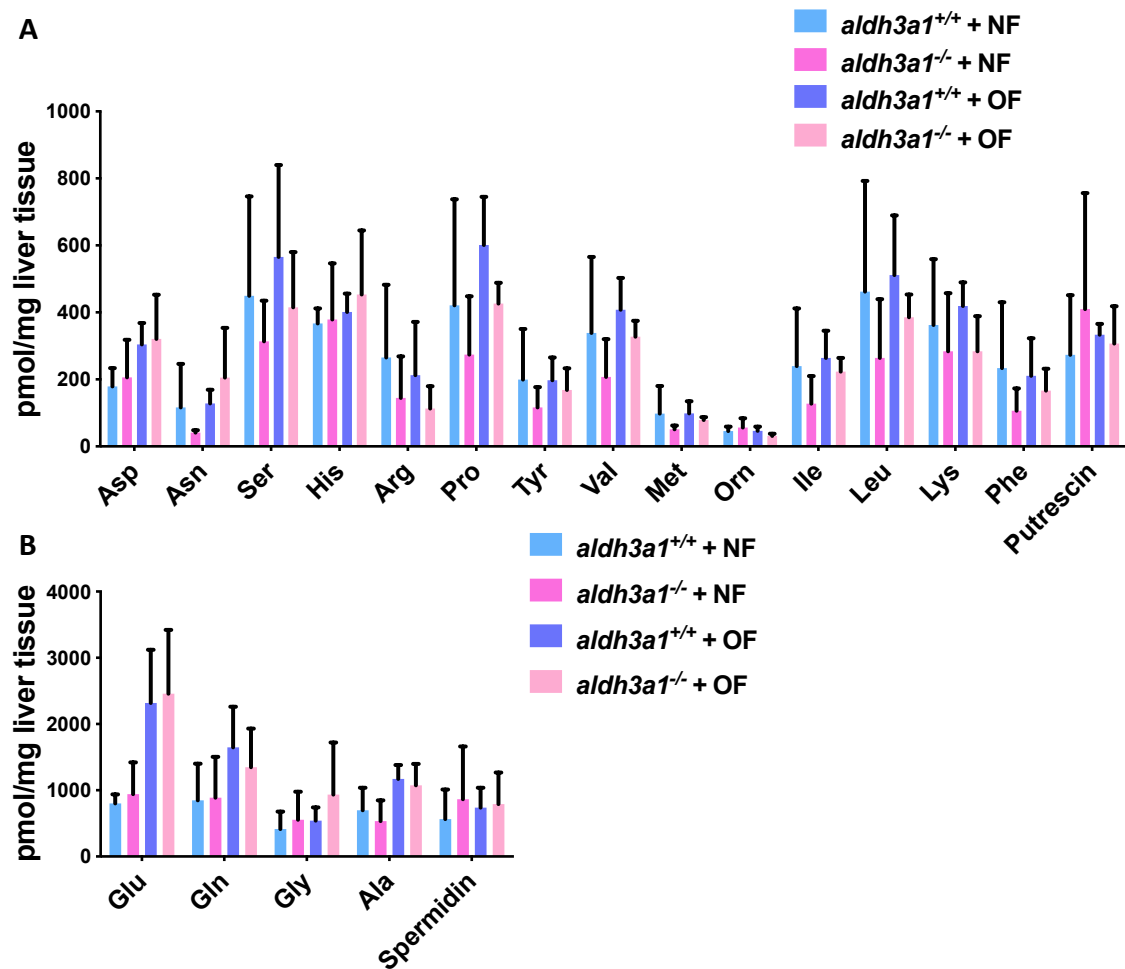


**Fig.23 Overfeeding does not alter the amino acid level in adult zebrafish liver.**

(A-B). Amino acids showed no alteration among each group. UPLC-MS was used to determine amino acids, thiols and adenosine in adult zebrafish livers after 8-week period normal and overfeeding. N=3-4 per group; mean  $\pm$  SD, for statistical analysis one-way ANOVA followed by Sidak's multiple comparison test was applied. NF, normal feeding; OF, overfeeding.

UPLC-MS analysis was performed by Gernot Poschet/Elena Heidenreich.

In summary, overfeeding leads obesity and alters retina morphology in  $aldh3a1^{-/-}$  adult zebrafish but the hyperglycaemia showed in Aldh3a1 knockout larvae disappeared in adult knockout animal. This may imply the regeneration of pancreas and  $\beta$  cell as a self-healing process during the growth to avoid the progression of impairment after loss of Aldh3a1.

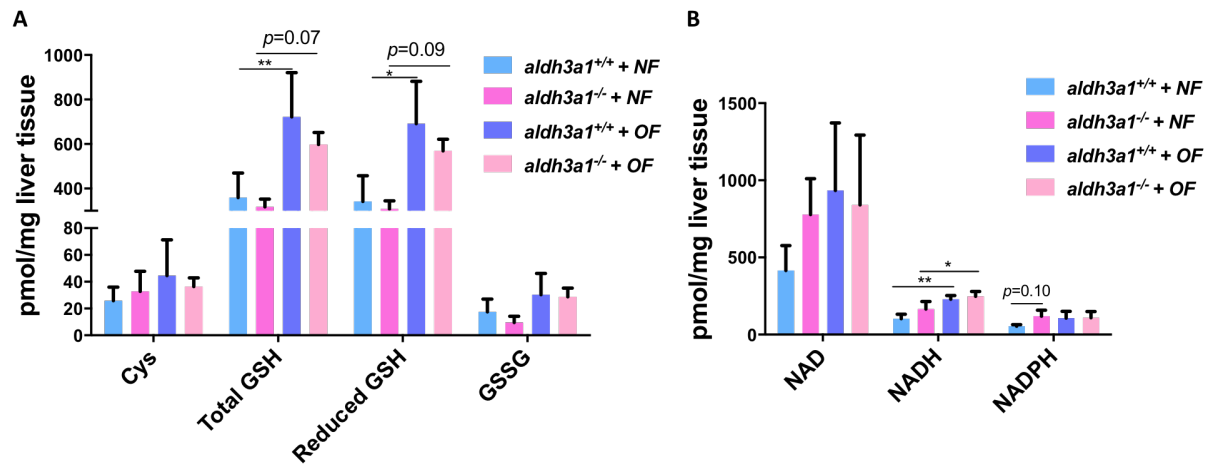


**Fig.24 Overfeeding leads to some alterations in adenosines and thiols in adult zebrafish liver.**

A. Total and reduced GSH were increased by overfeeding in both knockout and wildtype animal livers. B. NADH increased significantly after overfeeding despite the genotype and NADPH showed an increased trend in knockout animal livers. UPLC-FSR was used to determine, thiols and adenosine in adult zebrafish livers after 8-week period normal and overfeeding. N=3-4 per group; mean  $\pm$  SD, for statistical analysis one-way ANOVA followed by Sidak's multiple comparison test was applied, \* $p < 0.05$ , \*\* $p < 0.01$ . GSH, glutathione; NADH, nicotinamide adenine dinucleotide; NADPH, nicotinamide adenine dinucleotide phosphate. NF, normal feeding; OF, overfeeding.

UPLC-FSR analysis was performed by Gernot Poschet/Elena Heidenreich.

## 4 DISCUSSION

In this study, the developmental and physiological function of Aldh3a1 enzyme system in zebrafish was investigated for the first time. Zebrafish Aldh3a1 knockout model was generated and characterized and the main findings are summarized in Fig.25: 1. Aldh3a1 enzyme system is comparable to human and mouse by displaying a similar sequence and active site. 2. Loss of Aldh3a1 causes decreased ALDH activities but healthy gross development in zebrafish. *Aldh3a1*<sup>-/-</sup> larvae exhibit abnormal angiogenesis in trunk and retina hyaloid vasculature formation and the whole process is accelerated via Pdx1 induced hyperglycaemia. 3. *Aldh3a1*<sup>-/-</sup> larvae display imbalance energy metabolism and moderate hyperglycaemia, which is caused by the destruction of pancreas development. 4. Defective 4-HNE detoxification and the elevation of internal 4-HNE after Aldh3a1 loss, emphasising 4-HNE as a vital intermediate to regulate metabolic diseases via glucose homeostasis. 5. Overfeeding leads to the obesity and alters retina vasculature but not develops hyperglycaemia in *aldh3a1*<sup>-/-</sup> adult zebrafish.

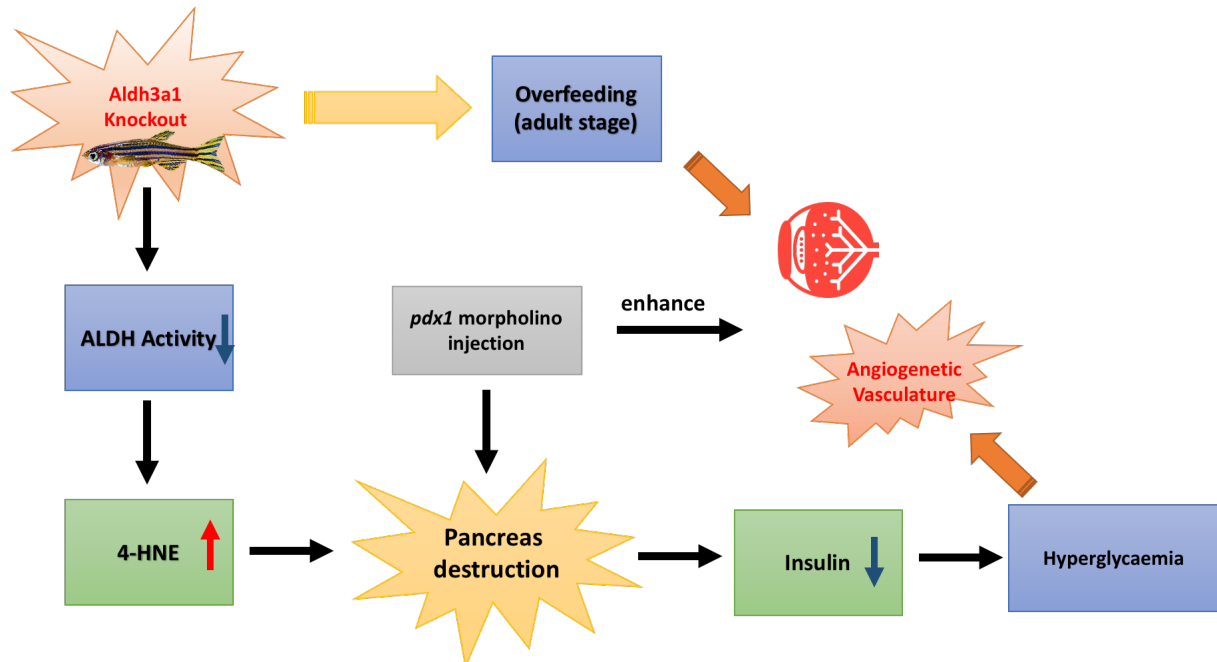


**Fig.25 Model for the role of the Aldh3a1 in zebrafish.**

In larvae stage, knock out of Aldh3a1 in zebrafish leads to decreased ALDH activity and increased 4-HNE amount, which destroys the structure of the pancreas and results in hyperglycaemia afterwards. Elevated glucose level causes increased angiogenetic formation in trunk and retinal hyaloid vasculature and can be enhanced via *pdx1* expression silencing. In adult Aldh3a1 knockout zebrafish, overfeeding alters retina vasculature but not develops hyperglycaemia.

#### 4.1 The Aldh3a1 enzyme system in zebrafish

The ALDH3 superfamily includes enzymes with the capacity to oxidize medium-chain aliphatic and aromatic aldehydes, such as peroxidic and fatty aldehydes. In addition, it also contains enzymes that have non-catalytic functions, including antioxidant functionalities<sup>76</sup>. ALDH3A1(Aldh3a1), one of the necessary members for aldehydes oxidation as well as being involved in several metabolisms, including but not limited to corticosteroids, biogenic amines, neurotransmitters, and lipid peroxidation, exists in zebrafish and almost every mammal but is missing in birds<sup>74</sup>. Several types of epithelial tissues in mammals, especially exposing to environmental stimulation continually, such as corneal epithelium, express ALDH3A1(Aldh3a1) at high levels. Its abundance in such tissues is perceived to help to maintain cellular homeostasis under oxidative stress. Metabolic as well as non-metabolic roles for ALDH3A1(Aldh3a1) have been associated with its mediated resistance to cellular oxidative stress<sup>124</sup>.

The protein sequence alignment of ALDH3A1(Aldh3a1) displayed a comparable signal peptide sequence and identical enzyme active sites (glutamic acid and cysteine) among zebrafish, human and mouse. This suggests zebrafish Aldh3a1 may behave similarly as mammals in both metabolic and non-metabolic roles while also emphasizing Aldh3a1 knockout zebrafish as a novel and appropriate model for human ALDH3A1 physiological and pathological functional study.

To get a basic understanding of Aldh3a1 character, a property of this enzyme distribution in zebrafish regarding the time and destination needs to be identified at first. So far, as the commercial antibody for zebrafish Aldh3a1 is not generated yet, qPCR-based mRNA expression of *aldh3a1* was performed instead. I found that the expression of *aldh3a1* is increased with developmental age in larvae, expressed in all adult organs and mostly in brain and eyes. Similar expression patterns were identified in mammals that *ALDH3A1 (Aldh3a1)* is highly expressed in the cornea<sup>125</sup>, and in mouse, *Aldh3a1* is also sufficient in lens and brain<sup>126, 127</sup>. Generally, the expression of zebrafish *aldh3a1* mRNA implies its essential role during growth, especially in eyes.

To sum, the data indicate that the Aldh3a1 enzyme system in zebrafish highly resembles the one in humans, by displaying similar enzyme characteristics and



expression pattern. Therefore, zebrafish is a suitable model to study this enzyme system *in vivo*.

#### 4.2 *Aldh3a1*<sup>-/-</sup>larvae exhibit abnormal angiogenesis in the trunk and retinal hyaloid vasculature, which was accelerated by hyperglycaemia.

Up to date, no *Aldh3a1* mutant was described in zebrafish. Yet, a study in mice showed that ALDH3A1-deficient mice developed cataracts because of the proteasome inhibition by lipid peroxidation<sup>86</sup>, but additional phenotypes in these mice have not been reported. Therefore, I have generated *Aldh3a1* knockout zebrafish for the first time by using CRISPR-Cas9 technology leading to an 11-base pair insertion. Amino sequence analysis of the 11-base pair *aldh3a1* mutant suggests the knock out by leading a Stop-codon in exon 2. Due to the lack of a specific commercial antibody for this zebrafish enzyme and own unsuccessful attempts to generate a new specific antibody together with the German Cancer Research Center (DKFZ) antibody core facility, I was not able to prove the knock out by western blot. Instead, acetaldehyde, one of the most common aldehydes and 4-HNE, a specific aldehyde showing high affinity with ALDH3A1(*Aldh3a1*), were used for ALDH activity measurement. Both acetaldehyde-dependent and 4-HNE-dependent ALDH activity decreased significantly in *aldh3a1* mutants, which confirms the knock out while also verifies the essential role of *Aldh3a1* for aldehydes detoxifying among ALDH superfamily.

Angiogenesis leads to the formation of the ISVs of the trunk during zebrafish development<sup>128</sup>. Although our study showed normal gross morphology of zebrafish larvae despite the genotype and *aldh3a1*<sup>-/-</sup>zebrafish larvae demonstrated no difference in hyper branches. However, a slight increase in abnormal ISVs was observed in *aldh3a1* mutant larvae at 96hpf. ISV development starts at 22hpf with the primary wave of endothelial cell sprouting and formation of the segmental artery (SA) originating from the dorsal aorta. Ten hours later, segmental vein(SV) is formed by a second endothelial cell wave originating from the common cardinal vein<sup>129</sup>. During the whole process, signalling through the VEGF/VEGF receptor (VEGFR) pathway is the driver for controlling physiological development and also in pathological conditions. *Vegfa* controls the formation of SA by primary angiogenesis wave, and *Vegfc* is essential for secondary angiogenesis, giving rise to SV and lymphatics<sup>130</sup>. Besides, Bower *et al.*

found that *Vegfd* plays context-specific and compensatory roles during both blood vessel angiogenesis and lymphangiogenesis, rather than being dispensable as a thought in the previous study<sup>131</sup>. Based on our RNA-Seq result, *vegfd* but not *vegfa* or *vegfc* altered in *aldh3a1* knockout mutants, indicating *Vegfd* may be the potential factors leading to abnormal formation of ISVs.

By using *pdx1* morpholino injection leading to hyperglycaemia and mimicking diabetic condition, I observed enhanced vasculature alternations with both increased hyper branches and abnormal ISV numbers in *aldh3a1* mutants. As mentioned before, VEGF is the most crucial mediator for angiogenesis, the question, how could the high glucose level induce the angiogenesis and via VEGF directly or indirectly, draws our attention.

Angiogenesis is controlled by both pro- and anti-angiogenic factors and an imbalance can result in the activation. Generally, VEGF expression is produced mainly by hypoxia via the activation of hypoxia-inducible transcription factor 1 (HIF1)<sup>132</sup>. Besides, several studies showed glucose itself leads to the increase of VEGF expression, including but not limited to retinal endothelial cells, epithelial cells, Müller cells, vascular smooth muscle cells and also in zebrafish larvae<sup>96, 133-136</sup>. One of the mechanisms is activation of PKC pathway by raised glucose, which induces the expression of VEGF in human vascular smooth muscle cells<sup>137</sup>. Additionally, increased ROS and ROS release orchestrated during hyperglycaemia by polyol and PKC pathway can stimulate VEGF signalling and drive the angiogenic process. In endothelial cells, NADPH oxidase (NOX) 4 derived H<sub>2</sub>O<sub>2</sub> in part activates Nox2 to increase mitochondria production via elevated S36 phosphorylation of p66Shc, therefore enhancing VEGFR2 signalling and angiogenesis<sup>138</sup>.

Several studies already explored the effects of hyperglycaemia in zebrafish retina hyaloid vasculature network. Treating with 130mM glucose from 3 days to 6 days after post fertilization (dpf), zebrafish larvae exhibited formation of dilated hyaloid-retinal vessels accompanied by disrupted tight junction proteins. All these alternations were related to the elevation of Nitrate Oxygen (NO) production and increased *vegfa* mRNA expression<sup>96</sup>. Incubation with 4% and 5% D-Glucose in a pulsatile manner from 3hpf to 5dpf, Singh *et al.* found numerous ocular dysfunctions in zebrafish larvae, which is associated with altered retinal cell layer thickness, increased presence of macrophages, and decreased number of Müller glial and retinal ganglion cells following

high-glucose exposure<sup>139</sup>. However, all the above studies showed the retinal alternations by external glucose intervention. Whether the induced angiogenic phenotype of the retina is driven by the internal hyperglycaemia or other metabolomics alternation or just the “unspecific feedback reaction” to the extremely high amount of external glucose even just the change of osmotic pressure, remains unknown.

Differently, our study focuses on the hyaloid vasculature while also the connection of internal metabolic change after the gene knock out. *Aldh3a1* mutants displayed the widen branches in retina hyaloid vasculature network, which drives our attention, if the alternations related to the glucose level in *aldh3a1* mutants? Also, *pdx1* knockout zebrafish model was successfully generated, and the knock down of Pdx1 is confirmed as an effective tool to study the influence of short-term high internal sugar level on retina vasculature<sup>92</sup>. The phenotype is enhanced with both widen IOC branch diameters and increased number of sprouts aggregately in *aldh3a1*<sup>-/-</sup> compared to *aldh3a1*<sup>+/+</sup> larvae after *pdx1* morpholino injection. Which further emphasises the question, if hyperglycaemia plays an essential role in the alternation after the loss of Aldh3a1, and can be activated via decreased Pdx1 expression as a cascade reaction to accelerate the whole angiogenetic process?

#### 4.3 *Aldh3a1*<sup>-/-</sup> larvae display imbalance energy metabolism and moderate hyperglycaemia, which is caused by the destruction of pancreas development.

To address the question: if hyperglycaemia plays an essential role in the alternation after the loss of Aldh3a1, and can be activated via decreased Pdx1 expression, body glucose was measured in the zebrafish larvae, and our results showed *aldh3a1* mutants exerted hyperglycaemia by 40% increase of the whole-body glucose. Furthermore, glucose levels were increased in both genotypes after a *pdx1* morpholino injection, and interestingly *aldh3a1*<sup>-/-</sup> mutants gained around 30% more glucose than *aldh3a1*<sup>+/+</sup> larvae. Which confirms, hyperglycaemia due to the Aldh3a1 loss results in the primary moderate vascular alternations, and decreased Pdx1 expression accelerate the pathological angiogenetic process by further glucose elevation.

During the first couple of days of the development, zebrafish embryos/larvae utilize energy and nutrition from the yolk sac until they are feeding from external food sources

starting at around 5dpf-6dpf<sup>140</sup>. Therefore, the direct link for hyperglycaemia should be a series of energy metabolisms regulation by itself.

ATP is a complex organic chemical that provides energy to drive many processes in living cells, such as muscle contraction, nerve impulse propagation and mass of chemical/bio synthesis<sup>141</sup>. A number of distinct cellular processes can produce ATP, and three main pathways in eukaryotes are 1). glycolysis, 2). the tricarboxylic acid (TCA) cycle and oxidative phosphorylation, and 3). beta-oxidation. In addition, it converts to ADP or AMP via dephosphorylation when consuming in metabolic process. The dynamic equilibrium of the ATP/ADP cycle is the basement of several biomedical activities, including intracellular signalling, DNA and RNA synthesis and amino acid activation in protein synthesis<sup>142</sup>.

ATP/ADP ratio, as the cellular "energy state", is responsible for coupling glucose stimulus to insulin secretion<sup>143</sup>. In physiological condition, the elevation of glucose level can result in increased glycolysis and thereby input reducing equivalents into both the citric acid cycle through pyruvate dehydrogenase (PDH) and respiratory chain through the glycerol phosphate shuttle. The influx of reducing equivalents is "greater" than what is needed for ATP synthesis, hence, leads to a reduction of the intra mitochondrial NAD pool and an increased ATP/ADP ratio in "energy state" <sup>143</sup>. However, decreased ATP amount and lower ATP/ADP ratio is measured in *aldh3a1* mutants after *pdx1* morpholino injection compared to wild type, suggesting the impaired metabolomic energy status to glucose intolerance after Aldh3a1 knock out. Patterson *et al.* found that Mitochondrial pyruvate carrier 1 (Mpc1) and Mitochondrial pyruvate carrier 2 (Mpc2) are essential for ATP-regulated potassium (KATP) channel pathways of insulin secretion regulation in clonal 832/13  $\beta$  cells as well as mammal islets. Inhibition of the MPC by both pharmacological inhibitors and siRNA-mediated knockdown blocked the insulin secretion through ATP/ADP ratio regulation and resulted in impaired glucose tolerance<sup>144</sup> Also significantly reduced mitochondrial pyruvate carriers (*mpc1* and *mpc2*) mRNA expression was observed in *aldh3a1* mutants, which may be the directly reason lead to energy metabolism imbalance and hyperglycaemia.

Until now, it was identified that glucose metabolism is impaired in *aldh3a1* mutants, which may be linked to insufficient insulin secretion on account of reduced *ins* mRNA level. Further investigation concerning its source, pancreas and  $\beta$  Cell, would be necessary. Keen interest is raised, particularly in understanding pancreas

development as it goes hand in hand to different forms of diagnoses and therapies for diabetes. Apart from *Pdx1*, the most crucial transcription factor gene for pancreatic development, the *Hb9(Mnx1)* gene encodes a homeobox transcription factor in vertebrates that has conserved functions in motoneuron differentiation and pancreas development<sup>145</sup>. In zebrafish, *hb9* plays an essential role in zebrafish endocrine cell fate decisions<sup>40</sup> and is required and sufficient for regulating expression in  $\beta$  cells prior to the onset of insulin expression<sup>146</sup>. By using zebrafish as a visual model for pancreas morphology study, a combination of *Aldh3a1* knockout and knockdown strategies identified a decreased pancreatic size in *Tg(hb9:GFP)* and reduced  $\beta$  Cell mass dimension in *Tg(ins:nfsB-mCherry)* zebrafish larvae, which indicates the destruction of the pancreas before decreased insulin secretion. Besides, Rna-Seq and qPCR-based mRNA expression results also showed: the expression of several genes involved into endocrine pancreas development was decreased in *aldh3a1* mutants, including but not limited to *pdx1*, *hb9*, *sox9b*, *rfx3*, *notch2*, *wnt5b*, *isl2b*, which hints the dysfunctional pancreas may result from the insufficiency of several transcription factors, such as Hb9 and Pdx1.

According to all the above data, we suppose two mechanisms which links to the insufficient insulin expression in *aldh3a1* mutants: 1) the imbalance energy metabolism including impaired ATP/ADP signalling pathway, which can be related to high sugar level directly in *aldh3a1* mutant larvae before external food intake. 2) the destruction of the early pancreas because of the dysfunction of several transcription factors such as Hb9 and Pdx1, which may be the initiative cause Nevertheless, how could the missing of *aldh3a1*, one enzyme gene, leading to these following changes to hyperglycaemia at the end?

#### 4.4 Defective 4-HNE detoxification and increased internal 4-HNE concentration regulate metabolic diseases via glucose homeostasis after *Aldh3a1* loss.

MG is a reactive organic compound involved in the biology of diabetes. Due to the increased blood sugar level, elevated MG levels can be observed in diabetes and thereby participates in the formation of AGEs<sup>147</sup>. In zebrafish larvae, one study revealed that MG induced pathological angiogenesis in the trunk vasculature, due to the activation of the VEGF/VEGFR2 signalling cascade<sup>148</sup>. Besides, a permanent

knock out of *Glo1* in zebrafish, the primary MG detoxifying system, led to a two-fold increase in ALDH activity and qPCR-based expression data identified increased mRNA levels of *aldh3a1* in the *glo1* mutants<sup>90</sup>. All of the above hints suggest Aldh3a1 as an alternative compensatory enzyme for the MG detoxification. The increased MG may cause hyperglycaemia and related phenotype after Aldh3a1 loss. However, neither the enzyme activity to detoxify MG nor the internal concentration of MG was changed in *aldh3a1* mutants.

4-HNE, one of the most prominent lipid peroxidation specific aldehydes, has shown a high affinity with ALDH3A1 in several studies. Treating with H<sub>2</sub>O<sub>2</sub>, Natalie *et al.* found increased 4-HNE adducted proteins in a rabbit corneal fibroblastic cell line (TRK43) without human ALDH3A1 transfection compared to ALDH3A1-TRK43 cells after the treatment of H<sub>2</sub>O<sub>2</sub><sup>88</sup>. Aglaia *et al.* showed that human corneal epithelial cell line (HCE) transfected with ALDH3A1 were more resistant to UV- and 4-HNE-induced cytotoxicity than mock-transfected cells<sup>149</sup>. M Hlaváčová *et al.* demonstrated increased plasma level of 4-HNE accompanied by decreased *Aldh3a1* gene expression in the liver in Wistar rats applied with conventional doxorubicin<sup>150</sup>. By measuring the 4-HNE concentration and ALDH activity *in vivo*, I identified the internal increased 4-HNE concentration and decreased ability to detoxify 4-HNE in *aldh3a1* knockout zebrafish for the first time.

The detrimental and cytotoxic effects of 4-HNE have been described in myriad tissues, organs and links to the pathological process. Also, pancreas and  $\beta$  cells are susceptible to the influence of 4-HNE. One study found a significant increase in interleukin-1 $\beta$  expression and 4-HNE formation in cat islet after a period of hyperglycaemia and obesity, suggested the elevation of inflammation and oxidative marker occurs very early during the diabetes development<sup>151</sup>. The destruction of rat pancreatic islet  $\beta$  cell by cytokine combination of IL-1 $\beta$ , TNF $\alpha$ , and IFN $\gamma$  was closely associated with aldehyde production, including 4-HNE and MDA<sup>152</sup>. Moreover, high levels of 4-HNE can induce massive  $\beta$  cell death. Rat pancreas islets treated with increasing 4-HNE concentration showed a dose-dependent decrease of glucose-stimulated insulin secretion<sup>153</sup>. In acute pancreatitis rats, pancreatic 4-HNE levels were increased by 300%, accompanied by the 50% reduction of glutathione peroxidase (GPx)<sup>154</sup>.

The general role of 4-HNE involved in  $\beta$  cell dysfunction can be described in two signalling mechanisms. First, via activating or inhibitory interactions with receptors, key signalling molecules, enzymes and other macromolecules such as mitochondrial, TCA cycle enzymes and lipoproteins<sup>68</sup>. Once the capacity of 4-HNE is exceeded, through increased lipid peroxidation and oxidative stress, it leads to structural and conformational modification of the macromolecules and ultimately attributes to the  $\beta$  cell dysfunction and failure.

The other role is that 4-HNE can regulate the expression of several major transcription factors. For instance, 4-HNE activated the pro-inflammatory transcription factor (nuclear factor kappa-light-chain-enhancer of activated B cells) NF- $\kappa$ B<sup>155</sup>, leading to deteriorating responses including hyperglycaemia. However, it remains unclear which transcription factor is influenced by high 4-HNE amounts during pancreas destruction. We identified that 4-HNE induced a similar phenotypes as seen in *aldh3a1* mutants when added on wild type larvae, with the destructed pancreas and decreased mRNA expression of *ins* and also of *pdx1*. However, potential transcription factors which can be targeted directly needs more exploration in the future.

Furthermore, 4-HNE treated wild type larvae exhibited altered angiogenesis in the retinal hyaloid vasculature network with both increased IOC diameters and sprouts formation. This may result from the double effects: 4-HNE induced hyperglycaemia and 4-HNE induced oxidative stress, which can activate the WNT pathway and cause diseases in retina directly<sup>156</sup>. Zhou *et al.* showed increased 4-HNE level in the retina of diabetic rats, accompanied with increased phosphorylated and total LDL receptor-related protein (LRP) 6, cytosolic  $\beta$ -catenin and connective tissue growth factor (CTGF), which can be attenuated by N-acetyl-cysteine (NAC), an antioxidant as well as a thiol-protective agent<sup>156</sup>. While retinal pigment epithelial cells and retinal capillary endothelial cells also exhibited activated WNT pathway after 4-HNE intervention *in vitro*, by increasing LRP6, cytosolic  $\beta$ -catenin and CTGF expression level<sup>156</sup>.

How could 4-HNE influence energy metabolism is still under investigation and several studies already illuminated the role of 4-HNE in mitochondria. Mitochondria are essential for the life of eukaryotic cells because of the critical functions including ATP generation and TCA metabolism, and these functions are tightly regulated by mitochondrial lipids such as cardiolipin (CL) and 4-HNE<sup>157</sup>. Increased oxidative stress

caused by exceed ROS may lead to the accumulation of lipid peroxidation, and these reactive lipid species cause mtDNA mutation, dysfunctional mitochondrial membrane, and protein modification. All these effects can lead to mitochondrial dysfunction and further exacerbate the ROS generation and oxidative stress. Moreover, the elevation of oxidative stress has been closely associated with insulin resistance and diabetes<sup>158</sup>. ROS activate mitochondrial uncoupling protein 2(UCP2) via Peroxidation of mitochondrial membrane phospholipids, can result in reduced ATP synthesis and pancreatic  $\beta$  cell dysfunction<sup>159</sup>. Decreased ATP level was displayed in *aldh3a1* mutants and after *pdx1* morpholino injection, which may be related to 4-HNE induced mitochondria dysfunction and further lead to reduced insulin expression.

To sum, I identified a defective 4-HNE detoxification system and increased internal 4-HNE concentration in *aldh3a1* mutants. Increased 4-HNE leads to hyperglycaemia by the destruction of the pancreas with both  $\beta$  cell mass reduction and  $\beta$  cell dysfunction, which may be regulated by the general role of increased oxidative stress in the mitochondrial and specific way of the inhibition of several pancreas transcription factors.

#### 4.5 Overfeeding induced obesity alters retina morphology in *aldh3a1*<sup>-/-</sup> adult zebrafish.

High nutrition intake is one of the main reasons for developing diabetes and accelerating the progression of diabetes complications, including diabetic retinopathy<sup>121</sup>. To assess the effects of Aldh3a1 loss in adult fish, overfeeding experiments were performed. Animals from overfeeding group displayed a significantly heavier bodyweight than normal feeding ones, regardless of genotype. However, hyperglycaemia as observed in *aldh3a1* mutant larvae did not continue into adulthood.

The zebrafish pancreas shares conserved functions with the mammal pancreas<sup>40</sup>. As the regenerative capacity of mammalian  $\beta$  cells is restricted, loss and dysfunction of  $\beta$  cells can result in diabetes. In contrast to mammals, zebrafish can regenerate functional pancreatic  $\beta$  cells throughout their whole life<sup>160</sup>. Several studies showed  $\alpha$  cells' potential contribution to  $\beta$  cell regeneration as well as neogenesis; Also, centroacinar cells, which are defined as specialized ductal epithelial cells located at



the ends of ducts within the acinar lumen, can form new endocrine cells after  $\beta$  cell ablation or partial pancreatectomy<sup>52, 53</sup>.

This suggests that the recovery of normal glucose level in adult fish after *Aldh3a1* loss results from the regeneration of pancreas and  $\beta$  cell as self-healing during the growth to avoid the progression of impairment. Anderson *et al.* demonstrated adenosine agonist NECA can increase  $\beta$  cell proliferation via acting the adenosine receptor A2aa, and promote the restoration of normal glucose level in zebrafish larvae [51], which suggests an evolutionarily conserved role for adenosine in  $\beta$  cell regeneration. Similarly, the significantly reduced adenosine amount in *aldh3a1*<sup>-/-</sup> larvae showed no difference in adult zebrafish regarding the genotype and feeding method, indicating the regained ability of  $\beta$  cell proliferation in *aldh3a1*<sup>-/-</sup> adult zebrafish.

Notably, *aldh3a1*<sup>-/-</sup> adult zebrafish after overfeeding displayed angiogenic retinal vasculature, which may be a “memory effect” of high glucose levels since the larva state<sup>139</sup> but not induced by hyperglycaemia in the adult stage<sup>139</sup>. Besides, overnutrition can lead to exceed-burden 4-HNE in *aldh3a1* adult mutants on account of dysfunctional detoxifying ability, which may further aggravate the phenotype via oxidative stress. Detailed mechanisms are necessary to be studied in the future.

## SUMMARY

Diabetes mellitus is a global disease with increasing prevalence worldwide. Long-standing diabetes mellitus leads to various microvascular, including diabetic nephropathy, neuropathy, retinopathy, cardiomyopathy etc, and several macrovascular complications such as coronary heart disease and stroke. In almost all high-income countries, diabetes is a leading cause of cardiovascular disease, blindness, kidney failure, and lower limb amputation. The treatment of diabetes and its complications results in enormous health expenditure all over the world.

The increased formation of methylglyoxal (MG) under hyperglycaemia is associated with the development of microvascular complications in patients with diabetes. However, in zebrafish, a permanent knock out of glyoxalase 1(Glo1), the central MG detoxifying system, only led to a two-fold elevation of endogenous MG levels. Importantly, a two-fold increase in aldehyde dehydrogenases (ALDH) activity, a group of enzymes which catalyse the oxidation of aldehydes, was observed. Furthermore, qPCR-based expression data identified increased mRNA levels of *aldh3a1* in the *glo1* mutants suggesting Aldh3a1 as an alternative protein for the detoxification of reactive metabolites. Thus, this project aimed to analyse *aldh3a1* mutant zebrafish on its function to potentially compensate for the loss of Glo1 in development and disease.

By using CRISPR/CAS9 technology, I generated Aldh3a1 knockout model in zebrafish. A series of experiments were performed regarding the function and morphology of pancreas, vasculature, glucose homeostasis and metabolism after Aldh3a1 loss. The main findings of this dissertation are: *Aldh3a1*<sup>-/-</sup> larvae exhibit impaired 4-Hydroxynonenal (4-HNE) detoxification ability and increased internal 4-HNE concentration, which destructs the pancreas development via  $\beta$  cell mass reduction and dysfunction and leads to hyperglycaemia. Impaired glucose homeostasis causes abnormal angiogenesis in trunk and retina hyaloid vasculature formation and can be further enhanced via down-regulated *pdx1* expression.

Although this study successfully linked a loss of Aldh3a1 to an elevation of 4-HNE to impaired glucose homeostasis, there are some limitations. First, due to the lack of specific and commercial antibodies for zebrafish Aldh3a1, to confirm the Aldh3a1

knockout in zebrafish by protein level is unavailable. Second, as *aldh3a1* mutants in zebrafish pancreas transgenic reporter line have not been generated yet, we cannot perform pancreas morphology study in knockout models directly. Additionally, our conclusion on how 4-HNE regulates pancreas and  $\beta$  cell morphology, as well as function, mostly are based on the qPCR-based mRNA expression data *in vivo*. It would be interesting to explore the potential pathways based on the alterations of protein levels. At last, in order to test the primary hypothesis if Aldh3a1 can compensate after Glo1 loss, the generation of *glo1/aldh3a1* double knockout mutants seems necessary in the future.

Overall, this dissertation provided patent evidence for the contribution of deficient 4-HNE detoxification and subsequent increased 4-HNE concentration to the development of hyperglycaemia via pancreas dysfunction in *aldh3a1* mutants, as a novel direction for future research regarding diabetic pathophysiology and therapy.

## REFERENCE

1. Cho, NH, Shaw, JE, Karuranga, S, Huang, Y, da Rocha Fernandes, JD, Ohlrogge, AW, Malanda, B: IDF Diabetes Atlas: Global estimates of diabetes prevalence for 2017 and projections for 2045. *Diabetes Res Clin Pract*, 138: 271-281, 2018.
2. Shaw, JE, Sicree, RA, Zimmet, PZ: Global estimates of the prevalence of diabetes for 2010 and 2030. *Diabetes Res Clin Pract*, 87: 4-14, 2010.
3. Saeedi, P, Petersohn, I, Salpea, P, Malanda, B, Karuranga, S, Unwin, N, Colagiuri, S, Guariguata, L, Motala, AA, Ogurtsova, K, Shaw, JE, Bright, D, Williams, R, Committee, IDFDA: Global and regional diabetes prevalence estimates for 2019 and projections for 2030 and 2045: Results from the International Diabetes Federation Diabetes Atlas, 9(th) edition. *Diabetes Res Clin Pract*, 157: 107843, 2019.
4. Bellamy, L, Casas, JP, Hingorani, AD, Williams, D: Type 2 diabetes mellitus after gestational diabetes: a systematic review and meta-analysis. *Lancet*, 373: 1773-1779, 2009.
5. Katsarou, A, Gudbjornsdottir, S, Rawshani, A, Dabelea, D, Bonifacio, E, Anderson, BJ, Jacobsen, LM, Schatz, DA, Lernmark, A: Type 1 diabetes mellitus. *Nat Rev Dis Primers*, 3: 17016, 2017.
6. Tisch, R, McDevitt, H: Insulin-dependent diabetes mellitus. *Cell*, 85: 291-297, 1996.
7. Petersmann, A, Nauck, M, Muller-Wieland, D, Kerner, W, Muller, UA, Landgraf, R, Freckmann, G, Heinemann, L: Definition, Classification and Diagnosis of Diabetes Mellitus. *Exp Clin Endocrinol Diabetes*, 126: 406-410, 2018.
8. Lotfy, M, Adeghate, J, Kalasz, H, Singh, J, Adeghate, E: Chronic Complications of Diabetes Mellitus: A Mini Review. *Curr Diabetes Rev*, 13: 3-10, 2017.
9. Ahlqvist, E, Storm, P, Karajamaki, A, Martinell, M, Dorkhan, M, Carlsson, A, Vikman, P, Prasad, RB, Aly, DM, Almgren, P, Wessman, Y, Shaat, N, Spegel, P, Mulder, H, Lindholm, E, Melander, O, Hansson, O, Malmqvist, U, Lernmark, A, Lahti, K, Forsen, T, Tuomi, T, Rosengren, AH, Groop, L: Novel subgroups of adult-onset diabetes and their association with outcomes: a data-driven cluster analysis of six variables. *Lancet Diabetes Endocrinol*, 6: 361-369, 2018.
10. Njeru, JW, Castro, MR, Carta, KG, Simon, G, Caraballo, PJ: Clinical Recognition and Management of Patients with Prediabetes. *Endocr Pract*, 25: 545-553, 2019.
11. Tokarz, VL, MacDonald, PE, Klip, A: The cell biology of systemic insulin function. *J Cell Biol*, 217: 2273-2289, 2018.
12. Boland, BB, Rhodes, CJ, Grimsby, JS: The dynamic plasticity of insulin production in beta-cells. *Mol Metab*, 6: 958-973, 2017.
13. Quesada, I, Tuduri, E, Ripoll, C, Nadal, A: Physiology of the pancreatic alpha-cell and glucagon secretion: role in glucose homeostasis and diabetes. *J Endocrinol*, 199: 5-19, 2008.
14. Ghezzi, C, Loo, DDF, Wright, EM: Physiology of renal glucose handling via SGLT1, SGLT2 and GLUT2. *Diabetologia*, 61: 2087-2097, 2018.
15. American Diabetes, A: 2. Classification and Diagnosis of Diabetes: Standards of Medical Care in Diabetes-2020. *Diabetes Care*, 43: S14-S31, 2020.

16. Warshauer, JT, Bluestone, JA, Anderson, MS: New Frontiers in the Treatment of Type 1 Diabetes. *Cell Metab*, 31: 46-61, 2020.
17. Libianto, R, Davis, TM, Ekinci, EI: Advances in type 2 diabetes therapy: a focus on cardiovascular and renal outcomes. *Med J Aust*, 2020.
18. Buse, JB, Wexler, DJ, Tsapas, A, Rossing, P, Mingrone, G, Mathieu, C, D'Alessio, DA, Davies, MJ: 2019 update to: Management of hyperglycaemia in type 2 diabetes, 2018. A consensus report by the American Diabetes Association (ADA) and the European Association for the Study of Diabetes (EASD). *Diabetologia*, 63: 221-228, 2020.
19. Umpierrez, G, Korytkowski, M: Diabetic emergencies - ketoacidosis, hyperglycaemic hyperosmolar state and hypoglycaemia. *Nat Rev Endocrinol*, 12: 222-232, 2016.
20. Brownlee, M: Biochemistry and molecular cell biology of diabetic complications. *Nature*, 414: 813-820, 2001.
21. Giacco, F, Brownlee, M: Oxidative stress and diabetic complications. *Circ Res*, 107: 1058-1070, 2010.
22. Domingueti, CP, Dusse, LM, Carvalho, M, de Sousa, LP, Gomes, KB, Fernandes, AP: Diabetes mellitus: The linkage between oxidative stress, inflammation, hypercoagulability and vascular complications. *J Diabetes Complications*, 30: 738-745, 2016.
23. Congdon, NG, Friedman, DS, Lietman, T: Important causes of visual impairment in the world today. *JAMA*, 290: 2057-2060, 2003.
24. Saaddine, JB, Honeycutt, AA, Narayan, KM, Zhang, X, Klein, R, Boyle, JP: Projection of diabetic retinopathy and other major eye diseases among people with diabetes mellitus: United States, 2005-2050. *Arch Ophthalmol*, 126: 1740-1747, 2008.
25. Wong, TY, Cheung, CM, Larsen, M, Sharma, S, Simo, R: Diabetic retinopathy. *Nat Rev Dis Primers*, 2: 16012, 2016.
26. Klein, R, Klein, BE, Moss, SE, Davis, MD, DeMets, DL: The Wisconsin epidemiologic study of diabetic retinopathy. III. Prevalence and risk of diabetic retinopathy when age at diagnosis is 30 or more years. *Arch Ophthalmol*, 102: 527-532, 1984.
27. Klein, R, Klein, BE, Moss, SE, Davis, MD, DeMets, DL: The Wisconsin epidemiologic study of diabetic retinopathy. II. Prevalence and risk of diabetic retinopathy when age at diagnosis is less than 30 years. *Arch Ophthalmol*, 102: 520-526, 1984.
28. Leasher, JL, Bourne, RR, Flaxman, SR, Jonas, JB, Keeffe, J, Naidoo, K, Pesudovs, K, Price, H, White, RA, Wong, TY, Resnikoff, S, Taylor, HR, Vision Loss Expert Group of the Global Burden of Disease, S: Global Estimates on the Number of People Blind or Visually Impaired by Diabetic Retinopathy: A Meta-analysis From 1990 to 2010. *Diabetes Care*, 39: 1643-1649, 2016.
29. Fenwick, EK, Pesudovs, K, Rees, G, Dirani, M, Kawasaki, R, Wong, TY, Lamoureux, EL: The impact of diabetic retinopathy: understanding the patient's perspective. *Br J Ophthalmol*, 95: 774-782, 2011.
30. Wang, W, Lo, ACY: Diabetic Retinopathy: Pathophysiology and Treatments. *Int J Mol Sci*, 19, 2018.

31. Kern, TS, Antonetti, DA, Smith, LEH: Pathophysiology of Diabetic Retinopathy: Contribution and Limitations of Laboratory Research. *Ophthalmic Res*, 62: 196-202, 2019.
32. Chen, J, Connor, KM, Aderman, CM, Smith, LE: Erythropoietin deficiency decreases vascular stability in mice. *J Clin Invest*, 118: 526-533, 2008.
33. Riva, CE, Logean, E, Falsini, B: Visually evoked hemodynamical response and assessment of neurovascular coupling in the optic nerve and retina. *Prog Retin Eye Res*, 24: 183-215, 2005.
34. Cheung, N, Mitchell, P, Wong, TY: Diabetic retinopathy. *Lancet*, 376: 124-136, 2010.
35. Watanabe, D, Suzuma, K, Matsui, S, Kurimoto, M, Kiryu, J, Kita, M, Suzuma, I, Ohashi, H, Ojima, T, Murakami, T, Kobayashi, T, Masuda, S, Nagao, M, Yoshimura, N, Takagi, H: Erythropoietin as a retinal angiogenic factor in proliferative diabetic retinopathy. *N Engl J Med*, 353: 782-792, 2005.
36. Fong, DS, Aiello, LP, Ferris, FL, 3rd, Klein, R: Diabetic retinopathy. *Diabetes Care*, 27: 2540-2553, 2004.
37. Riaskoff, S: Photocoagulation treatment of proliferative diabetic retinopathy. *Bull Soc Belge Ophtalmol*, 197: 9-17, 1981.
38. Whitehead, M, Wickremasinghe, S, Osborne, A, Van Wijngaarden, P, Martin, KR: Diabetic retinopathy: a complex pathophysiology requiring novel therapeutic strategies. *Expert Opin Biol Ther*, 18: 1257-1270, 2018.
39. Mitchell, P, Wong, TY, Diabetic Macular Edema Treatment Guideline Working, G: Management paradigms for diabetic macular edema. *Am J Ophthalmol*, 157: 505-513 e501-508, 2014.
40. Prince, VE, Anderson, RM, Dalgin, G: Zebrafish Pancreas Development and Regeneration: Fishing for Diabetes Therapies. *Curr Top Dev Biol*, 124: 235-276, 2017.
41. Ehrhardt, JD, Gomez, F: Embryology, Pancreas. In: *StatPearls*. Treasure Island (FL), 2019.
42. Dolensek, J, Rupnik, MS, Stozar, A: Structural similarities and differences between the human and the mouse pancreas. *Islets*, 7: e1024405, 2015.
43. Jennings, RE, Berry, AA, Strutt, JP, Gerrard, DT, Hanley, NA: Human pancreas development. *Development*, 142: 3126-3137, 2015.
44. Gao, T, McKenna, B, Li, C, Reichert, M, Nguyen, J, Singh, T, Yang, C, Pannikar, A, Doliba, N, Zhang, T, Stoffers, DA, Edlund, H, Matschinsky, F, Stein, R, Stanger, BZ: Pdx1 maintains beta cell identity and function by repressing an alpha cell program. *Cell Metab*, 19: 259-271, 2014.
45. Talchai, C, Xuan, S, Lin, HV, Sussel, L, Accili, D: Pancreatic beta cell dedifferentiation as a mechanism of diabetic beta cell failure. *Cell*, 150: 1223-1234, 2012.
46. Weedon, MN, Cebola, I, Patch, AM, Flanagan, SE, De Franco, E, Caswell, R, Rodriguez-Segui, SA, Shaw-Smith, C, Cho, CH, Allen, HL, Houghton, JA, Roth, CL, Chen, R, Hussain, K, Marsh, P, Vallier, L, Murray, A, International Pancreatic Agenesis, C, Ellard, S, Ferrer, J, Hattersley, AT: Recessive mutations in a distal PTF1A enhancer cause isolated pancreatic agenesis. *Nat Genet*, 46: 61-64, 2014.

47. Shaw-Smith, C, De Franco, E, Lango Allen, H, Battle, M, Flanagan, SE, Borowiec, M, Taplin, CE, van Alfen-van der Velden, J, Cruz-Rojo, J, Perez de Nanclares, G, Miedzybrodzka, Z, Deja, G, Wlodarska, I, Mlynarski, W, Ferrer, J, Hattersley, AT, Ellard, S: GATA4 mutations are a cause of neonatal and childhood-onset diabetes. *Diabetes*, 63: 2888-2894, 2014.
48. Smith, SB, Qu, HQ, Taleb, N, Kishimoto, NY, Scheel, DW, Lu, Y, Patch, AM, Grabs, R, Wang, J, Lynn, FC, Miyatsuka, T, Mitchell, J, Seerke, R, Desir, J, Vanden Eijnden, S, Abramowicz, M, Kacet, N, Weill, J, Renard, ME, Gentile, M, Hansen, I, Dewar, K, Hattersley, AT, Wang, R, Wilson, ME, Johnson, JD, Polychronakos, C, German, MS: Rfx6 directs islet formation and insulin production in mice and humans. *Nature*, 463: 775-780, 2010.
49. Flanagan, SE, De Franco, E, Lango Allen, H, Zerah, M, Abdul-Rasoul, MM, Edge, JA, Stewart, H, Alamiri, E, Hussain, K, Wallis, S, de Vries, L, Rubio-Cabezas, O, Houghton, JA, Edghill, EL, Patch, AM, Ellard, S, Hattersley, AT: Analysis of transcription factors key for mouse pancreatic development establishes NKX2-2 and MNX1 mutations as causes of neonatal diabetes in man. *Cell Metab*, 19: 146-154, 2014.
50. Pisharath, H, Rhee, JM, Swanson, MA, Leach, SD, Parsons, MJ: Targeted ablation of beta cells in the embryonic zebrafish pancreas using E. coli nitroreductase. *Mech Dev*, 124: 218-229, 2007.
51. Andersson, O, Adams, BA, Yoo, D, Ellis, GC, Gut, P, Anderson, RM, German, MS, Stainier, DY: Adenosine signaling promotes regeneration of pancreatic beta cells in vivo. *Cell Metab*, 15: 885-894, 2012.
52. Delaspre, F, Beer, RL, Rovira, M, Huang, W, Wang, G, Gee, S, Vitery Mdel, C, Wheelan, SJ, Parsons, MJ: Centroacinar Cells Are Progenitors That Contribute to Endocrine Pancreas Regeneration. *Diabetes*, 64: 3499-3509, 2015.
53. Ye, L, Robertson, MA, Hesselson, D, Stainier, DY, Anderson, RM: Glucagon is essential for alpha cell transdifferentiation and beta cell neogenesis. *Development*, 142: 1407-1417, 2015.
54. Poli, G, Schaur, RJ: 4-Hydroxynonenal in the pathomechanisms of oxidative stress. *IUBMB Life*, 50: 315-321, 2000.
55. Esterbauer, H, Schaur, RJ, Zollner, H: Chemistry and biochemistry of 4-hydroxynonenal, malonaldehyde and related aldehydes. *Free Radic Biol Med*, 11: 81-128, 1991.
56. Camara, AK, Lesnefsky, EJ, Stowe, DF: Potential therapeutic benefits of strategies directed to mitochondria. *Antioxid Redox Signal*, 13: 279-347, 2010.
57. Schaur, RJ, Siems, W, Bresgen, N, Eckl, PM: 4-Hydroxy-nonenal-A Bioactive Lipid Peroxidation Product. *Biomolecules*, 5: 2247-2337, 2015.
58. Fukumoto, J, Fukumoto, I, Parthasarathy, PT, Cox, R, Huynh, B, Ramanathan, GK, Venugopal, RB, Allen-Gipson, DS, Lockey, RF, Kolliputi, N: NLRP3 deletion protects from hyperoxia-induced acute lung injury. *Am J Physiol Cell Physiol*, 305: C182-189, 2013.
59. Ayala, A, Munoz, MF, Arguelles, S: Lipid peroxidation: production, metabolism, and signaling mechanisms of malondialdehyde and 4-hydroxy-2-nonenal. *Oxid Med Cell Longev*, 2014: 360438, 2014.

60. Benedetti, A, Comporti, M, Esterbauer, H: Identification of 4-hydroxynonenal as a cytotoxic product originating from the peroxidation of liver microsomal lipids. *Biochim Biophys Acta*, 620: 281-296, 1980.
61. Dalleau, S, Baradat, M, Gueraud, F, Huc, L: Cell death and diseases related to oxidative stress: 4-hydroxynonenal (HNE) in the balance. *Cell Death Differ*, 20: 1615-1630, 2013.
62. Cohen, G, Riahi, Y, Sunda, V, Deplano, S, Chatgillaloglu, C, Ferreri, C, Kaiser, N, Sasson, S: Signaling properties of 4-hydroxyalkenals formed by lipid peroxidation in diabetes. *Free Radic Biol Med*, 65: 978-987, 2013.
63. Benedetti, E, D'Angelo, B, Cristiano, L, Di Giacomo, E, Fanelli, F, Moreno, S, Cecconi, F, Fidoamore, A, Antonosante, A, Falcone, R, Ippoliti, R, Giordano, A, Cimini, A: Involvement of peroxisome proliferator-activated receptor beta/delta (PPAR beta/delta) in BDNF signaling during aging and in Alzheimer disease: possible role of 4-hydroxynonenal (4-HNE). *Cell Cycle*, 13: 1335-1344, 2014.
64. Zhong, H, Yin, H: Role of lipid peroxidation derived 4-hydroxynonenal (4-HNE) in cancer: focusing on mitochondria. *Redox Biol*, 4: 193-199, 2015.
65. Pashkow, FJ: Oxidative Stress and Inflammation in Heart Disease: Do Antioxidants Have a Role in Treatment and/or Prevention? *Int J Inflam*, 2011: 514623, 2011.
66. Okamoto, K, Toyokuni, S, Uchida, K, Ogawa, O, Takenawa, J, Kakehi, Y, Kinoshita, H, Hattori-Nakakuki, Y, Hiai, H, Yoshida, O: Formation of 8-hydroxy-2'-deoxyguanosine and 4-hydroxy-2-nonenal-modified proteins in human renal-cell carcinoma. *Int J Cancer*, 58: 825-829, 1994.
67. Sasson, S: 4-Hydroxyalkenal-activated PPARdelta mediates hormetic interactions in diabetes. *Biochimie*, 136: 85-89, 2017.
68. Sasson, S: Nutrient overload, lipid peroxidation and pancreatic beta cell function. *Free Radic Biol Med*, 111: 102-109, 2017.
69. Liu, G, Ji, W, Huang, J, Liu, L, Wang, Y: 4-HNE expression in diabetic rat kidneys and the protective effects of probucol. *J Endocrinol Invest*, 39: 865-873, 2016.
70. Akude, E, Zherebitskaya, E, Roy Chowdhury, SK, Girling, K, Fernyhough, P: 4-Hydroxy-2-nonenal induces mitochondrial dysfunction and aberrant axonal outgrowth in adult sensory neurons that mimics features of diabetic neuropathy. *Neurotox Res*, 17: 28-38, 2010.
71. Mori, A, Takei, T, Sakamoto, K, Nakahara, T, Ishii, K: 4-Hydroxy-2-nonenal attenuates beta2-adrenoceptor-mediated vasodilation of rat retinal arterioles. *Naunyn Schmiedebergs Arch Pharmacol*, 388: 575-582, 2015.
72. Vasiliou, V, Thompson, DC, Smith, C, Fujita, M, Chen, Y: Aldehyde dehydrogenases: from eye crystallins to metabolic disease and cancer stem cells. *Chem Biol Interact*, 202: 2-10, 2013.
73. Ahmed Laskar, A, Younus, H: Aldehyde toxicity and metabolism: the role of aldehyde dehydrogenases in detoxification, drug resistance and carcinogenesis. *Drug Metab Rev*, 51: 42-64, 2019.
74. Jackson, B, Brocker, C, Thompson, DC, Black, W, Vasiliou, K, Nebert, DW, Vasiliou, V: Update on the aldehyde dehydrogenase gene (ALDH) superfamily. *Hum Genomics*, 5: 283-303, 2011.



75. Sophos, NA, Vasiliou, V: Aldehyde dehydrogenase gene superfamily: the 2002 update. *Chem Biol Interact*, 143-144: 5-22, 2003.
76. Marchitti, SA, Brocker, C, Stagos, D, Vasiliou, V: Non-P450 aldehyde oxidizing enzymes: the aldehyde dehydrogenase superfamily. *Expert Opin Drug Metab Toxicol*, 4: 697-720, 2008.
77. Pappa, A, Brown, D, Koutalos, Y, DeGregori, J, White, C, Vasiliou, V: Human aldehyde dehydrogenase 3A1 inhibits proliferation and promotes survival of human corneal epithelial cells. *J Biol Chem*, 280: 27998-28006, 2005.
78. Evces, S, Lindahl, R: Characterization of rat cornea aldehyde dehydrogenase. *Arch Biochem Biophys*, 274: 518-524, 1989.
79. Estey, T, Piatigorsky, J, Lassen, N, Vasiliou, V: ALDH3A1: a corneal crystallin with diverse functions. *Exp Eye Res*, 84: 3-12, 2007.
80. King, G, Holmes, RS: Human corneal aldehyde dehydrogenase: purification, kinetic characterisation and phenotypic variation. *Biochem Mol Biol Int*, 31: 49-63, 1993.
81. Mitchell, J, Cenedella, RJ: Quantitation of ultraviolet light-absorbing fractions of the cornea. *Cornea*, 14: 266-272, 1995.
82. Uma, L, Hariharan, J, Sharma, Y, Balasubramanian, D: Corneal aldehyde dehydrogenase displays antioxidant properties. *Exp Eye Res*, 63: 117-120, 1996.
83. Piatigorsky, J: Multifunctional lens crystallins and corneal enzymes. More than meets the eye. *Ann N Y Acad Sci*, 842: 7-15, 1998.
84. Manzer, R, Pappa, A, Estey, T, Sladek, N, Carpenter, JF, Vasiliou, V: Ultraviolet radiation decreases expression and induces aggregation of corneal ALDH3A1. *Chem Biol Interact*, 143-144: 45-53, 2003.
85. Voulgaridou, GP, Tsochantaridis, I, Tolkas, C, Franco, R, Giatromanolaki, A, Panayiotidis, MI, Pappa, A: Aldehyde dehydrogenase 3A1 confers oxidative stress resistance accompanied by altered DNA damage response in human corneal epithelial cells. *Free Radic Biol Med*, 2020.
86. Lassen, N, Bateman, JB, Estey, T, Kuszak, JR, Nees, DW, Piatigorsky, J, Duester, G, Day, BJ, Huang, J, Hines, LM, Vasiliou, V: Multiple and additive functions of ALDH3A1 and ALDH1A1: cataract phenotype and ocular oxidative damage in *Aldh3a1(-/-)/Aldh1a1(-/-)* knock-out mice. *J Biol Chem*, 282: 25668-25676, 2007.
87. Black, W, Chen, Y, Matsumoto, A, Thompson, DC, Lassen, N, Pappa, A, Vasiliou, V: Molecular mechanisms of ALDH3A1-mediated cellular protection against 4-hydroxy-2-nonenal. *Free Radic Biol Med*, 52: 1937-1944, 2012.
88. Lassen, N, Pappa, A, Black, WJ, Jester, JV, Day, BJ, Min, E, Vasiliou, V: Antioxidant function of corneal ALDH3A1 in cultured stromal fibroblasts. *Free Radic Biol Med*, 41: 1459-1469, 2006.
89. Maessen, DE, Stehouwer, CD, Schalkwijk, CG: The role of methylglyoxal and the glyoxalase system in diabetes and other age-related diseases. *Clin Sci (Lond)*, 128: 839-861, 2015.
90. Lodd, E, Wiggerhauser, LM, Morgenstern, J, Fleming, TH, Poschet, G, Buttner, M, Tabler, CT, Wohlfart, DP, Nawroth, PP, Kroll, J: The combination of loss of glyoxalase1 and obesity results in hyperglycemia. *JCI Insight*, 4, 2019.

91. Schmohl, F, Peters, V, Schmitt, CP, Poschet, G, Buttner, M, Li, X, Weigand, T, Poth, T, Volk, N, Morgenstern, J, Fleming, T, Nawroth, PP, Kroll, J: CNDP1 knockout in zebrafish alters the amino acid metabolism, restrains weight gain, but does not protect from diabetic complications. *Cell Mol Life Sci*, 76: 4551-4568, 2019.
92. Wigganhauser, LM, Qi, H, Stoll, SJ, Metzger, L, Bennewitz, K, Poschet, G, Krenning, G, Hillebrands, JL, Hammes, HP, Kroll, J: Activation of retinal angiogenesis in hyperglycemic *pdx1 (-/-)* zebrafish mutants. *Diabetes*, 2020.
93. Lawson, ND, Weinstein, BM: In vivo imaging of embryonic vascular development using transgenic zebrafish. *Dev Biol*, 248: 307-318, 2002.
94. Flanagan-Steet, H, Fox, MA, Meyer, D, Sanes, JR: Neuromuscular synapses can form in vivo by incorporation of initially aneural postsynaptic specializations. *Development*, 132: 4471-4481, 2005.
95. Kimmel, CB, Ballard, WW, Kimmel, SR, Ullmann, B, Schilling, TF: Stages of embryonic development of the zebrafish. *Dev Dyn*, 203: 253-310, 1995.
96. Jung, SH, Kim, YS, Lee, YR, Kim, JS: High glucose-induced changes in hyaloid-retinal vessels during early ocular development of zebrafish: a short-term animal model of diabetic retinopathy. *Br J Pharmacol*, 173: 15-26, 2016.
97. Oka, T, Nishimura, Y, Zang, L, Hirano, M, Shimada, Y, Wang, Z, Umemoto, N, Kuroyanagi, J, Nishimura, N, Tanaka, T: Diet-induced obesity in zebrafish shares common pathophysiological pathways with mammalian obesity. *BMC Physiol*, 10: 21, 2010.
98. Wigganhauser, LM, Kohl, K, Dietrich, N, Hammes, HP, Kroll, J: Studying Diabetes Through the Eyes of a Fish: Microdissection, Visualization, and Analysis of the Adult *tg(fli:EGFP)* Zebrafish Retinal Vasculature. *J Vis Exp*, 2017.
99. TW, HB, Girke, T: systemPipeR: NGS workflow and report generation environment. *BMC Bioinformatics*, 17: 388, 2016.
100. Bray, NL, Pimentel, H, Melsted, P, Pachter, L: Near-optimal probabilistic RNA-seq quantification. *Nat Biotechnol*, 34: 525-527, 2016.
101. Ritchie, ME, Phipson, B, Wu, D, Hu, Y, Law, CW, Shi, W, Smyth, GK: limma powers differential expression analyses for RNA-sequencing and microarray studies. *Nucleic Acids Res*, 43: e47, 2015.
102. Gu, Z, Eils, R, Schlesner, M: Complex heatmaps reveal patterns and correlations in multidimensional genomic data. *Bioinformatics*, 32: 2847-2849, 2016.
103. Vander Jagt, DL, Hunsaker, LA: Methylglyoxal metabolism and diabetic complications: roles of aldose reductase, glyoxalase-I, betaine aldehyde dehydrogenase and 2-oxoaldehyde dehydrogenase. *Chem Biol Interact*, 143-144: 341-351, 2003.
104. McLellan, AC, Thornalley, PJ: Glyoxalase activity in human red blood cells fractionated by age. *Mech Ageing Dev*, 48: 63-71, 1989.
105. Rabbani, N, Thornalley, PJ: Measurement of methylglyoxal by stable isotopic dilution analysis LC-MS/MS with corroborative prediction in physiological samples. *Nat Protoc*, 9: 1969-1979, 2014.
106. Weger, BD, Weger, M, Gorling, B, Schink, A, Gobet, C, Keime, C, Poschet, G, Jost, B, Krone, N, Hell, R, Gachon, F, Luy, B, Dickmeis, T: Extensive Regulation of

- Diurnal Transcription and Metabolism by Glucocorticoids. *PLoS Genet*, 12: e1006512, 2016.
107. Beale, DJ, Pinu, FR, Kouremenos, KA, Poojary, MM, Narayana, VK, Boughton, BA, Kanojia, K, Dayalan, S, Jones, OAH, Dias, DA: Review of recent developments in GC-MS approaches to metabolomics-based research. *Metabolomics*, 14: 152, 2018.
108. Holmes, RS, Hempel, J: Comparative studies of vertebrate aldehyde dehydrogenase 3: sequences, structures, phylogeny and evolution. Evidence for a mammalian origin for the ALDH3A1 gene. *Chem Biol Interact*, 191: 113-121, 2011.
109. Agalou, A, Thrapsianiotis, M, Angelis, A, Papakyriakou, A, Skaltsounis, AL, Aligiannis, N, Beis, D: Identification of Novel Melanin Synthesis Inhibitors From *Crataegus pycnoloba* Using an in Vivo Zebrafish Phenotypic Assay. *Front Pharmacol*, 9: 265, 2018.
110. Konermann, S, Brigham, MD, Trevino, AE, Joung, J, Abudayyeh, OO, Barcena, C, Hsu, PD, Habib, N, Gootenberg, JS, Nishimasu, H, Nureki, O, Zhang, F: Genome-scale transcriptional activation by an engineered CRISPR-Cas9 complex. *Nature*, 517: 583-588, 2015.
111. Cook, OF: The Mendelian Inheritance of Mutations. *Science*, 28: 86-88, 1908.
112. Babu, DA, Deering, TG, Mirmira, RG: A feat of metabolic proportions: Pdx1 orchestrates islet development and function in the maintenance of glucose homeostasis. *Mol Genet Metab*, 92: 43-55, 2007.
113. Wangsa-Wirawan, ND, Linsenmeier, RA: Retinal oxygen: fundamental and clinical aspects. *Arch Ophthalmol*, 121: 547-557, 2003.
114. Alvarez, Y, Cederlund, ML, Cottell, DC, Bill, BR, Ekker, SC, Torres-Vazquez, J, Weinstein, BM, Hyde, DR, Vihtelic, TS, Kennedy, BN: Genetic determinants of hyaloid and retinal vasculature in zebrafish. *BMC Dev Biol*, 7: 114, 2007.
115. Kimmel, RA, Meyer, D: Molecular regulation of pancreas development in zebrafish. *Methods Cell Biol*, 100: 261-280, 2010.
116. Roder, PV, Wu, B, Liu, Y, Han, W: Pancreatic regulation of glucose homeostasis. *Exp Mol Med*, 48: e219, 2016.
117. Papasani, MR, Robison, BD, Hardy, RW, Hill, RA: Early developmental expression of two insulins in zebrafish (*Danio rerio*). *Physiol Genomics*, 27: 79-85, 2006.
118. Yano, K, Morinaka, Y, Wang, F, Huang, P, Takehara, S, Hirai, T, Ito, A, Koketsu, E, Kawamura, M, Kotake, K, Yoshida, S, Endo, M, Tamiya, G, Kitano, H, Ueguchi-Tanaka, M, Hirano, K, Matsuoka, M: GWAS with principal component analysis identifies a gene comprehensively controlling rice architecture. *Proc Natl Acad Sci U S A*, 116: 21262-21267, 2019.
119. Subramanian, A, Tamayo, P, Mootha, VK, Mukherjee, S, Ebert, BL, Gillette, MA, Paulovich, A, Pomeroy, SL, Golub, TR, Lander, ES, Mesirov, JP: Gene set enrichment analysis: a knowledge-based approach for interpreting genome-wide expression profiles. *Proc Natl Acad Sci U S A*, 102: 15545-15550, 2005.
120. Breitzig, M, Bhimineni, C, Lockey, R, Kolliputi, N: 4-Hydroxy-2-nonenal: a critical target in oxidative stress? *Am J Physiol Cell Physiol*, 311: C537-C543, 2016.
121. Forbes, JM, Cooper, ME: Mechanisms of diabetic complications. *Physiol Rev*, 93: 137-188, 2013.

122. Wigganhauser, LM, Kroll, J: Vascular Damage in Obesity and Diabetes: Highlighting Links Between Endothelial Dysfunction and Metabolic Disease in Zebrafish and Man. *Curr Vasc Pharmacol*, 17: 476-490, 2019.
123. Lechner, J, O'Leary, OE, Stitt, AW: The pathology associated with diabetic retinopathy. *Vision Res*, 139: 7-14, 2017.
124. Voulgaridou, GP, Tsochantaridis, I, Mantso, T, Franco, R, Panayiotidis, MI, Pappa, A: Human aldehyde dehydrogenase 3A1 (ALDH3A1) exhibits chaperone-like function. *Int J Biochem Cell Biol*, 89: 16-24, 2017.
125. Stagos, D, Chen, Y, Cantore, M, Jester, JV, Vasiliou, V: Corneal aldehyde dehydrogenases: multiple functions and novel nuclear localization. *Brain Res Bull*, 81: 211-218, 2010.
126. Estey, T, Chen, Y, Carpenter, JF, Vasiliou, V: Structural and functional modifications of corneal crystallin ALDH3A1 by UVB light. *PLoS One*, 5: e15218, 2010.
127. Kijewska, M, Viski, C, Turrell, F, Fitzpatrick, A, van Weverwijk, A, Gao, Q, Iravani, M, Isacke, CM: Using an in-vivo syngeneic spontaneous metastasis model identifies ID2 as a promoter of breast cancer colonisation in the brain. *Breast Cancer Res*, 21: 4, 2019.
128. Tobia, C, Gariano, G, Guerra, J, Presta, M: Zebrafish embryo intersegmental vessels: a tool for investigating sprouting angiogenesis. *Methods Mol Biol*, 1214: 173-184, 2015.
129. Ellertsdottir, E, Lenard, A, Blum, Y, Krudewig, A, Herwig, L, Affolter, M, Belting, HG: Vascular morphogenesis in the zebrafish embryo. *Dev Biol*, 341: 56-65, 2010.
130. Hogan, BM, Herpers, R, Witte, M, Helotera, H, Alitalo, K, Duckers, HJ, Schulte-Merker, S: Vegfc/Flt4 signalling is suppressed by Dll4 in developing zebrafish intersegmental arteries. *Development*, 136: 4001-4009, 2009.
131. Bower, NI, Vogrin, AJ, Le Guen, L, Chen, H, Stacker, SA, Achen, MG, Hogan, BM: Vegfd modulates both angiogenesis and lymphangiogenesis during zebrafish embryonic development. *Development*, 144: 507-518, 2017.
132. Barben, M, Samardzija, M, Grimm, C: The Role of Hypoxia, Hypoxia-Inducible Factor (HIF), and VEGF in Retinal Angiomatous Proliferation. *Adv Exp Med Biol*, 1074: 177-183, 2018.
133. Sone, H, Kawakami, Y, Okuda, Y, Kondo, S, Hanatani, M, Suzuki, H, Yamashita, K: Vascular endothelial growth factor is induced by long-term high glucose concentration and up-regulated by acute glucose deprivation in cultured bovine retinal pigmented epithelial cells. *Biochem Biophys Res Commun*, 221: 193-198, 1996.
134. Sun, Y, Wang, D, Ye, F, Hu, DN, Liu, X, Zhang, L, Gao, L, Song, E, Zhang, DY: Elevated cell proliferation and VEGF production by high-glucose conditions in Muller cells involve XIAP. *Eye (Lond)*, 27: 1299-1307, 2013.
135. Betts-Obregon, BS, Vellanki, S, Buikema, J, Tsin, AT, Wright, K: Effect of Glucose on Retinal Endothelial Cell Viability and VEGF Secretion. *HSOA J Cell Biol Cell Metabol*, 3, 2016.
136. Doronzo, G, Viretto, M, Russo, I, Mattiello, L, Anfossi, G, Trovati, M: Effects of high glucose on vascular endothelial growth factor synthesis and secretion in aortic vascular smooth muscle cells from obese and lean Zucker rats. *Int J Mol Sci*, 13: 9478-9488, 2012.

137. Williams, B, Gallacher, B, Patel, H, Orme, C: Glucose-induced protein kinase C activation regulates vascular permeability factor mRNA expression and peptide production by human vascular smooth muscle cells in vitro. *Diabetes*, 46: 1497-1503, 1997.
138. Kim, YM, Kim, SJ, Tatsunami, R, Yamamura, H, Fukai, T, Ushio-Fukai, M: ROS-induced ROS release orchestrated by Nox4, Nox2, and mitochondria in VEGF signaling and angiogenesis. *Am J Physiol Cell Physiol*, 312: C749-C764, 2017.
139. Singh, A, Castillo, HA, Brown, J, Kaslin, J, Dwyer, KM, Gibert, Y: High glucose levels affect retinal patterning during zebrafish embryogenesis. *Sci Rep*, 9: 4121, 2019.
140. Geisler, R, Borel, N, Ferg, M, Maier, JV, Strahle, U: Maintenance of Zebrafish Lines at the European Zebrafish Resource Center. *Zebrafish*, 13 Suppl 1: S19-23, 2016.
141. Bonora, M, Patergnani, S, Rimessi, A, De Marchi, E, Suski, JM, Bononi, A, Giorgi, C, Marchi, S, Missiroli, S, Poletti, F, Wieckowski, MR, Pinton, P: ATP synthesis and storage. *Purinergic Signal*, 8: 343-357, 2012.
142. Maldonado, EN, Lemasters, JJ: ATP/ADP ratio, the missed connection between mitochondria and the Warburg effect. *Mitochondrion*, 19 Pt A: 78-84, 2014.
143. Matschinsky, FM, Wilson, DF: The Central Role of Glucokinase in Glucose Homeostasis: A Perspective 50 Years After Demonstrating the Presence of the Enzyme in Islets of Langerhans. *Front Physiol*, 10: 148, 2019.
144. Patterson, JN, Cousteils, K, Lou, JW, Manning Fox, JE, MacDonald, PE, Joseph, JW: Mitochondrial metabolism of pyruvate is essential for regulating glucose-stimulated insulin secretion. *J Biol Chem*, 289: 13335-13346, 2014.
145. Tanabe, Y, William, C, Jessell, TM: Specification of motor neuron identity by the MNR2 homeodomain protein. *Cell*, 95: 67-80, 1998.
146. Arkhipova, V, Wendik, B, Devos, N, Ek, O, Peers, B, Meyer, D: Characterization and regulation of the hb9/mnx1 beta-cell progenitor specific enhancer in zebrafish. *Dev Biol*, 365: 290-302, 2012.
147. Bellier, J, Nokin, MJ, Larde, E, Karoyan, P, Peulen, O, Castronovo, V, Bellahcene, A: Methylglyoxal, a potent inducer of AGEs, connects between diabetes and cancer. *Diabetes Res Clin Pract*, 148: 200-211, 2019.
148. Jorgens, K, Stoll, SJ, Pohl, J, Fleming, TH, Sticht, C, Nawroth, PP, Hammes, HP, Kroll, J: High tissue glucose alters intersomitic blood vessels in zebrafish via methylglyoxal targeting the VEGF receptor signaling cascade. *Diabetes*, 64: 213-225, 2015.
149. Pappa, A, Chen, C, Koutalos, Y, Townsend, AJ, Vasiliou, V: Aldh3a1 protects human corneal epithelial cells from ultraviolet- and 4-hydroxy-2-nonenal-induced oxidative damage. *Free Radic Biol Med*, 34: 1178-1189, 2003.
150. Hlavacova, M, Gumulec, J, Stracina, T, Fojtu, M, Raudenska, M, Masarik, M, Novakova, M, Paulova, H: Different doxorubicin formulations affect plasma 4-hydroxy-2-nonenal and gene expression of aldehyde dehydrogenase 3A1 and thioredoxin reductase 2 in rat. *Physiol Res*, 64 Suppl 5: S653-660, 2015.
151. Herndon, AM, Breshears, MA, McFarlane, D: Oxidative modification, inflammation and amyloid in the normal and diabetic cat pancreas. *J Comp Pathol*, 151: 352-362, 2014.

152. Suarez-Pinzon, WL, Strynadka, K, Rabinovitch, A: Destruction of rat pancreatic islet beta-cells by cytokines involves the production of cytotoxic aldehydes. *Endocrinology*, 137: 5290-5296, 1996.
153. Miwa, I, Ichimura, N, Sugiura, M, Hamada, Y, Taniguchi, S: Inhibition of glucose-induced insulin secretion by 4-hydroxy-2-nonenal and other lipid peroxidation products. *Endocrinology*, 141: 2767-2772, 2000.
154. Jaworek, J, Szklarczyk, J, Bonior, J, Kot, M, Goralska, M, Pierzchalski, P, Reiter, RJ, Czech, U, Tomaszewska, R: Melatonin metabolite, N(1)-acetyl-N(1)-formyl-5-methoxykynuramine (AFMK), attenuates acute pancreatitis in the rat: in vivo and in vitro studies. *J Physiol Pharmacol*, 67: 411-421, 2016.
155. Lee, SJ, Seo, KW, Yun, MR, Bae, SS, Lee, WS, Hong, KW, Kim, CD: 4-Hydroxynonenal enhances MMP-2 production in vascular smooth muscle cells via mitochondrial ROS-mediated activation of the Akt/NF-kappaB signaling pathways. *Free Radic Biol Med*, 45: 1487-1492, 2008.
156. Zhou, T, Zhou, KK, Lee, K, Gao, G, Lyons, TJ, Kowluru, R, Ma, JX: The role of lipid peroxidation products and oxidative stress in activation of the canonical wingless-type MMTV integration site (WNT) pathway in a rat model of diabetic retinopathy. *Diabetologia*, 54: 459-468, 2011.
157. Xiao, M, Zhong, H, Xia, L, Tao, Y, Yin, H: Pathophysiology of mitochondrial lipid oxidation: Role of 4-hydroxynonenal (4-HNE) and other bioactive lipids in mitochondria. *Free Radic Biol Med*, 111: 316-327, 2017.
158. Paglialunga, S, van Bree, B, Bosma, M, Valdecantos, MP, Amengual-Cladera, E, Jorgensen, JA, van Beurden, D, den Hartog, GJM, Ouwens, DM, Briede, JJ, Schrauwen, P, Hoeks, J: Targeting of mitochondrial reactive oxygen species production does not avert lipid-induced insulin resistance in muscle tissue from mice. *Diabetologia*, 55: 2759-2768, 2012.
159. Ma, ZA: The role of peroxidation of mitochondrial membrane phospholipids in pancreatic beta -cell failure. *Curr Diabetes Rev*, 8: 69-75, 2012.
160. Matsuda, H: Zebrafish as a model for studying functional pancreatic beta cells development and regeneration. *Dev Growth Differ*, 60: 393-399, 2018.

## PUBLICATION LIST

Some parts of the experimental work, although not included in this written thesis, has been published in the following journal:

### **Genetic Compensation by *epob* in Pronephros Development in *epoa* Mutant Zebrafish**

Jianqing She\*, Yue Wu\*, **Bowen Lou\***, Elisabeth Lodd, Alina Klems, Felix Schmoehl, Zuyi Yuan, Ferdinand Le Noble, Jens Kroll

Cell Cycle, 18 (20), 2683-2696, Oct 2019; DOI: 10.1080/15384101.2019.1656019

\* These authors contributed equally to the publication.

The main parts of this thesis are currently in preparation for publication:

### **Elevated level of 4-hydroxynonenal in *aldh3a1* mutants causes hyperglycaemia leading to diabetic complications**

**Bowen Lou**, Thomas Fleming, Jakob Morgenstern, Poschet Gernot, Elena Heidenreich, Carsten Sticht, Stefan Kopf, Britta Brügger, Peter Paul Nawroth, Jens Kroll

Planned for submission in May 2020.

## CURRICULUM VITAE

### Personal Information

Name:	Bowen Lou
Date of birth:	19.05.1992
Place of birth:	Ankang, Shaanxi, China
Marital status:	unmarried
Father:	Wei Lou, civil servant
Mother:	Shanli Ke, bank employee

### Primary School Education

09.1998-06.2004	Chengguan Town First Primary School, Shiquan, Shaanxi, China.
09.2004-06.2007	Hanbin Junior High School, Ankang, Shaanxi, China
09.2007-06.2010	Shaanxi Ankang High School, Ankang, Shaanxi, China

### University Education

09.2010-06.2015	BM in Clinic Medicine (7 years) School of Health Science Center, Xi'an Jiaotong University
07.2015-06.2017	MD in Internal Medicine School of Health Science Center, Xi'an Jiaotong University
09.2017-	Universitätsmedizin Mannheim, Heidelberg University



## ACKNOWLEDGEMENT

I thank everyone who contributed to the successful accomplishment of this work.

At first, my special thanks go to Prof. Dr. Jens Kroll, who made it possible for me to carry out my MD/Dr.med. in his lab, for the patient guidance, encouragement and advice he has provided throughout all my research.

Then, I want to give my sincere thanks to the whole Kroll-Lab team, which has accompanied and assisted me in the past three years. Katrin Bennewitz, Elisabeth Lodd, Xiaogang Li, Silas Soleymani, Felix Schmöhl, Utsho Ali-Hader, Mike Boger, Haozhe Qi (Ryan), David Wohlfart, and everyone else, who has brought the laboratory to life, thank you.

I also thank, Dr. Gernot Poschet, Elena Heidenreich, Dr. Carsten Sticht, Dr. Carolina De La Torre, Dr. Thomas Flemming, Dr. Jakob Morgenstern, Prof. Dr. Karen Bieback, Prof. Dr. Peter Paul Nawroth, Prof. Dr. Hans-Peter Hammes and Live Cell Imaging Mannheim, for all the technical sustentation, excellent instruction and cooperation.

Furthermore, I would like to thank all the support from the SFB1118, the GRK 1874 DIAMICOM and China Scholarship Council (CSC).

I thank all my friends, for the care and help from Mannheim, Aachen, Paris, Xi'an, Lanzhou, Beijing, Hangzhou, Lincoln and Philadelphia, always at my side warmly, scientifically and personally.

Last, I would like to say thanks to my whole family, to two people who first showed me how to speak and walk. Thanks, mom and dad, for everything I can imagine.

As well, thanks for being all the things that make you.